UNIVERSIDADE ESTADUAL DE CAMPINAS
Instituto de Geociências

ULISSES MIGUEL DA COSTA CORREIA

# THE IMPACT OF POST-DEPOSITIONAL STRUCTURES IN CARBONATE RESERVOIRS: EXAMPLES OF IGNEOUS INTRUSIONS, FRACTURES, AND KARST

# O IMPACTO DE ESTRUTURAS PÓS-DEPOSICIONAIS EM RESERVATÓRIOS CARBONÁTICOS: EXEMPLOS DE INTRUSÕES ÍGNEAS, FRATURAS E CARSTE

CAMPINAS
2019

ULISSES MIGUEL DA COSTA CORREIA

# THE IMPACT OF POST-DEPOSITIONAL STRUCTURES IN CARBONATE RESERVOIRS: EXAMPLES OF IGNEOUS INTRUSIONS, FRACTURES, AND KARST

# O IMPACTO DE ESTRUTURAS PÓS-DEPOSICIONAIS EM RESERVATÓRIOS CARBONÁTICOS: EXEMPLOS DE INTRUSÕES ÍGNEAS, FRATURAS E CARSTE

THESIS PRESENTED TO THE INSTITUTE OF GEOSCIENCES OF THE UNIVERSITY OF CAMPINAS TO OBTAIN THE DEGREE OF DOCTOR IN SCIENCES IN AREA OF GEOLOGY AND NATURAL RESOURCES

TESE APRESENTADA AO INSTITUTO DE GEOCIÊNCIAS DA UNIVERSIDADE ESTADUAL DE CAMPINAS PARA OBTENÇÃO DO TÍTULO DE DOUTOR EM CIÊNCIAS NA ÁREA DE GEOLOGIA E RECURSOS NATURAIS

ORIENTADOR: PROF. DR. ALEXANDRE CAMPANE VIDAL

ESTE EXEMPLAR CORRESPONDE À VERSÃO FINAL DA TESE DEFENDIDA PELO ALUNO ULISSES MIGUEL DA COSTA CORREIA E ORIENTADA PELO PROF. DR. ALEXANDRE CAMPANE VIDAL

CAMPINAS

2019

**Agência(s) de fomento e nº(s) de processo(s):** CAPES
**ORCID:** https://orcid.org/0000-0002-3734-8022

Ficha catalográfica
Universidade Estadual de Campinas
Biblioteca do Instituto de Geociências
Marta dos Santos - CRB 8/5892

C817i

Correia, Ulisses Miguel da Costa, 1989-
The impact of post-depositional structures in carbonate reservoirs : examples of igneous intrusions, fractures, and karst / Ulisses Miguel da Costa Correia. – Campinas, SP : [s.n.], 2019.

Orientador: Alexandre Campane Vidal.
Tese (doutorado) – Universidade Estadual de Campinas, Instituto de Geociências.

1. Magmatismo. 2. Fraturas. 3. Carste. 4. Campos, Bacia de (RJ). I. Vidal, Alexandre Campane, 1969-. II. Universidade Estadual de Campinas. Instituto de Geociências. III. Título.

Informações para Biblioteca Digital

**Título em outro idioma:** O impacto de estruturas pós-deposicionais em reservatórios carbonáticos : exemplos de intrusões ígneas, fraturas e carste
**Palavras-chave em inglês:**
Magmatism
Fractures
Karst
Campos Basin (Brazil)
**Área de concentração:** Geologia e Recursos Naturais
**Titulação:** Doutor em Ciências
**Banca examinadora:**
Alexandre Campane Vidal [Orientador]
Janaína Teixeira Lobo
Anna Eliza Svartman Dias
Giorgio Basilici
Manuel Gomes Correia
**Data de defesa:** 28-02-2019
**Programa de Pós-Graduação:** Geociências

**UNIVERSIDADE ESTADUAL DE CAMPINAS**
**INSTITUTO DE GEOCIÊNCIAS**

**AUTOR**: Ulisses Miguel da Costa Correia

THE IMPACT OF POST-DEPOSITIONAL STRUCTURES IN CARBONATE RESERVOIRS: EXAMPLES OF IGNEOUS INTRUSIONS, FRACTURES, AND KARST

O IMPACTO DE ESTRUTURAS PÓS-DEPOSICIONAIS EM RESERVATÓRIOS CARBONÁTICOS: EXEMPLOS DE INTRUSÕES ÍGNEAS, FRATURAS E CARSTE

**ORIENTADOR**: Prof. Dr. Alexandre Campane Vidal

Aprovado em: 28 / 02 / 2019

**EXAMINADORES:**

Prof. Dr. Alexandre Campane Vidal - Presidente

Prof. Dr. Giorgio Basilici

Prof. Dr. Manuel Gomes Correia

Dra. Janaína Teixeira Lobo

Dra. Anna Eliza Svartman Dias

**A Ata de defesa com as respectivas assinaturas dos membros, encontra-se disponível no SIGA - Sistema de Fluxo de Tese e na Secretaria de Pós-graduação do IG.**

Campinas, 28 de fevereiro de 2019.

## SÚMULA/BIOGRAFIA

Ulisses Miguel da Costa Correia, geólogo, formado em Geologia e Recursos Naturais pela Faculdade de Ciências da Universidade de Lisboa (2012), obteve o grau de mestre pelo Instituto de Geociências da Universidade Estadual de Campinas (2015) onde desenvolveu trabalho na área de modelagem geológica de reservatórios siliciclásticos, num caso de estudo na Bacia de Campos. Pela mesma instituição se candidata à obtenção do grau de doutor em ciências com o presente trabalho. Atualmente tem se dedicado ao reconhecimento e caracterização geométrica de intrusões magmáticas e estruturas relacionadas, através de interpretação sísmica, para entender o impacto do magmatismo em sistemas petrolíferos.

*À minha família que eu tanto amo.*

*Aos meus pais Luis Correia e Epifânia Malam da Costa Correia.*

*Aos meus irmãos Bruno Correia, Adelina Correia, e Wilma Correia.*

## AGRADECIMENTO

Devo começar por agradecer pela oportunidade que me foi concedida pelo meu orientador Professor Doutor Alexandre Campane vidal, que me proporcionou junto do Laboratório de Modelagem Geológica de Reservatórios condições para participar em projetos de pesquisa com a Equinor, numa primeira instânica, e mais tarde com a Shell. Por isso, também agradeço a essas empresas pela excelente oportunidade de trabalhar sob as suas orientações. Ter trabalhado nesses dois projetos de pesquisa me proporcionou, ao final, uma maior experiência que de certeza me fez um geólogo com um pouco mais de conhecimento. Um especial agradecimento à Susana da Graça Santos, que sempre esteve disponível para rever todos os textos e todas as discussões desde o ínicio deste trabalho. Muito também se deve a ela, e em particular à sua excelente capaciade de transmitir a mensagem através de textos científicos. A paciência foi de Santa. Agradeço aos meus eternos mentores e conselheiros, Doutor Hugo Matias, Professor Doutor Leonardo Azevedo, e Professor Doutor Nuno Pimentel. Devo agradecer também à Coordenação de Aperfeiçoamento de Pessoal de Nível Superior (CAPES) - Código de Financiamento 001, pela bolsa de Doutorado que me foi concedida, e também ao Banco de Dados de Exploração e Produção (BDEP) da Agência Nacional do Petróleo, Gás Natural e Biocombustíveis (ANP) por ter disponiblizado dados de poço e de sísmica 2D e 3D. Às empresas, dGB Earth Sciences, Schlumberger, IHS Markit, Ikon Science agradeço por terem cedido licenças académicas dos programas, OpendTect, Petrel, Kingdom, e RokDoc, respectivamente. Ao Departamento de Geologia e Recursos Naturais (DGRN) do Instituto de Geociências (IG), também devo um especial agradecimento por me ter acolhido durante todos estes anos, desde 2013 (Mestrado), até agora com muito carinho, e todo o apoio que sempre precisei, principalmente da Valdirene Pinotti, Gorete Bernardelli, e Cristina Moraes, da Secretaria da Pós-Graduação, e ao Maicon, Moacir, Ricardo, e Paulo da informática do instituto. Aos meus amigos do laboratório Modelagem Geológica de Reservatórios (MGR) do Centro de Estudos de Petróleo (CEPETRO) devo um especial agradecimento por todos os momentos, conhecimento, e orientação que sempre me concederam (e concedem) na academia e na vida. Tem sido uma honra conhecê-los. Foram, sem dúvida, uma peça fundamental do puzzle. Agradeço ao Doutor Manuel Correia, à Doutora Janaína Lobo, e ao Professor Doutor Ticiano dos Santos pelas valiosas contribuições na qualificação (primeiro estágio de avaliação) do trabalho, que se encontra melhor que antes. E por fim aos últimos avaliadores do trabalho na banca final de defesa, agradeço ao Professor Giorgio Basilici e à Doutora Anna Eliza Svartman que tiveram contribuições muito valiosas.

## RESUMO

A caracterização geológica de reservatórios tem-se tornado cada vez mais desafiante. Com o rápido avanço de processos e métodos para a caracterização de reservatórios também surgem soluções e propostas para os mais variados problemas. Esses problemas e desafios incluem a interpretação e caracterização de estruturas pós-deposicionais para a sua representação através de modelos geológicos tridimensionais. Exemplos dessas estruturas são intrusões ígneas e as estruturas internas e externas associadas, fraturas de escala sub-sísmica, e feições relacionadas a carste. Na seção pós-sal da Bacia de Campos e no pré-sal da Bacia de Santos são aplicadas técnicas para identificar e caracterizar estruturas pós-deposicionais. O principal propósito deste trabalho é contribuir para o aumento do conhecimento em caracterização de reservatórios e para o impacto que as estruturas pós-deposicionais podem ter nos sistemas petrolíferos, particularmente nos reservatórios. Os dados utilizados são constituídos por duas aquisições sísmicas e dois conjuntos de poços das bacias de Campos e Santos. A caracterização de rochas ígneas intrusivas, na Bacia de Campos, se baseou na análise morfométrica que permitiu caracterizar as intrusões, e entender a relação que existe com as estruturas associadas que ocorrem em torno das intrusões. Com base na análise quantitativa das soleiras foi possível inferir os limites em que as geometrias ocorrem, assim como quais as estruturas mais prováveis a serem geradas. Essas estruturas de soleiras magmáticas são caracterizadas por dobras forçadas (estruturas externas), degraus, pontes, e dedos (estruturas internas). Em particular, neste trabalho, concluí-se que provavelmente existem outros fatores importantes para o controlo da formação das dobras forçadas, uma vez que nem todas as vezes que o rácio indicador, a partir do qual a rocha hospedeira é dobrada, está dentro do intervalo de interesse se forma uma dobra forçada. Em relação à caracterização das redes de fraturas e feições relacionadas a carste, na Bacia de Santos, foi construído um modelo de dupla-porosidade, dupla-permeabilidade e utilizou-se uma abordagem de multi-atributos sísmicos para detectar e caracterizar as anomalias de alta amplitude que possivelmente estariam associadas a feições cársticas. Na fase da modelagem, foram distribuídos atributos geométricos de fratura na malha geológica para quantificar a porosidade e permeabilidade equivalente de fratura, e para melhorar a previsão do comportamento estático do reservatório em regiões fraturadas. A fase da modelagem ajudou na estimativa do campo de tensões tectónico local, que também foi importante para a previsão e localização de regiões potencialmente fraturadas.



**Palavras-chave:** Soleiras magmáticas, estruturas ígneas, redes de fraturas, carste, bacias de Campos e Santos

## ABSTRACT

The geological characterization of petroleum reservoirs has been very challenging. The fast-paced evolution of processes and methods for reservoir characterization have been giving rise to different solutions and proposals for the most varied issues in geological modeling. These issues and challenges include the interpretation of post-depositional structures and their representation in three-dimensional geological models. Examples of these structures are igneous intrusions and related internal and external structures, sub-seismic fractures, and karst-related features. In the post-salt of the Campos Basin and in the pre-salt of the Santos Basin we applied techniques to identify and characterize the post-depositional structures. The main objective of this work is to contribute to the scientific knowledge in the reservoir characterization and to understand the impact that such structures may have in the petroleum systems, particularly in the carbonate reservoirs. The dataset used in this work include two three-dimensional seismic surveys and two sets of borehole data, both from Campos and Santos Basins. The characterization of the intrusive igneous rocks in the Campos Basin was based on the morphometric analysis that allowed the understanding of the relation between the sills and the structures occurring within and around them. Based on the quantitative analysis of sills we were able to infer at which ranges the sill geometries occur in terms of area and length for example. In addition to which external structures are more likely to be generated according to the different sill geometries. Examples of these structures are, forced folds (external structures), steps, bridges, and fingers (internal structures). In particular, in this work, we found that probably there are other factors that control the formation of forced folds, since not always that the indicator ratio, from which country rock is folded, are within the interval of interest it forms a forced fold. Regarding the characterization of the fracture networks and karst-related features, in the Santos Basin, we built dual-porosity, dual-permeability model and used a seismic multi-attribute approach to detect and characterize the high-amplitude anomalies possibly associated with karst-related features. In the modeling stage, we distributed the key fracture geometrical attributes in the geological grid, to quantify the fracture equivalent porosity and permeability, and to enhance the prediction of the reservoir static behavior in fractured regions. The modeling stage helped to predict the local tectonic stress field, which is key to predict and locate potential fractured regions.



**Keywords:** Magmatic sills, igneous-related structures, fracture networks, karst, Campos and Santos basins

# CONTENTS

# 1. INTRODUCTION

Across several sedimentary basins worldwide with magmatic activity and associated hydrocarbons occur both intrusions and extrusions of magmatic material within the sedimentary successions. Such magmatic activity, most of the times occur in the form of sills (roughly tabular bodies) and dykes (approximately sub-vertical bodies) if associated with intrusions. In particular, these sills may form a variety of enigmatic geometries that are usually conditioned to the sedimentary packages they are intruding in. When associated with extrusions, these basins may record structures like volcanoes, vents, pipes, and conduits that are most of the times geometrically associated with intrusions.

Carbonate reservoirs, often naturally fractured, are characterized by different scale fractures arranged in a complex framework (Price and Cosgrove, 1990). Such fractures play a major role in the characterization of the geological media due to its influence on the fluids in general, from storage to transfer (e.g. Narr, 1996; Singhal and Gupta, 2000).

All the previous efforts made to characterize complex fracture networks have been leading current research on challenging issues regarding fractures in geological formations. These efforts include research on mapping critical areas for the development of karst features (e.g. Yu et al., 2016), the communicability indices (Santiago et al., 2016), and on the understanding of the connectivity of such fracture networks (Sanderson and Nixon, 2015).

According to Singhal and Gupta (2010), fractures often occur as complex networks, associated to major fault damage zones, arranged in systems (known as systematic fractures), or without following the predefined background structure (known as non-systematic fractures). Geologic faults always occur in systems within the major background structure (Price and Cosgrove, 1990; Nelson, 2001). However, it is worth noting that closely spaced fractures not always represent clusters of interconnected fractures (Manzochhi, 2002). The fracture pattern and orientation are important due to the likelihood to affect permeability anisotropy (Bisdom et al., 2017).

According to Ghosh and Mitra (2009), the controlling factors of the fractures on carbonate reservoirs are mainly of structural origin including, type, orientation, and intensity, which help to understand the complexity and heterogeneity of fractured reservoirs. In addition, Gong and Rossen (2017) emphasize the contributing role of the connectivity between fractures for flow control.

The pre-salt cluster reservoirs in Santos Basin are composed of proximal microbial and stromatolite carbonates locally dolomitized, and distal shales from Barra Velha Formation, with different geometrical features depending on the basin setting. Deposits from a transitional environment, between continental and shallow marine, characterize this formation (Moreira et al., 2007). Most of the times, these carbonates occur fractured. The fractures present in the Barra Velha Fm. have been a great deal in the productivity of the exceptionally heterogeneous carbonates. The heterogeneity of these carbonates is mainly due to the later structuration of the reservoirs and to the facies variations. The role of fractures in the fluids communicability in these reservoirs is still unclear, and this study helps to narrow the understanding of some of the probable contributing factors.

## 1.1. Motivation

The main motivation of this integrated study is to develop series of interpretations of post-depositional structures, such as igneous intrusions, fractures, and karst, so it is possible to constrain their incorporation into the geological modeling of carbonate reservoirs. Furthermore, these structures may have an important role in the pre-salt massive oil discoveries in both the Brazilian and African counterparts. The influence of the aforementioned structures might be related to hydrothermal activity characterized by heated fluids ascending and circulating through the faults and fractures, and lastly contributing to the hypogenic karst processes.

There are main challenges and questions still unanswered in the literature. (1) Are the characterization of the fracture networks, by the current methods, representative of the whole scenarios of study areas? (2) Are the fracture properties consistent with implicit conceptual structural models? (3) Are there any pieces of evidence supporting the impact of fractures on the karst distribution (Yu et al., 2016)?

## 1.2. Scope and Objectives

The purpose of the documentation of magmatic activity through the seismic characterization of seismic high-amplitude anomalies as igneous intrusions is to provide insights and geometrical constraints on the impact of such structures in the petroleum systems. To understand the geometries of these structures, a quantitative analysis of

morphometry plays a key role. In the light of that, this may be also applicable largely in the study area and its surroundings or to comparable geologic settings.

The purpose of the structural analysis is to characterize the fracture patterns in the study area and to understand the relationship between these patterns and the karst features in carbonates. To do so, a fundamental part of the work is the establishment of the connectivity degree of the fractures that may have great implications in the fluids communication.

## 1.3. Structure of the thesis

This doctoral thesis is organized in three themes intended to be peer-reviewed articles, which are described in the following sections. Two of the themes (Article 1 and Article 2) are related to the magmatic intrusions and their related structures within oil-bearing sedimentary basins. A dataset composed of borehole and seismic data, from the southern Campos Basin is used as a case study for the characterization of the igneous intrusions and the related structures. Furthermore, an emphasis was given to the impact of such structures on the petroleum systems. The other theme (Article 3) is related to the characterization of fracture networks and karst features. In particular, we characterized faults, fractures, and karst structures. Then, we modeled the fractures using discrete fracture networks approach to assess the impact of such networks on the petrophysical characteristics of the reservoir. A dataset composed of borehole image log, conventional wireline log, and seismic data, from the pre-salt Santos Basin is used as a case study for the characterization of the fracture networks.

### 1.3.1. Article 1: Geometric Characterization of Igneous Intrusions: 3-D Seismic Insights from the Campos Basin, SE Brazil

*Ulisses M.C. Correia, Bruno C.Z. Honório, Michelle C. Kuroda, Leandro H. Melani, Alexandre C. Vidal*

*Published in a peer-reviewed journal, Marine and Petroleum Geology*

In this manuscript, through a systematic approach, using seismic attributes and an artificial neural network, we were able to interpret the geometries of igneous sills in southern Campos Basin, southeastern Brazilian margin. By systematically measuring morphometric parameters of sills, thus reducing interpretation bias, we were able to identify five different types of sill geometries. We established a comparison with similar sills recognized from other sedimentary basins. We also demonstrate that a multi-attribute analysis can also be used to

improve the seismic expression of sills, in particular, Root Mean Square amplitude, variance, dip and azimuth, and spectral decomposition).

The objective was to provide with insights for assessment of the impact of magmatic emplacement on hydrocarbon systems in the study area and in similar geologic contexts. Therefore, this manuscript might offer a contribution for both researchers, helping them handle geometric characterization of sills in larger datasets, and for explorationists, helping them mitigating risks associated with geological interpretation with the presence of such distinctive seismic features, the so-called high-amplitude anomalies.

### 1.3.2. Article 2: The importance igneous-related structures for petroleum reservoirs: examples from the Campos Basin, SE Brazil

*Ulisses M.C. Correia, Bruno C.Z. Honório, Leandro H. Melani, Michelle C. Kuroda, Alexandre C. Vidal*

*To be submitted to a peer-reviewed journal*

In this manuscript, we applied a volume rendering technique to unravel the architecture of the igneous intrusions bodies that are somehow associated with the magmatic structures, such as vents, bridges and forced folds. These structures may be used to constrain the impact of the magmatic activity in the study area on the petroleum systems. We used a three-dimensional seismic survey from the southern Campos Basin and a few borehole data to constrain the seismic.

We were able to extract the exact architecture of the igneous bodies through the application of the volume rendering technique. In addition, we also were able to identify some structures related to the mapped intrusions.

The objective was to understand how such structures related to intrusions might influence the petroleum systems.

### 1.3.3. Article 3: The impact of faults, fractures, and karst in carbonate rocks: examples from a pre-salt reservoir

*Ulisses M.C. Correia, Leandro H. Melani, Felipe M. Oliveira, Luana G. Lima, Michelle C. Kuroda, Alexandre C. Vidal*

*To be submitted to a peer-reviewed journal*

In this manuscript, we mapped and characterized the regional faults of the study area in order to build a structural framework. Therefore, we would use this built structural

framework to base all the modeling and interpretation stage. We also computed several seismic texture attributes to detect high-amplitude anomalies that in this work, we associated with possible karst-related features. We use the fracture data from the borehole data to estimate an in situ tectonic stress field that would be correlated to the far field tectonic stress field estimated from the interpreted seismic horizons encompassing the reservoir, the Barra Velha Formation of the pre-salt Santos Basin.

We compared the tectonic stress field estimated via borehole image fracture data (in situ field stress) and via the interpreted seismic horizons (local far-field stress). From this comparison of both stress fields, we obtained a reasonable correlation between the main directions of the fracture sets. This help to test the implicit structural conceptual model.

We conducted fracture modeling using the discrete fracture networks modeling approach to incorporate the petrophysical properties of the fractures within the geological model grid. This enabled the generation of the permeability tensor anisotropy, which is the variation of permeability per grid cell in the three directions.

The objective of this work was to run an assessment of the possible impacts of the faults, fractures, and karst structures on carbonate reservoirs, and to conduct this work we used an example from the pre-salt Santos Basin, the Barra Velha Formation.

# 2. GEOMETRIC CHARACTERIZATION OF IGNEOUS INTRUSIONS: 3-D SEISMIC INSIGHTS FROM THE CAMPOS BASIN, SE BRAZIL

Ulisses M.C. Correia, Bruno C.Z. Honório, Michelle C. Kuroda, Leandro H. Melani, Alexandre C. Vidal

Published in a peer-reviewed journal, *Marine and Petroleum Geology*

# GEOMETRIC CHARACTERIZATION OF IGNEOUS INTRUSIONS: 3-D SEISMIC INSIGHTS FROM THE CAMPOS BASIN, SE BRAZIL

## ABSTRACT

Igneous intrusions are important for the exploration and appraisal phases of an oilfield due to their impact on petroleum systems. Their presence can be associated with the generation, migration, accumulation, and entrapment of hydrocarbons. In particular, (1) sills with low permeability might form barriers to fluid flow and migration; (2) sills may re-use fracture networks, providing insights on fluid migration and interaction(s); (3) sills may influence source rock maturation, (4) sill-induced uplifting of overburden and faulting may generate traps, and (5) their geometric complexities enables the understanding of the interconnectedness of sill complexes, which is the focus of this study. Therefore, we provide a systematic characterization of sill geometries and their morphometric parameters. We used three-dimensional seismic data, calibrated with well logs, to interpret sills in the southern Campos Basin, Brazil. Throughout the Late Cretaceous until the Paleogene, sills intruded into the Cretaceous to the Eocene post-salt sedimentary sequence, including shallow-platform carbonates, transgressive marls, and shales. A morphometric analysis assisted by seismic attributes allowed the geometric characterization of sills, namely: (1) saucer-shaped; (2) slightly saucer-shaped; (3) climbing saucer-shaped; (4) transgressive; and (5) rough layer-parallel. The documented sills comprise a wide range of sizes (0.43-14.35 km2) that increase with depth (up to 3.18 km), extend vertically from 0.06 to 0.23 km, and vary from low (1.82-3.31°) to high dip (6.05-15.74°). The sill complex area extends over 67.35 km2. This study suggests that a thorough characterization of sill intrusions may have a substantial influence on the prediction of other igneous occurrences. The mapped sills might have implications not just on the acoustically similar shallow platform Albian carbonates of the Macaé Group but may also provide insightful geometric constraints on the Brazilian pre-salt igneous intrusions.

**Keywords:** Igneous intrusions; Geometric characterization; Morphometric analysis; Post-salt; Campos Basin

## 2.1. INTRODUCTION

The geometric style of igneous sills is a primary concern for understanding magma flow patterns and their effect on hydrocarbons, i.e., generation, migration, accumulation, and entrapment in sedimentary basins (e.g. Smallwood and Maresh, 2002; Schutter, 2003; Thomson, 2007; Senger et al., 2017; Spacapan et al., 2018). Seismic-, borehole-, and outcrop-based studies on igneous intrusions have made possible the detailed mapping of entire bodies to assess different sub-seismic scale features (Francis, 1982; Planke et al., 2005; Galerne et al., 2011; Jackson et al., 2013; Alves et al., 2015; Walker, 2016). Therefore, extensive literature on the distribution and geometry of igneous sills through morphometric analyses have been published (Planke et al., 2005; Cartwright and Hansen, 2006; Hansen and Cartwright, 2006; Polteau et al., 2008; Hansen et al., 2008; Jackson et al., 2013; Sun et al., 2014; Magee et al., 2014; Walker, 2016). However, studies are still required to understand and evaluate the effects of sills on hydrocarbon systems (Omosanya et al., 2017; Mark et al., 2018).

The geometry of sills, often controlled by pre-existing faults (Magee et al., 2013), may compartmentalize petroleum reservoirs to strongly affect their structural framework (Rateau et al., 2013). Faults that may provide pathways for magmatic emplacement may also facilitate hydrocarbons migration (Thomaz Filho et al., 2008; Schofield et al., 2017). In the long run, sill emplacement may uplift the overburden and influence the formation of structures for the accumulation of oil and gas (Jackson et al., 2013; Magee et al., 2013). Sills may also have a positive effect on the generation and early maturation of hydrocarbons by heat release (Svensen et al., 2004; Sydnes et al., 2018).

In order to better assess some of the effects sills may have on petroleum systems, they have been characterized by size, geometric style, area, and dimension (e.g. Thomson and Hutton, 2004; Planke et al., 2005; Hansen and Cartwright, 2006; Galerne et al., 2008; Magee et al. 2014; Omosanya et al., 2017; Mark et al., 2018). Additionally, well logs are used to constrain the physical properties of intrusions (e.g. Planke et al., 2000; Smallwood and Maresh, 2002; Delpino and Bermúdez, 2009; Mark et al., 2018; Spacapan et al., 2018).

Sills range from less than one meter to several hundred meters in lateral extension (e.g. Hansen et al., 2011, Sun et al., 2014) and most of them terminate abruptly within the host-rock strata (Planke et al., 2005). The plan-view morphologies of saucer-shaped sills are characterized by closed sub-circular to sub-elliptical features, comprising (1) sub-horizontal to

flat inner centers, forming the base, (2) peripheral inclined segments that cross-cut the stratigraphy upwards, and (3) sub-horizontal outer rims ending at the sill tip (Polteau et al., 2008). The outer rim forms a plateau at a higher stratigraphic level than the inner center. Transgressive sills are mostly characterized by an inclined segment, sometimes separated by a slight step feature. Sills can also be thick, long and layer-parallel, i.e. generally strata-concordant, occasionally forming transgressive segments (Planke et al., 2005; Polteau et al., 2008).

To characterize igneous sills in seismic-based studies, interpreters usually seek out homogeneity, which is a typical texture for igneous crystalline rocks that contrasts with the host rock, to produce strong amplitude contrasts. In addition, these amplitude contrasts are characterized by a downward increase in acoustic impedance also known as hard-on-soft reflections (Smallwood and Maresh, 2002; Alves et al., 2015; Omosanya et al., 2016). However, seismic features that are similar to intrusions have been misinterpreted as channels, salt-related structures, or hydrocarbon-related bright spots (Fiduk et al., 2004). In particular, Alves et al. (2015) and Omosanya et al. (2016) described bright spots as soft-on-hard reflections. Furthermore, hydrocarbon-related high amplitude anomalies are often associated with the underlying low amplitude and low-frequency shadow zones (Taner et al., 1979; Castagna et al., 2003; Ebrom, 2004). Other techniques, such as spectral decomposition and red-green-blue (RGB) color blending, have also been used for quantitative interpretation of igneous-related structures (McArdle et al., 2014).

Previous studies on magmatic events in the Campos Basin emphasized the effects of both intrusive and extrusive bodies on hydrocarbons exploration (e.g. Thomaz Filho et al., 2008). Cortez and Santos (2016) provided insights on the interconnection of intrusions emplaced in the Upper Cretaceous post-salt succession and their effects on the Lower Cretaceous pre-salt sequences. Likewise, Penna et al. (2018) emphasize the concerns about the presence of several intrusive and extrusive igneous bodies in production areas from the Santos Basin on the production and reservoir management. However, the role of emplacement of sills and their respective geometries on both carbonates from the Albian shallow platform of the Macaé Group and the pre-salt of the Barra Velha and Itapema Formations is still unclear.

As a result, we used three-dimensional seismic data calibrated with borehole data in this study for morphometric analysis of magmatic sills in the southern Campos Basin. The calibration of the seismic with borehole data enables us to ground-truth the magmatic

occurrences and more robust characterization of the igneous rocks. The aim of this work is to perform a quantitative characterization of the geometries of magmatic sills and, therefore, provide morphometric constraints to help understand the magmatic emplacement in the study area. This study may also provide insightful geometric constraints for both pre-salt and post-salt reservoirs.

## 2.2. GEOLOGICAL SETTING OF THE CAMPOS BASIN

The Campos Basin is a South Atlantic basin, lying between the Vitoria-Trindade Arch to the north and the Cabo Frio High to the south, and limited by the compressional salt front and the oceanic crust to the east (Ojeda, 1982) (Fig. 1). The initial structures of the basin are associated with the lateral movement produced by NW-SE striking faults (Chang et al., 1992). During the Mesozoic drifting phase, NE-trending normal faults and inherited-basement structures were reactivated as horsts and grabens (Fetter, 2009).

The basin stratigraphy consists of five main sequences: (1) continental rift, from the Early Neocomian to Early Aptian, (2) transitional evaporitic, from Middle Aptian to Late Aptian, (3) restricted shallow marine carbonate platform, from the Lower to the Middle Albian, (4) open marine transgressive, from the Late Albian to Eocene, and (5) marine regressive, from the Eocene until present (Mohriak et al., 2008).

Several magmatic events took place on the Brazilian sedimentary basins. In particular, (1) tholeiitic dykes and flood basalts around the Triassic (*c*. 215 Ma) and Jurassic (*c*. 180 Ma) periods; (2) tholeiitic to intermediate dykes and flood basalts around the Lower Cretaceous (*c*. 130 Ma); (3) low to intermediate silica content intrusions around Upper Cretaceous (*c*. 80-90 Ma); (4) intermediate to alkaline volcanic cones around the Eocene (*c*. 40-60 Ma) and from then to recent times (below 50 Ma) (Thomaz Filho et al., 2008).

Igneous intrusions were emplaced in the post-Aptian sedimentary succession through several pulses, from the late Upper Cretaceous to Early Eocene (Oreiro et al., 2008), as indicated by the intercalation of basaltic and andesitic sills and dykes (Ojeda, 1982). The magmatic activity in the southern Brazilian margin, over the major volcanic complex Cabo Frio High, was characterized by intrusions and extrusions (Thomaz Filho et al., 2005). Northeast-trending intrusions are intercalated with volcaniclastic and lower-impedance sedimentary sequences (Meisling et al., 2001; Oreiro et al., 2008). While sills and dykes

characterize the intrusions, lava flows and volcanic mounds characterize the extrusive bodies from the Albian to the Eocene (Oreiro et al., 2008).

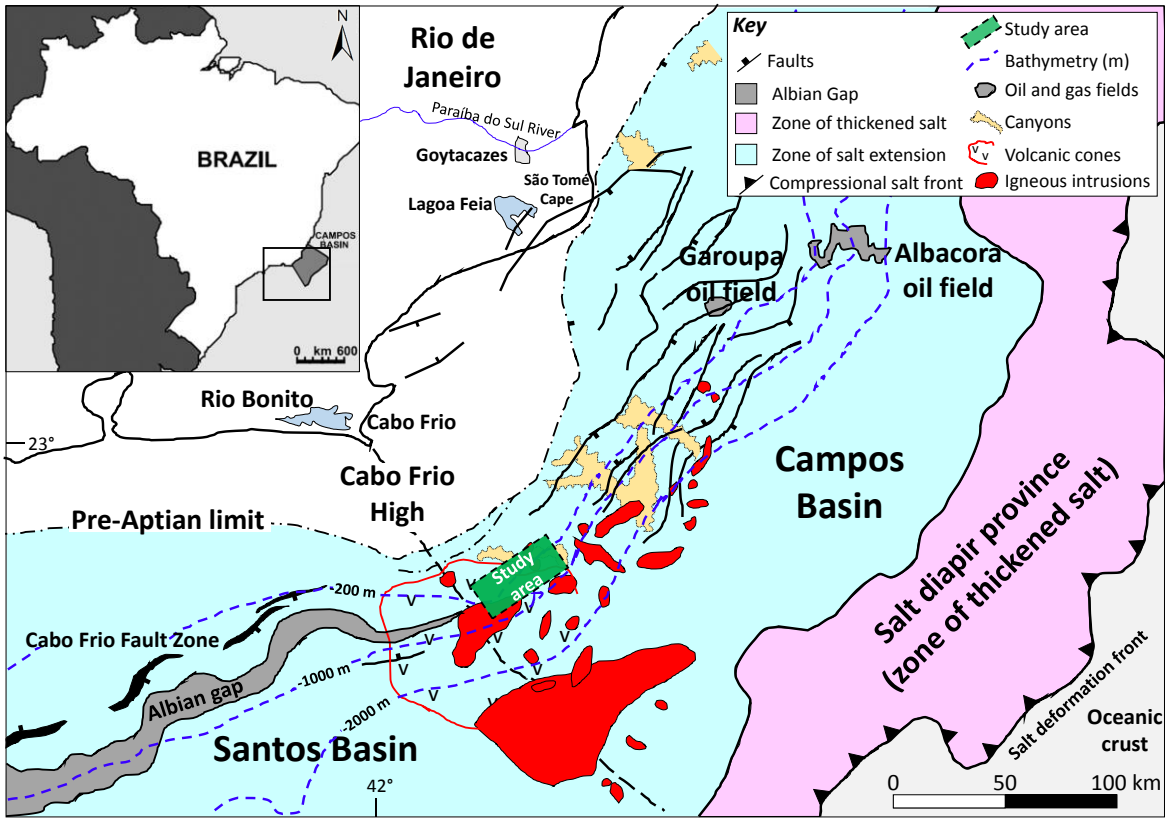


**Fig. 1.** Location map of the Campos Basin along the Brazilian southeastern margin (modified from Mohriak et al., 2008).

## 2.3. DATABASE

The 3-D seismic data covers approximately 183 km$^2$ in area and is located in the southern part of the Campos Basin (Fig. 2). The bin spacing of the seismic data is 18.75 m in the inline direction and 12.50 m in the crossline direction. Therefore, the horizontal seismic resolution is given by the bin spacing. The seismic volume record 1,250 samples at a vertical interval of 4 ms. The estimated dominant frequency is approximately 35 Hz. The estimated vertical resolution is 23.21 m, for a velocity of 3250 m/s. We used the American convention for seismic display (Brown, 2009); hence, a downward increase in acoustic impedance generates a positive reflection, resulting in a red-to-yellow peak. Wireline data from seven (7) exploration wells include: (1) gamma-ray (GR), (2) density (DEN), (3) neutron (NEU), and (4) sonic logs (DTC). This is in addition to geological descriptions of drill cuttings and cores, available from the ANP-BDEP well reports.

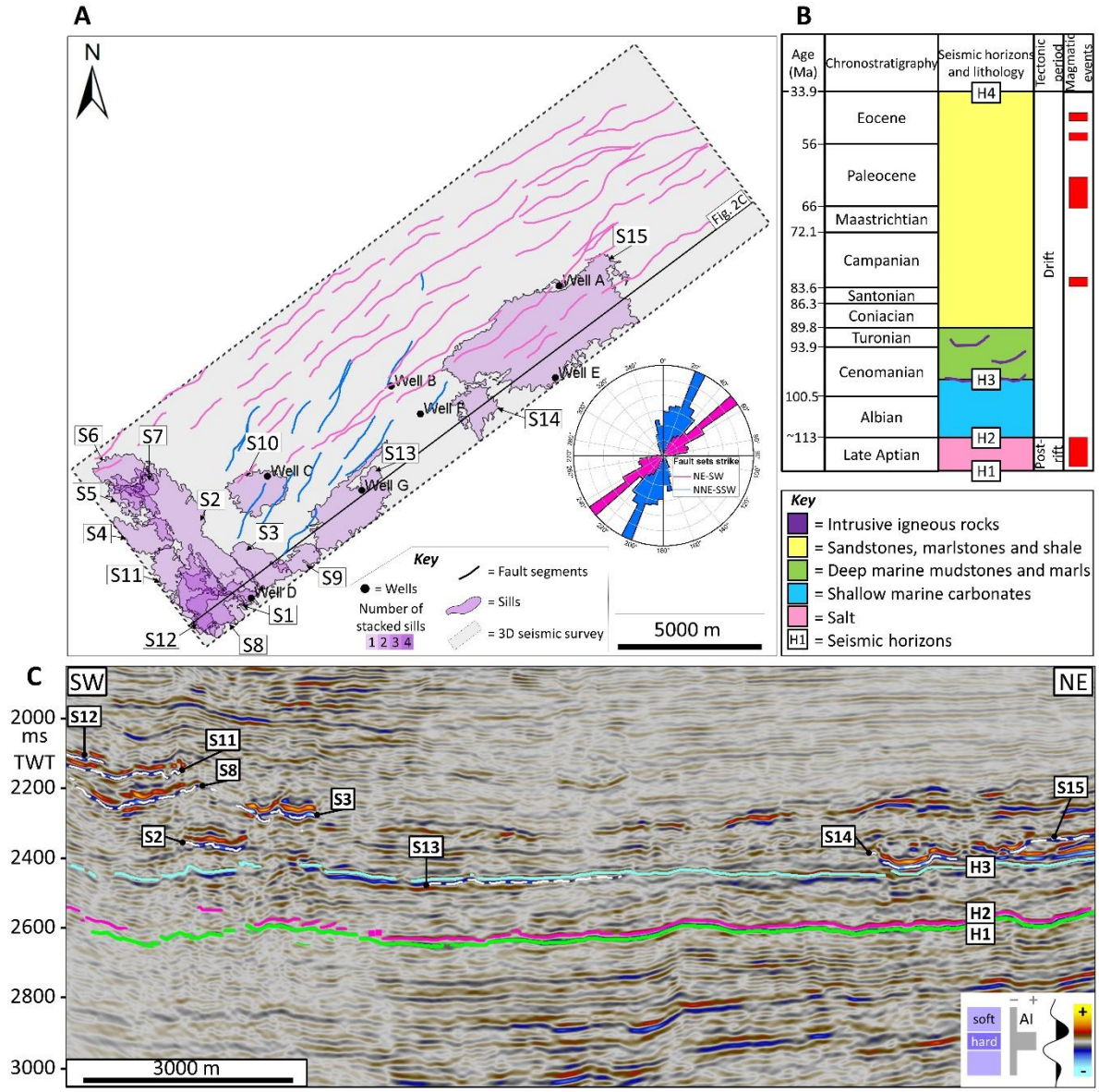


**Fig. 2.** (A) Outline of the 3-D seismic data used in this study (dashed rectangle), depicting (i) interpreted sills (polygons S1-S15); (ii) number of vertically stacked sills (1-4); (iii) interpreted fault segments; and (iv) location of the seven wells. (B) A simplified chronostratigraphic framework of the studied interval with interpreted horizons (H1-H4), main lithologies, and main tectonic and magmatic events (modified from Mohriak et al., 2008). (C) Interpreted seismic strike cross-section (NE-SW), highlighting sill geometries.

## 2.4. METHODS AND APPLICATIONS

We used wireline log data to constrain the physical properties of igneous rocks. According to Delpino and Bermúdez (2009), mafic rocks (decreased $SiO_2$ content) often present low GR values (21-34 gAPI) due to their low content in radioactive minerals. Conversely, intermediate to felsic rocks tend to present medium (52-63 gAPI) to high GR values (63-75 gAPI), respectively. Mafic igneous rocks generally record higher densities (approximately 2.80-3.00 g/cm$^3$) than intermediate (2.54-2.69 g/cm$^3$) to felsic (2.55-2.62 g/cm$^3$) rocks (Delpino and Bermúdez, 2009; Mark et al., 2018; Spacapan et al., 2018). As for velocity, mafic rocks commonly record high values, between 5500 and 6600 m/s, depending on the degree of alteration and the presence of vesicles (Planke et al., 2000; Planke et al., 2005; Mark et al., 2018). Thus, the higher the alteration degree and number of vesicles, the lower the velocity (Delpino and Bermúdez, 2009; Omosanya et al., 2016).

Four major seismic horizons (H1 to H4) were recognized, mapped, and used to perform time to depth conversions based on the velocity data from wells (Fig. 2). We used the following interval velocities: (1) 1500 m/s from mean sea level to the seabed, (2) 2100 m/s from the seabed to H4, (3) 2500 m/s from H4 to H3, and (4) 3250 m/s from H3 to H1.

Different sill types were classified by interpreting well-tied seismic horizons and high amplitude reflections, following the criteria described in Planke et al. (2005), which included the detection of: (1) high amplitude events, (2) local sheet transgressions, (3) saucer-shapes, and (4) blunt terminations. Planke et al. (2005) described the fundamental geometries of igneous sills to include (1) saucer-shaped, (2) planar transgressive, (3) layer-parallel, and (4) fault block. Jackson et al. (2013) identified some variations of the geometries described by Planke et al. (2005) for strata-concordant sills (similar to layer-parallel sills). For terminology clarity, we refer to igneous sill intrusions and positive high-amplitude seismic anomalies as sills (Fig. 3).

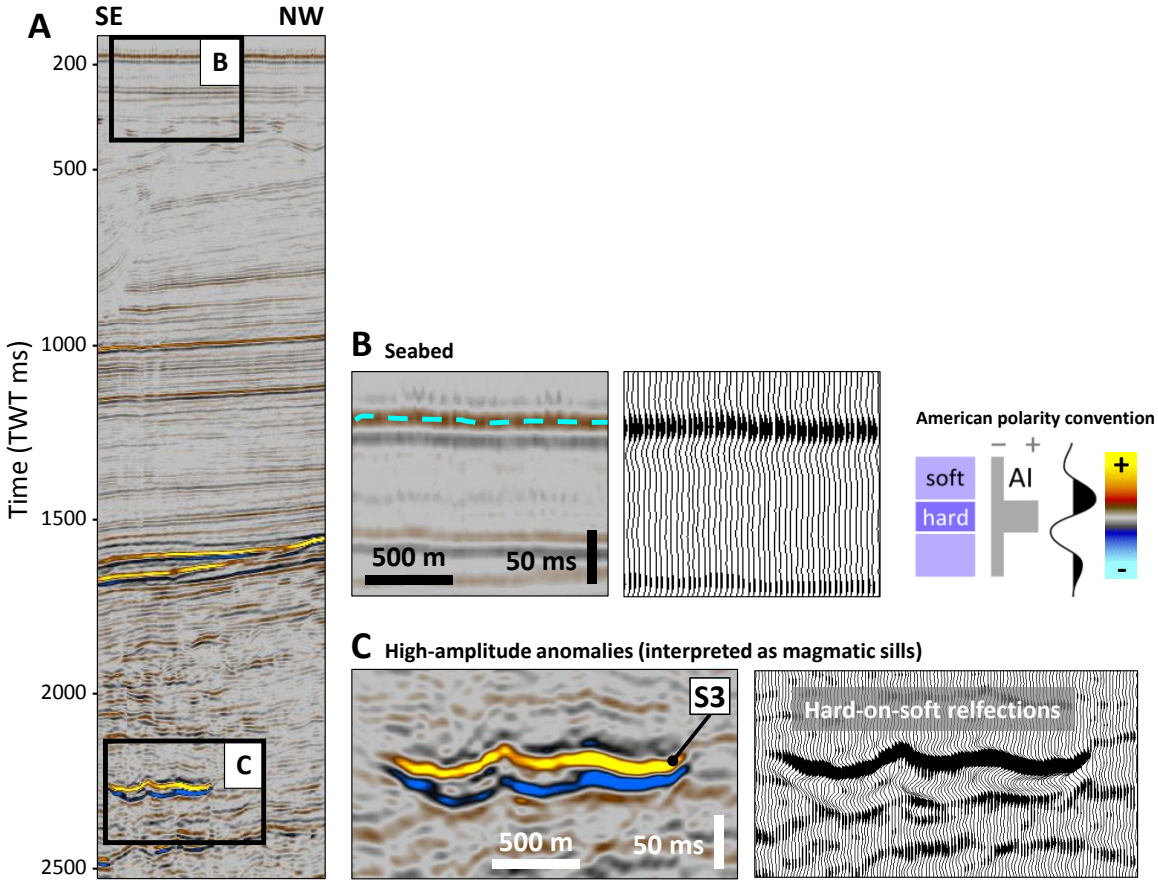


**Fig. 3.** Part of a seismic section showing the typical response of mapped high-amplitude anomalies, laterally discontinuous, that were interpreted as magmatic sills.

In this work, the classification of sills followed the prior studies of Planke et al. (2005), Polteau et al. (2008), Jackson et al. (2013), and Magee et al. (2014), which are mostly based on the analysis of the following morphometric parameters: (1) area, (2) thickness, (3) diameter or length, (4) depth of emplacement, (5) diameter-to-depth ratio, (6) diameter-to-thickness ratio, and (7) dip. We distinguished the different types of sills based on quantitative analysis of morphometric parameters, including: (1) area, (2) long and short axis length, (3) long axis azimuth, (4) sill height (vertical extension), (5) sill depth, (6) flat sections dip, (7) inclined segments dip, (8) mean dip azimuth, and (9) eccentricity (Fig. 4A). The dip angles of the sills were extracted from the seismic attribute dip magnitude. The minimum dips are associated with flat sections, and maximum dips with inclined segments. In addition, so as to minimize biases in horizon picking and interpretation, we defined cutoffs for the calculated dips as follows: 25th percentile for the flat sections, 90th for the inclined segments, and 95th as outliers. In order to obtain some of the properties of the method of Magee et al. (2014; 2015), we used a Matlab function "*regionprops*" to extract the best-fit ellipse eccentricity,

long and short axis length, and azimuth (Fig. 4B). The eccentricity is the ratio of the distance between foci of the ellipse and its major axis length.

We used a particular set of seismic attributes that are effective in illuminating and characterizing the expression of sills from relatively noise-free seismic data; Root-Mean Square amplitude, variance, dip and azimuth, spectral decomposition and RGB color blending, and vertical amplitude gradient (Chopra and Marfurt, 2007; Alves et al., 2015; Marfurt and Alves, 2015). The RMS amplitude seismic attribute highlights both negative and positive amplitude, find their squares and average, and then the square root. Sills have high amplitude contrast, due to their generally high acoustic impedance values, which is what makes the usage of these attributes suitable (See Omosanya and Alves, 2013a; 2013b). The variance attribute, which is best known for the ability to highlight discontinuities in the seismic reflection data, shows much more detail than the original amplitude, allowing the delineation of sills and near-vertical dikes by quantifying the differences between seismic traces (Brown, 2004; Chopra et al., 2011; Omosanya and Alves, 2013a; Infante-Paez and Marfurt, 2017). The dip and azimuth attributes that give the instantaneous dip magnitude and dip azimuth of the reflections, are suitable for the identification of the direction and magnitude in which sills are dipping (Marfurt et al., 1998; Marfurt, 2006). The spectral decomposition and the RGB color blending, used to highlight subtle stratigraphic features within the selected range of frequencies, allow the extraction of the frequency signatures that best characterize the sills (Henderson et al., 2007; Alves et al., 2015). We combined the three frequency volumes in the RGB blend to ensure the maximum expression of the sills is captured. To better highlight the seismic expression of magmatic sills, we also used the vertical amplitude gradient difference to extract the high amplitude anomaly features that characterize the sills (Maoshan et al., 2011). The use of these attributes could help define the boundaries and the seismic expression of the sills.

We interpreted faults based on seismic structural attributes using time slices and cross-sections to obtain the orientation and distribution of the faults. To do so, we co-rendered the following attributes: (1) background dip-steering cube for the extraction of global dip trends, while preserving the regional structure (Höcker and Fehmers, 2002); (2) maximum curvature, which indicates possible fault plane lineaments (Roberts, 2001); and (3) differential resolution similarity (DRS) to extract dissimilar features and to illuminate discontinuities in a given frequency range (Honório et al., 2017).

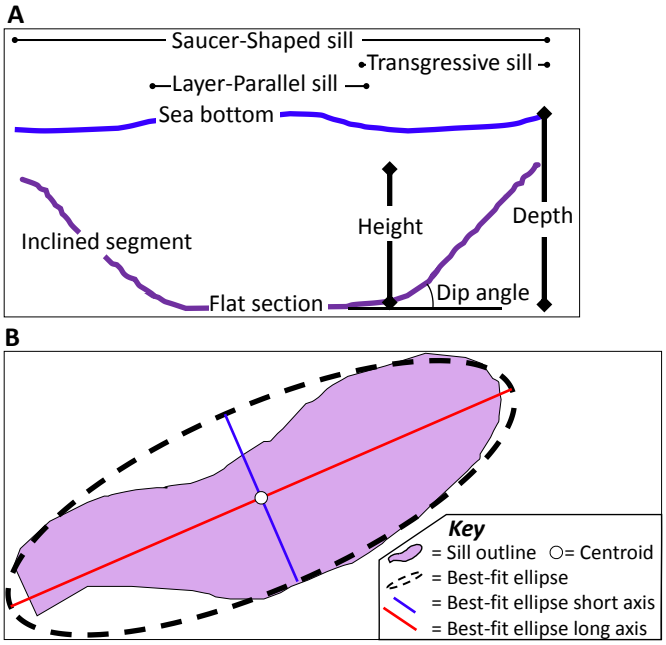


**Fig. 4.** Technique for the morphometric analysis of sill geometries in (A) cross-section and in (B) plan view (adapted from Magee et al., 2014).

## 2.5. RESULTS

### 2.5.1. Well-log pattern of igneous rocks

The symmetric and asymmetric box-shaped low-GR log values generally characterize the drilled igneous rocks in the seven wells used in this study. The characteristic response of the GR log corresponds to high-impedance layers given by the values in the DTC and DEN logs, which is typical of low-silica content igneous rocks (Fig. 5 and Fig. 6) (Delpino and Bermúdez, 2009; Mark et al., 2018; Watson et al., 2019). The constant blocky low-GR values may be an evidence for igneous rocks with little variations in composition and homogenously distributed minerals. However, in the uppermost section of the Well D (Fig. 6) there is a high-GR value, contrasting with the lower section low-GR values.

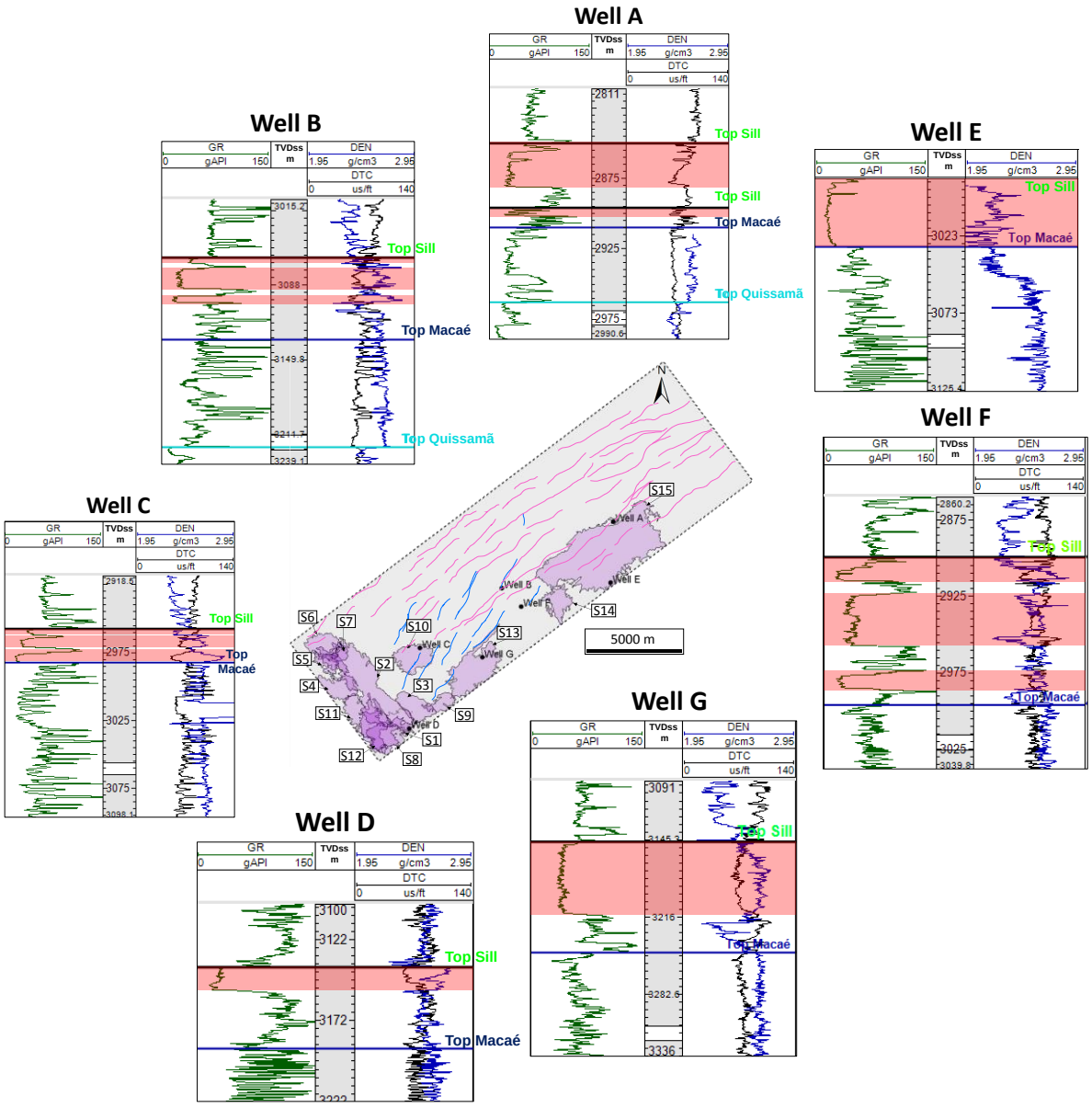


**Fig. 5.** The seven wells used in this study, depicting the typical response of mafic intrusions, characterized by low-silica content, for GR, DEN and DTC logs. The GR shows a constant interval for most of the wells. Some of the sills are not drilled, as is possible to see in this figure, and also not all the drilled igneous rocks were identified on seismic interpretation.

Well D demonstrates the correlation between well logs and igneous rocks (Fig. 6). In this well, four igneous intervals were identified; in addition, drill cuttings and core samples confirmed the presence of igneous rocks. GR, DEN, and DTC logs show distinct patterns from intervals 1 to 4, respectively, including (1) low box-shaped, (2) high symmetric, (3) irregular and abrupt, and (4) combined irregular and symmetric well-log signatures. In the synthetic seismic trace, a high amplitude characterizes the tops of igneous intervals. Well D drilled igneous rocks with intermediate to acidic chemical composition, yielding high GR values, whereas basic rocks record the opposite. A good correlation was found between the

density and sonic logs for igneous lithofacies in all wells, featuring layers of high acoustic impedance (Fig. 6). Additionally, decreases in gamma-ray follow increased density and decreased sonic transit time, featuring higher velocities (Fig. 6).

The differences in log responses within the igneous rocks at shallow levels suggest different rock types, possibly associated with distinct silica content (Delpino and Bermudez, 2009). Furthermore, drilled igneous rocks corroborate the distinction between felsic, intermediate, and mafic rock types. As the alteration processes involve potassium (*K*) losses, the rocks become more acidic. Thus, the GR log is able to record the systematic variation of *K*, which increases with the silica content, as the rock becomes more felsic (Delpino and Bermúdez, 2009). Based on these criteria, we may associate the results from this study with the different magmatic pulses that generated distinct silica-content intrusions, characterized by intermediate-to-acidic and basic sills in the Cabo Frio area, as described by Oreiro et al. (2008). Furthermore, impedance properties such as density and velocity allowed us to distinguish the presence of igneous rocks with different chemical properties, comparable to Cortez and Santos (2016), who described high-velocity (6500 m/s) and high-density (2.88 g/cc) sills in the Cabo Frio area. As the available well data does not drill all the interpreted sills, we cannot establish a pattern of silica content variations in the study area. However, most of the drilled igneous rocks are of basic composition and, therefore, dominantly depleted in silica.

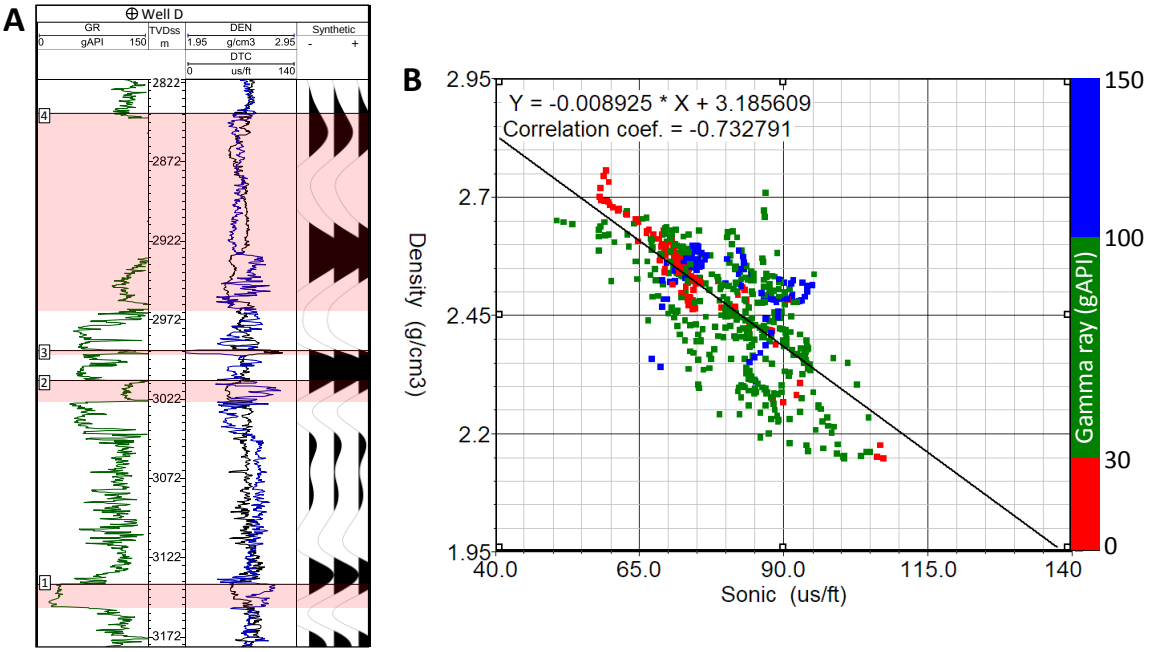


**Fig. 6.** (A) Well D highlights a typical response of the igneous rocks for GR, DEN, and DTC logs. Some of the top and bottom of the igneous rocks (1 to 4) are represented by a peak and a trough on the synthetic seismic expression. (B) cross-plot between the sonic velocity and the density logs. Note the good correlation between the two variables. The low-GR values represent the probable low-silica content igneous rocks contrasting with the shallower rocks of high-GR values.

### 2.5.2. Seismic expression of sills

The cross-plot between the apparent time thickness and the actual time thickness enables to calculate the tuning thickness of the seismic beds in the selected interval. The extraction of the deterministic wavelet and the selection of the area of interest to build the time-frequency panels are key to perform a seismic tuning thickness analysis (Fig. 7).

The tuning thicknesses calculated for various areas of interest over the study area allow us to confirm that in this dataset the magmatic sills are tuned reflections and we cannot properly distinguish the top from the base. It is possible to confirm that by giving different velocities, for a given frequency and a model for seismic resolution calculation (Widess, 1973; Zeng and Backus, 2005), we may obtain scenarios for the tuning thickness in meters by multiplying a velocity to the one-way time.

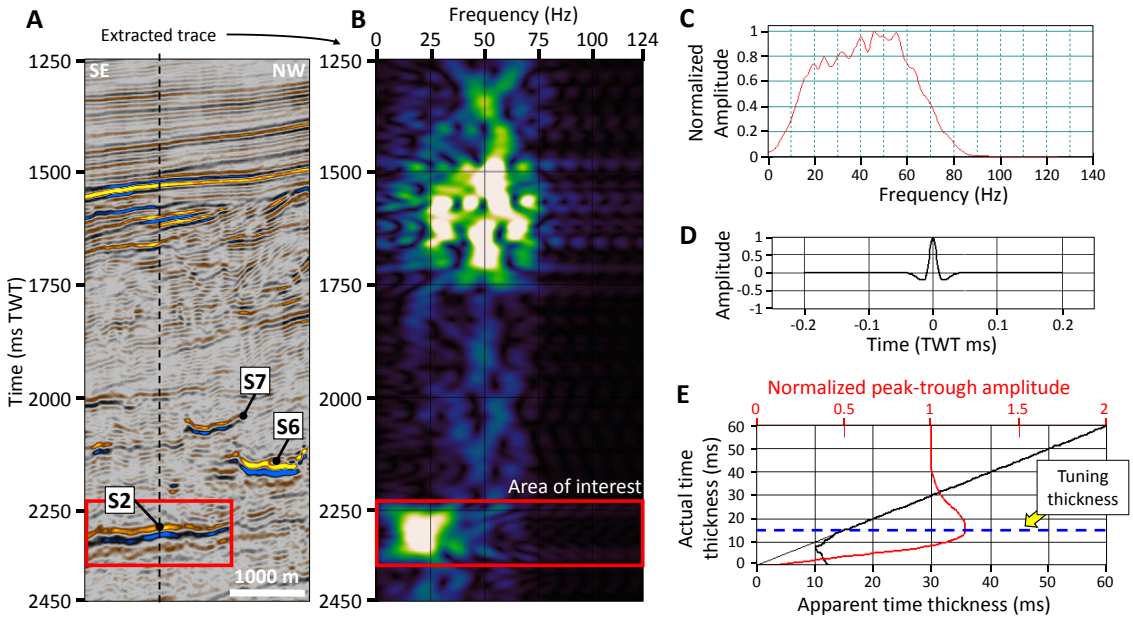


**Fig. 7.** (A) Part of a seismic cross section showing some of the interpreted sills and sill S2 on which was built the time-frequency panel, extracted a deterministic wavelet and computed the tuning thickness. (B) time-frequency 2D panel showing the frequency response over time. Particularly in the area of interest that encompasses sill S2 note that the frequencies have low values. (C) Amplitude spectrum for the seismic section presented in (A). (D) extracted deterministic wavelet from the seismic data. (E) Tuning thickness chart showing the tuning thickness in time (c. 15 ms TWT). The top reflection constructively interferes with the base reflection to form tuned reflectors with increased amplitude values, which according to Magee et al. (2015) and Mark et al. (2018), commonly presents a challenge to estimate the sill thickness.

The fifteen identified sills are characterized by positive high-amplitudes with high-impedance contrast to the host rock. This seismic expression of sills is depicted in the amplitude, vertical QR gradient, and RGB frequency blending attribute time-slices (Fig. 8). The variance attribute time slices show the outline of sills and also show how homogeneous is the expression of the inner sill parts.

For sill S6, however, the time slices of amplitude, vertical QR gradient, and RGB frequency blending highlight only the inner sill. This is due to the inclined sheets (c. 12.96º) at the border of the saucer-shaped sill, which offsets the outer sill and do not enhance it in the same time slice. On the other hand, depth-structure and RMS amplitude maps enhance the outer sill and are clearly distinctive from the inner sill (Fig. 8 and Fig. 9).

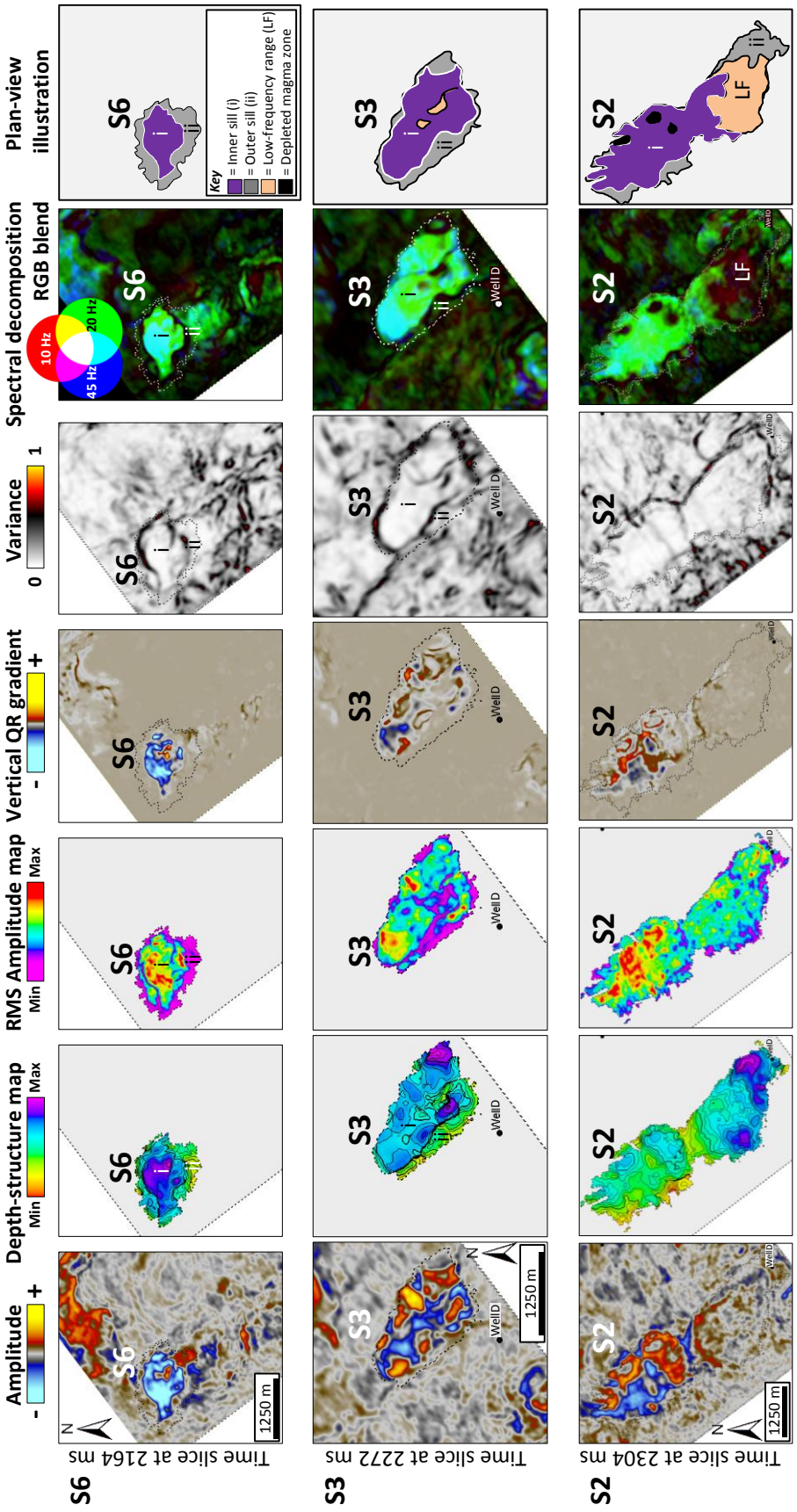


**Fig. 8.** Multi-attribute co-visualization of time slices and depth maps for S2, S3, and S6.

From the RGB color-blended panels, the prevalence of green color (frequency tuning at *c*. 20 Hz) is evident and highlights the bright and homogeneous texture for S2, S3, and S6. However, in some inner parts of sill S6, and some parts of sill S3 and S2, the green and blue are overlapping. This means that the dominant frequency for the sills lie approximately between 20 and 45 Hz. The red color dominance in the southern part for sill S2 suggests a frequency tuning of approximately 10 Hz. These evidences from the spectral decomposition and RGB frequency blending allowed the quantitative analysis of the amplitude data.

From the interpretation we also noted that structures that resemble sill steps tend to climb the stratigraphy, which to some extent are consistent with features observed in the Streymoy sill, Faroe Islands (e.g. Walker, 2016). The distinct separated transgressive reflectors suggest sills splitting into separate segments while accommodated by the host rock (Fig. 9).

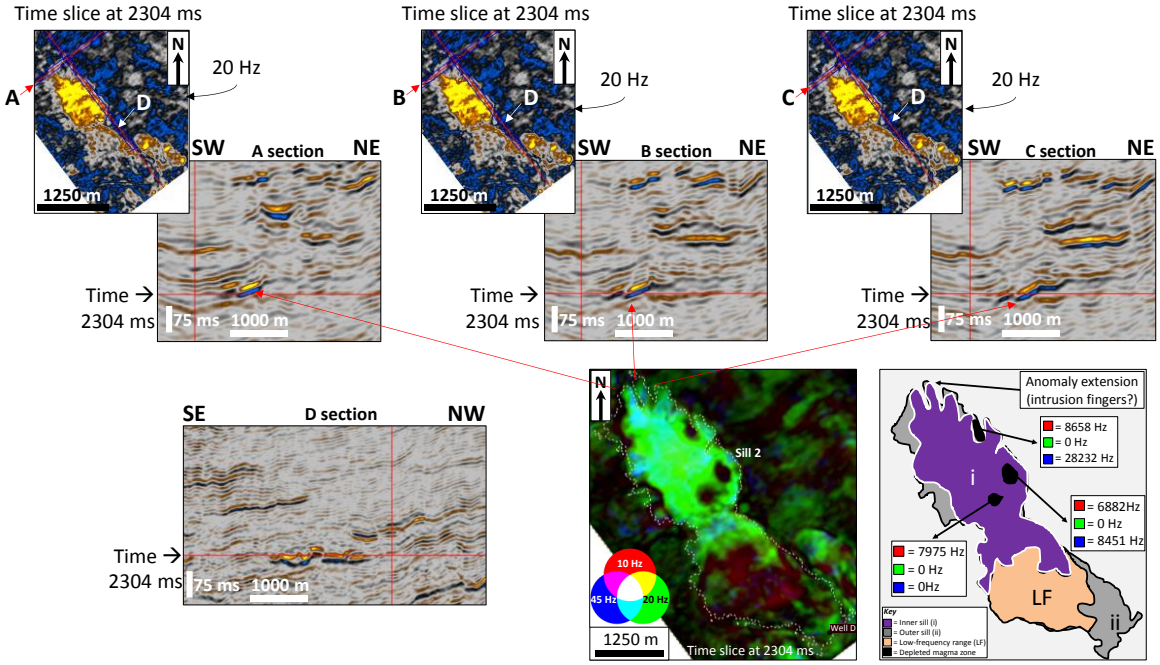


**Fig. 9.** Spectral decomposition at 2304 ms time slice displayed as a RGB blend (R = 10 Hz, G = 20 Hz, B = 45 Hz) that enables the characterization of the seismic expression of sill S2. Illustration of sill S2 highlighting features that look like the internal structures of this sill and the extraction of RGB values for each of the small sub-circular structures inferred as depleted magma zones (black polygons). The location of the cross sections highlighting the internal structures of sill S2 are shown on the time slices of the iso-frequency volume 20 Hz.

### 2.5.3. Geometry and distribution of sills

Most sills occur on the H3 and between the H4 and H3 seismic horizons, inferred as the top Albian post-salt carbonates within the Upper Cretaceous succession. We illustrate one sill from each of the five geometric types within a total of fifteen sills studied.

*Type I* – The saucer-shaped geometry is characterized by an approximately flat-lying and slightly convex upward inner sill (dipping between 2.58º and 3.05º) thinning towards its edge (Fig. 10). At this edge, an inclined segment that transgresses upwards at angles from 11.56º to 15.74º connects the inner sill to a gently dipping outer sill (Fig. 10A and Fig. 10B). The relatively small areas range from 1.12 to 1.67 km$^2$. The long and short axes range from 1.43 to 2.03 km and from 1.11 to 1.28 km, respectively, with an average ratio of approximately 1.46. These sills extend vertically to a maximum of 0.18 km and are emplaced between depths of 2.70 and 2.99 km (Table 1).

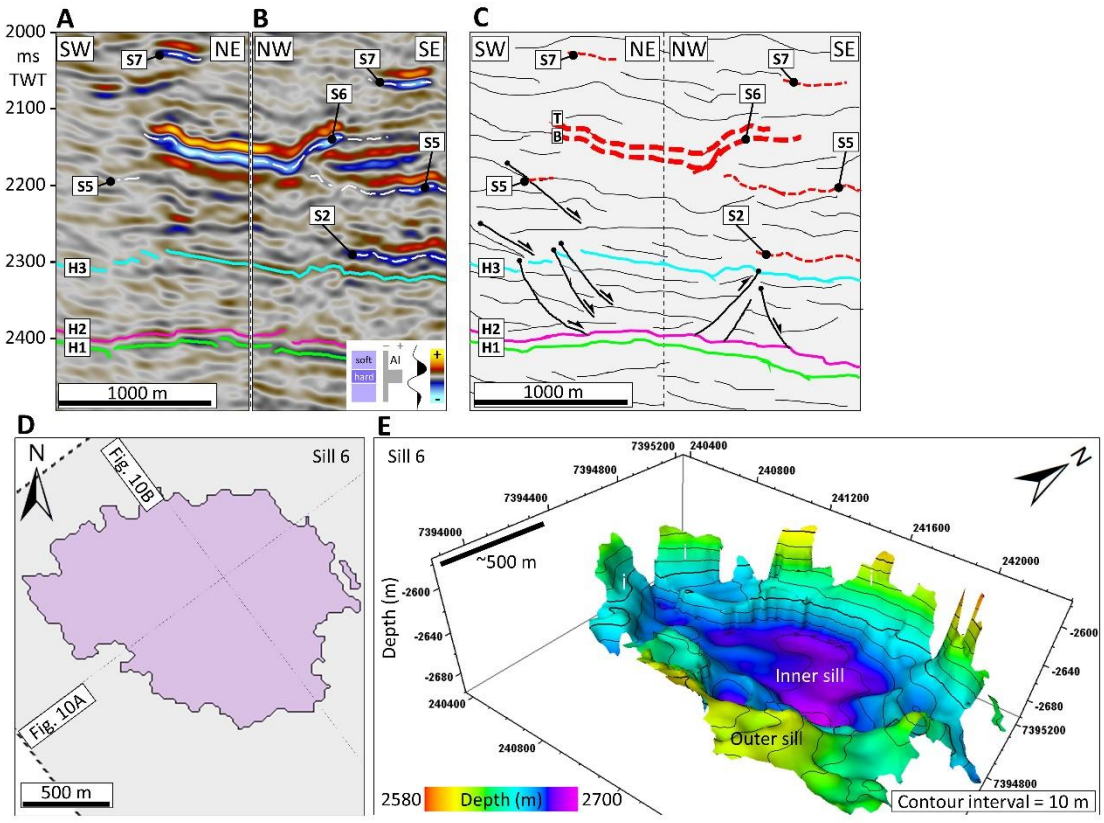


**Fig. 10.** Interpreted seismic sections along (A) strike (SW-NE) and (B) dip directions (NW-SE), highlighting the morphology of sill S6. (C) Geological model emphasizing sill geometry, faults, reflectors configuration, and the main interpreted horizons. (D) Plan-view morphology. (E) 3-D view of a saucer-shaped sill (Type I) depicting inclined segments (i), inner and outer sill.

*Type II* – The slightly saucer-shaped geometry, featured by only one sill (S3), is dominantly characterized by an inflated inner sill (dipping 2.61º) with a gently developed central ridge (Fig. 11). On the periphery, just like Type I, the inclined segments dip 11.23º. The area of S3 is 1.79 km$^2$ and is characterized by a 2.15-km long axis and a 1.16-km short axis with a ratio of 1.86 and an eccentricity of 0.84. Emplaced at a depth of 2.86 km, it extends vertically 0.12 km (Table 1). Similarly to S6, S3 thins laterally and towards the top.

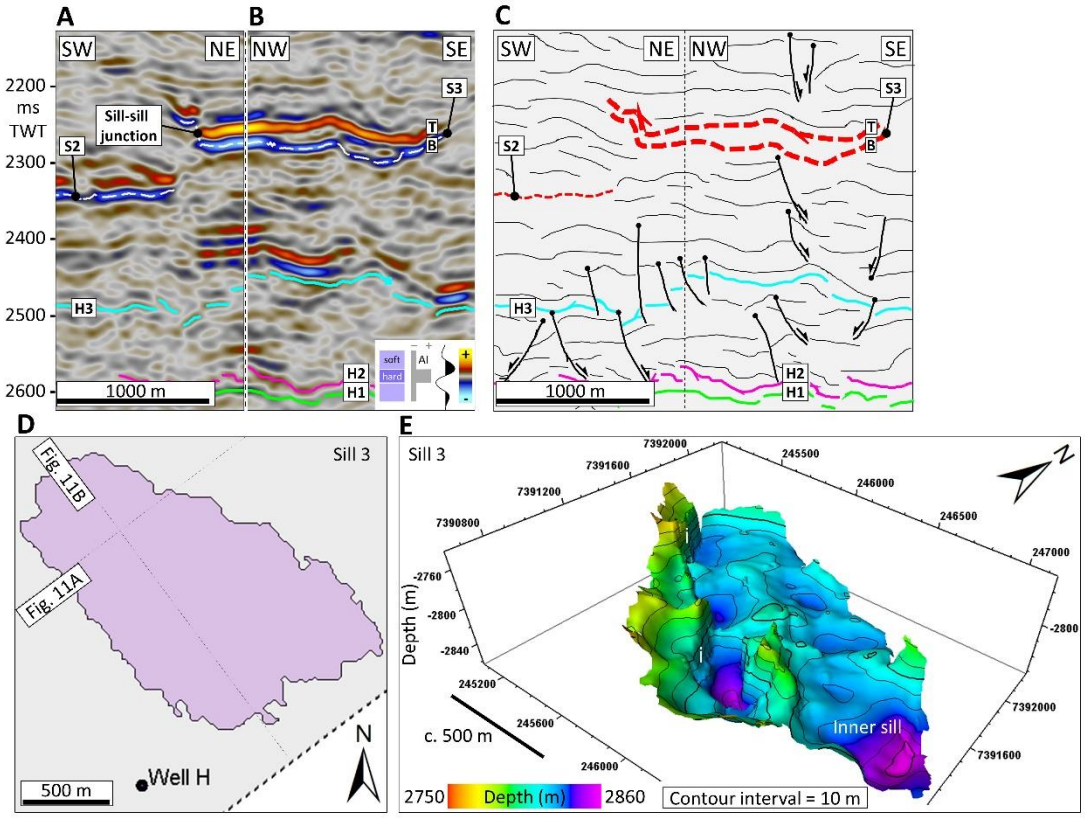


**Fig. 11.** Interpreted seismic sections along (A) strike (SW-NE) and (B) dip directions (NW-SE), highlighting the morphology of sill S3. (C) Geological model emphasizing sill geometry, faults, reflector configuration, and main interpreted horizons. (D) Plan-view morphology. (E) 3-D view of a slightly saucer-shaped sill (Type II), depicting inclined segments (i) and inner sill.

*Type III* – The climbing saucer-shaped geometry, featured by only one sill (S14), lies between transgressive and saucer-shaped geometries due to an asymmetry characterized by a large and shallower segment on one of its sides (Fig. 12A). Similarly to Type I (Fig. 10), and Type II (Fig. 11) sills, these Type III sills is also characterized by an inner and outer sill connected by an inclined segment. The flat section dips 2.76º and the inclined segments dip 12.11º. The length of the long and short axes is 1.69 km and 1.24 km, respectively, with an area of 1.27 km$^2$. A long-to-short axis ratio of 1.36 characterizes this sill, which is lower than the average for other saucer-shaped sills (Type I and Type II). S14 developed almost on the

horizon H3 (Fig. 12A-B). The plan-view morphology is sub-elliptical with an eccentricity of 0.68 (Fig. 12D). The vertical extent is 0.19 km, a little higher than the average for Type I and is emplaced at a depth of 3.11 km, deeper than the average for Types I and II (Table 1).

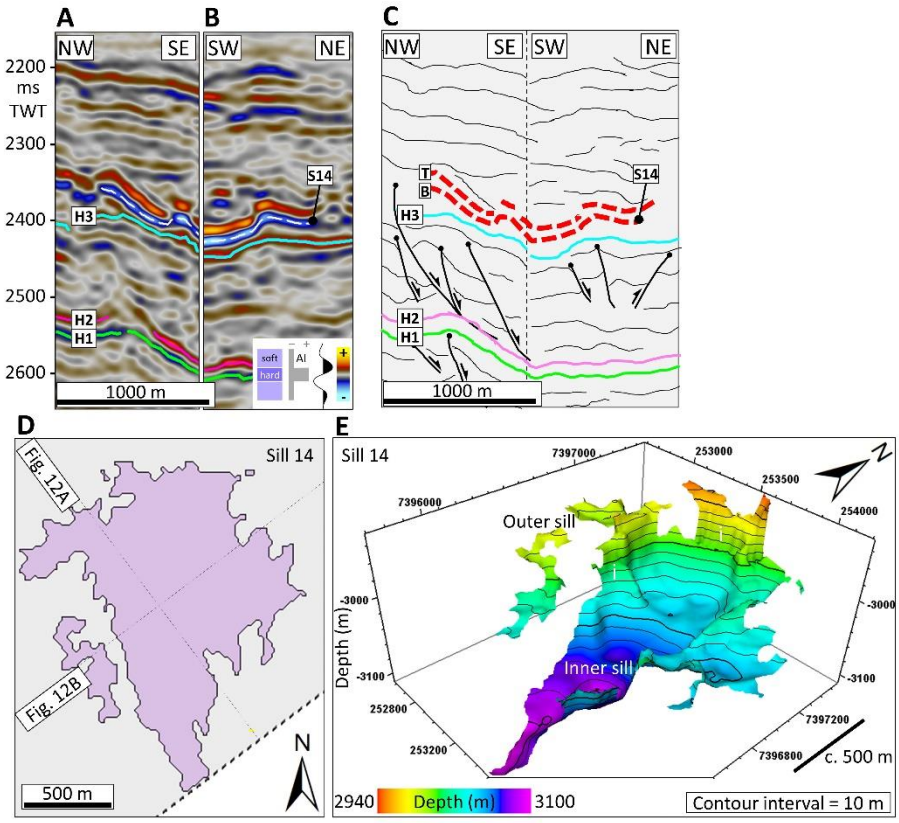


**Fig. 12.** Interpreted seismic sections along (A) dip (NW-SE) and (B) strike directions (NE-SW), highlighting the morphology of sill S14. (C) Geological model emphasizing the sill geometry, faults, reflectors configuration, and main interpreted horizons. (D) Plan-view morphology. (E) 3-D view of a climbing saucer-shaped sill (Type III) depicting inclined segments (i), inner and outer sill.

*Type IV* – The transgressive geometry is characterized by an upward stepped shape that crosscuts the stratigraphy at angles of 7.30-13.41º, with a minimum dip of 2.46º (Fig. 13A-B; Table 1). The area ranges from 0.43 to 0.82 km$^2$. The length of the long axis ranges between 1.01 and 2.71 km and the short axis from 0.78 to 1.93 km. The ratio between the long and short axis is between 1.30 and 1.99. These sills are characterized by irregular plan-view morphologies with eccentricities ranging from 0.45 to 0.83. They extend vertically from 0.13 to 0.25 km and are emplaced at 2.56-2.94 km depths (Table 1). Fig. 13E shows the steeply inclined segments on the inner sill periphery and the sill inclination towards NW.

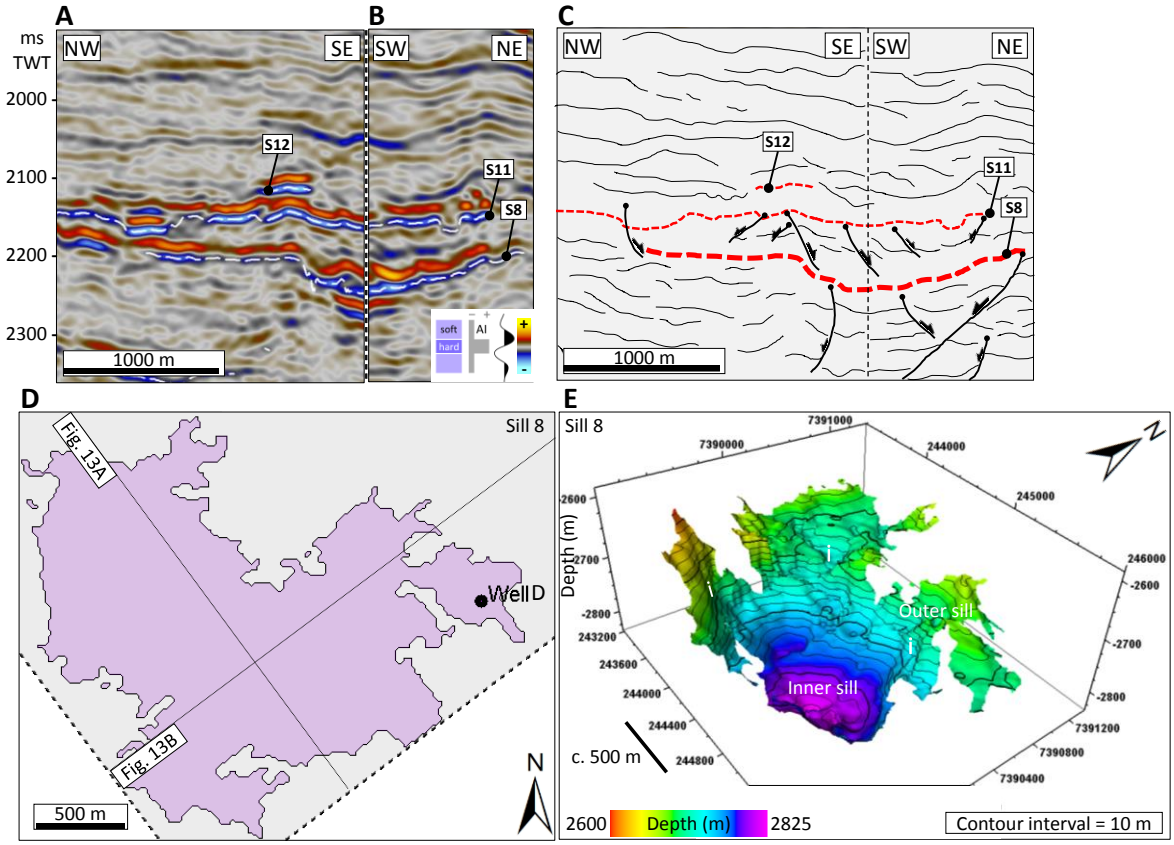


**Fig. 13.** Interpreted seismic sections along (A) dip (NW-SE) and (B) strike directions (NE-SW), highlighting the morphology of sill S8. (C) Geological model emphasizing the sill geometry, faults, and reflectors configuration. (D) Plan-view morphology. (E) 3-D view of a transgressive sill (Type IV) depicting inclined segments (i), inner and outer sill.

*Type V* – The rough layer-parallel geometry is characterized by dominantly strata-concordant segments (Fig. 14). This sill type extends over large areas (up to 14.35 km$^2$) with long and short axes ranging from 1.56 to 6.82 km and from 0.98 to 3.04 km, respectively, greater than the other types (I to IV). The vertical extent ranges between 0.06 and 0.23 km. In addition to lower vertical extents, these are emplaced at deeper levels (2.61-3.18 km) when compared to the other types. Approximately elongated ellipses with eccentricities ranging between 0.53 and 0.95 characterize the plan-view morphologies and comprise the highest eccentricity of the sills (Fig. 14D; Table 1).

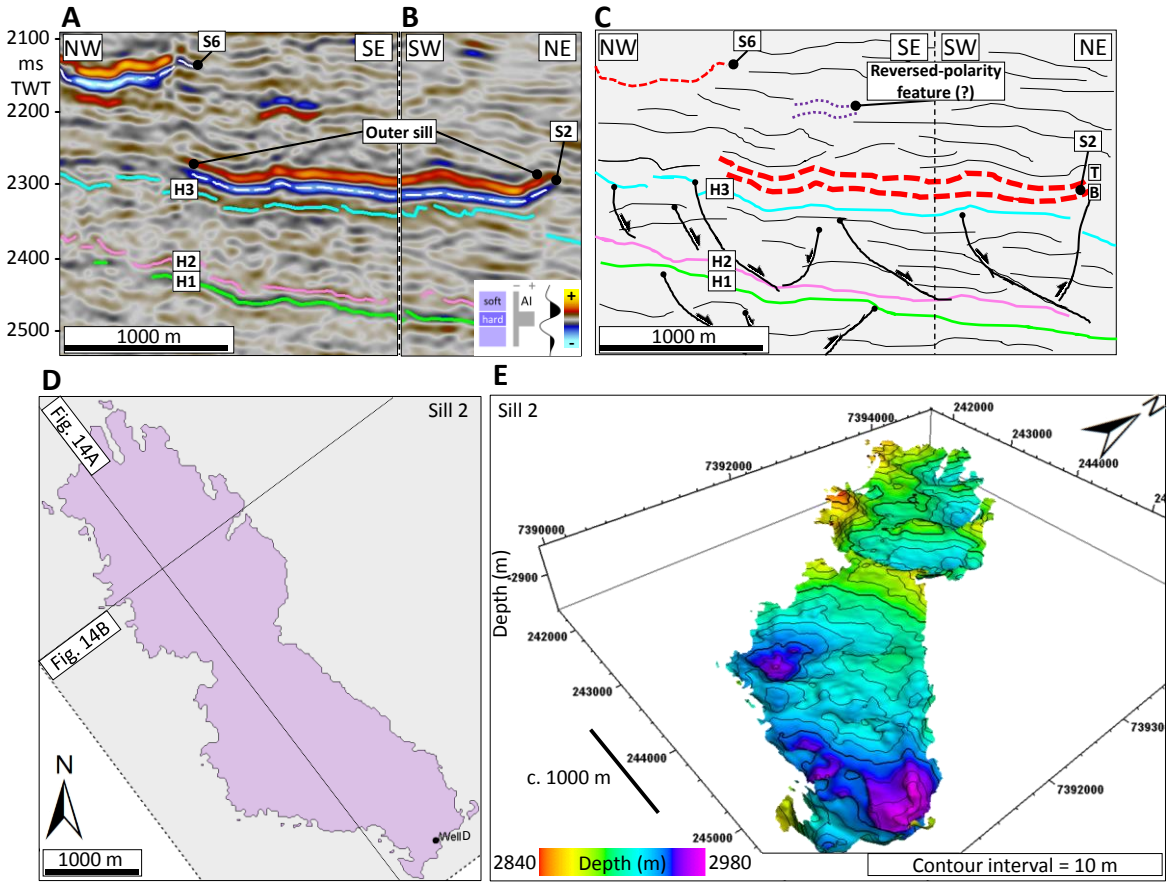


**Fig. 14**. Interpreted seismic sections along (A) dip (NW-SE) and (B) strike directions (NE-SW), highlighting the morphology of sill S2. (C) Geological model emphasizing the sill geometry, faults, reflectors configuration, and main interpreted horizons. (D) Plan-view morphology. (E) 3-D view of a layer-parallel sill (Type V).

We delineated structures in sills S2 and S3 that are characterized by small- (0.02-0.07 km$^2$) to medium-scale (up to 2.20 km$^2$) in size. In plan view, these structures present sub-circular to elliptical shapes in both sills, which is seen from the RGB frequency blending panels (Fig. 8 and Fig. 9). In sill S2, these structures are not detected at any of the selected frequencies, from the RGB blend panels, though appearing as approximately black (Fig. 8). Some extensions of sill S2 slightly branch off to form small-scale features further north. In addition, sill S2 appears red at the southern tip, on which we call a low-frequency range feature (LF), as also observed in other regions (Fig. 8).

**Table 1.** Summary of morphometric data for the interpreted sills.

| Sill | Sill type | Area ($km^2$) | Long axis (km) | Short axis (km) | Long/short axis ratio | Long axis orientation | | Sill height (km) | Sill depth (km) | Flat sections dip angle (°) | Inclined segments dip angle (°) | Mean dip orientation | | Area/ depth ratio | Eccentricity | Geometry |
|---|---|---|---|---|---|---|---|---|---|---|---|---|---|---|---|---|
| | | | | | | Azimuth (°) | Direction | | | | | Azimuth (°) | Direction | | | |
| S1 | I | 1.12 | 1.43 | 1.11 | 1.29 | 116 | NW-SE | 0.09 | 2.99 | 2.58 | 11.56 | 164 | S | 2.67 | 0.97 | Saucer-Shaped |
| S2 | VI | 7.55 | 6.23 | 1.83 | 3.41 | 142 | NW-SE | 0.15 | 2.99 | 2.19 | 7.75 | 162 | S | 0.40 | 0.95 | Layer-Parallel Rough |
| S3 | II | 1.79 | 2.15 | 1.16 | 1.86 | 120 | NW-SE | 0.12 | 2.86 | 2.61 | 11.23 | 157 | SE | 1.60 | 0.84 | Slightly Saucer-Shaped |
| S4 | I | 1.61 | 2.03 | 1.20 | 1.69 | 101 | NE-SW | 0.18 | 2.83 | 3.05 | 15.74 | 176 | S | 1.76 | 0.81 | Saucer-Shaped |
| S5 | V | 1.16 | 1.80 | 0.98 | 1.83 | 113 | NW-SE | 0.10 | 2.76 | 2.07 | 8.87 | 155 | SE | 2.38 | 0.84 | Layer-Parallel Rough |
| S6 | I | 1.67 | 1.81 | 1.28 | 1.41 | 103 | NE-SW | 0.13 | 2.70 | 2.63 | 12.96 | 161 | S | 1.62 | 0.71 | Saucer-Shaped |
| S7 | IV | 0.43 | 1.01 | 0.78 | 1.30 | 150 | NW-SE | 0.13 | 2.56 | 2.46 | 7.30 | 128 | SE | 5.99 | 0.45 | Transgressive |
| S8 | IV | 3.12 | 2.71 | 1.93 | 1.41 | 105 | NW-SE | 0.25 | 2.84 | 3.31 | 13.41 | 148 | SE | 0.91 | 0.70 | Transgressive |
| S9 | IV | 0.82 | 1.59 | 0.80 | 1.99 | 62 | NE-SW | 0.09 | 2.94 | 2.66 | 8.50 | 166 | S | 3.61 | 0.83 | Transgressive |
| S10 | V | 2.11 | 2.05 | 1.44 | 1.42 | 79 | NE-SW | 0.06 | 3.03 | 1.82 | 7.05 | 192 | S | 1.44 | 0.71 | Layer-Parallel Rough |
| S11 | V | 4.39 | 3.68 | 1.71 | 2.15 | 138 | NW-SE | 0.15 | 2.68 | 2.29 | 8.89 | 159 | S | 0.61 | 0.89 | Layer-Parallel Rough |
| S12 | VI | 0.85 | 1.56 | 0.99 | 1.57 | 9 | NNW-SSE | 0.09 | 2.61 | 3.13 | 9.42 | 122 | SE | 3.06 | 0.77 | Layer-Parallel Rough |
| S13 | VI | 4.21 | 3.63 | 1.76 | 2.07 | 41 | NE-SW | 0.17 | 3.18 | 1.82 | 7.37 | 181 | S | 0.76 | 0.53 | Layer-Parallel Rough |
| S14 | III | 1.27 | 1.69 | 1.24 | 1.36 | 168 | N-S | 0.19 | 3.11 | 2.76 | 12.11 | 173 | S | 2.44 | 0.68 | Climbing saucer-shaped |
| S15 | VI | 14.35 | 6.82 | 3.04 | 2.24 | 63 | NE-SW | 0.23 | 3.01 | 1.83 | 6.05 | 179 | S | 0.21 | 0.90 | Layer-Parallel Rough |

### 2.5.4. Distribution and pattern of faults

We identified two distinct fault sets in the study area: (1) NE-SW (striking N45º-50ºE) and (2) NNE-SSW (striking N15º-20ºE), based on the density, plan-view morphology, and mean strike (see rose diagram in Fig. 2A). Over the northeastern to the central study area, the fault density increased, the morphology is curved depicting concave and, to a smaller extent, linear structures, and the major azimuth is NE-SW (89% of the total). Over the southwestern area, the fault density decreases as the space between fault lineaments increases; the faults are linear and NNE-SSW oriented, intersecting the NE-SW striking faults set. The geometry of the interpreted faults on seismic cross-sections is typical of an extensional setting. The majority of faults developed within the H3 and H2 interval. However, some major faults extend into the overlying strata, while others are produced within the underlying strata.

## 2.6. DISCUSSION

### 2.6.1. Morphometric controls on the sills geometry

Our results support that depth (c. 2300 ms) conditions the size of sills, i.e. the size increases with depth. A high area-to-depth ratio reflects increased conditions for the formation of transgressive and layer-parallel sills. We expected a much lower dip of inclined segments for the layer-parallel sills, i.e., a sub-horizontal dip implying that parallel and concordant sills would broadly follow the dip of regional stratigraphy.

The high eccentricity values (0.71-0.97) of saucer-shaped sills cannot corroborate the circular plan-view morphology suggested by the 1.46 long-to-short axis ratio. Conversely, the slightly saucer-shaped sill long-to-short axis ratio (1.86) suggests a moderately circular shape and elliptical plan-view morphology (0.84 of eccentricity). Transgressive sills support a connection between a deeper sill (S8) with a relatively flat layer-parallel sill (S11), suggested by the morphology and position of the steeply inclined peripheral segments (Fig. 13A-B). Although classified as layer-parallel rough sills with gently dipping flat sections, these sills comprise peripherally minor inclined segments (Fig. 14A-B). The relatively high dip for a layer-parallel sill should be explained by the handpicking of seismic horizons, even though the vertical extension corroborates this geometry.

The RGB blending was important to describe the sill extensions structure (i.e., fingers; Schofield et al., 2010), as well as to reveal the seismic expression of high-amplitude anomalies, such as those generated by sills (Fig. 9).

The low-frequency range features may be associated with zones of depleted magma and compared with internal depletion zones, described in Alves et al. (2015). However, in the S2, we observed a large zone of low-frequency features, which may be associated with a different magmatic pulse. The homogeneous texture for each sill, observed in the variance attribute time slices, could be associated with fine-grained crystalline rocks (Alves et al., 2015) in the post-salt sequence of the Espírito Santo Basin, in the southeastern Brazilian offshore. The red color dominance corroborates an increased sill thickness in that region, marked by frequency and amplitude variation, such as the examples from McArdle et al. (2014). Furthermore, another magmatic pulse in that region would make the sill seems thicker. The fact that the interpreted small-scale sub-circular features appear as approximately black suggests a non-detection of any of the selected frequencies (10-20-45 Hz). This could be associated with zones of depleted magma, where the thickness is minimum, as suggested by the blue color detected (*c.* 45 Hz) over the red and green (greater thicknesses) on S2 in the RGB blend. In addition, this can be corroborated by the increased thickness far from these zones.

The range of measured size, depth, vertical extent, and dips for the flat-lying sections and inclined segments in the studied saucer-shaped, transgressive, and layer-parallel sills, is in accordance with previous studies (Fig. 15). Schofield et al. (2010) measured dips <5º for the flat sections and 25-30º for the inclined segments, which are similar to the overall geometric shape that we have mapped. Hansen et al. (2008) described that sill transgresses at <20º in the saucer-shaped periphery, similar to this study, in which sill type I inclined segments crosscut the stratigraphy at approximately 11 to 16º.

Saucer-shaped sills (Type I, II, and III) thin outwards, from the inner sill to the inclined segments and outer sill. Similarly, other seismic-based studies described a thickening towards the saucer axis and an outwards tapering (e.g. Hansen and Cartwright, 2006; Hansen et al., 2011).

In the saucer-shaped sills, we observed reflectors continuity breaks from the inner sill to the inclined sheets and outer sill. In addition, their relatively shallow depth of emplacement makes us favor that layer-parallel sills are at the base and limit sill complexes (Planke et al., 2005). The broad geometry and plan-view morphology resemble the saucer-shaped sill described by Polteau et al. (2008).

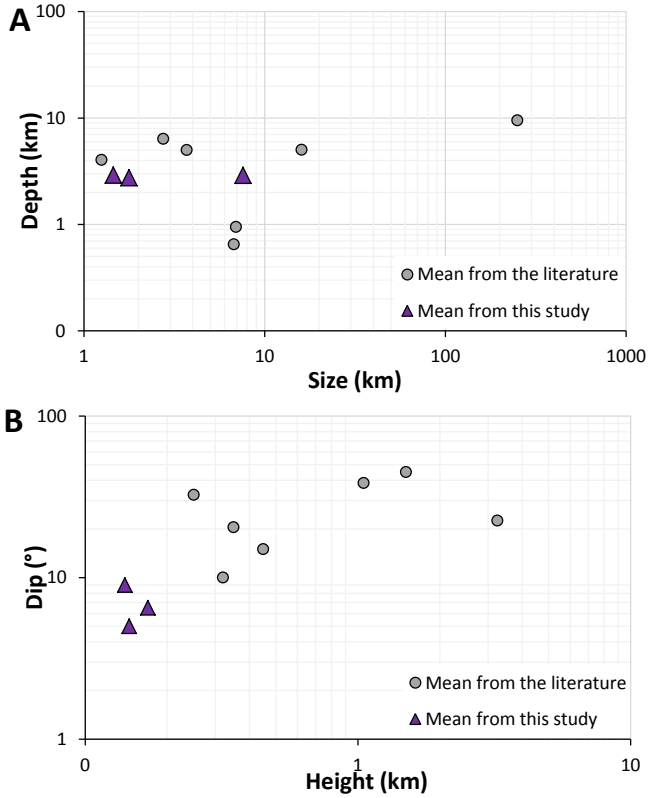


**Fig. 15.** Cross-plots between (A) size and depth and (B) vertical extent and dip from the studied sills and the literature (Hansen et al., 2004; Thomson and Hutton, 2004; Cartwright and Hansen, 2006; Hansen and Cartwright, 2006; Polteau et al., 2008; Magee et al., 2014; Sun et al., 2014).

### 2.6.2. Seismic resolution

Although sills are most prone to be mapped from seismic data by recognizing the top reflection as the base is usually more difficult due to the interference and tuning effects (e.g. Smallwood and Maresh, 2002; Trude et al., 2003; Magee et al., 2015). In our study, although we are able to map two distinct seismic reflections, we may not be able to resolve them in a way we can compute the real thickness of the seismic beds. The upper and lower contacts of the intrusive bodies may not be distinguishable at all since the vast majority of the

magmatic sills mapped worldwide are described as tuned reflections with indistinct upper and lower contacts (Smallwood and Maresh, 2002; Planke et al., 2015, Omosanya et al., 2018).

## 2.7. CONCLUSIONS

We mapped igneous sills in the southern Campos Basin, southeastern Brazil, and improved the understanding of their geometries, based on quantitative morphometric analysis supported by seismic attributes. This study will assist further global research on the formation of sills. The scarcity of data is a limitation that may compromise the representativeness of this study. Nonetheless, our results support the following conclusions:

(1) High-amplitude seismic anomalies, with a tuning frequency of approximately 20-45 Hz, characterize the fifteen interpreted magmatic sills.

(2) Layer-parallel sills occur as thick extensive intrusions and feature a strong stratigraphic relationship with the top seismic reflection of Albian carbonates of the Macaé Group. Inner and outer approximately-flat section linked through inclined sheets characterizes the saucer-shaped sills. Continuous and slightly stepped-like reflectors characterize transgressive sills.

(3) The deepest sills are generally associated with larger sizes (e.g. layer-parallel sills), a result supported by similar ratios documented for igneous sills in other basins. Sills usually thin out laterally. However, the higher the dip at the periphery, the higher the contrast in the sill tapering toward its tips.

(4) The interpreted magmatic sills present a stacking pattern, characterized by two main trends: (1) NW-trending and (2) NE-trending, generally dipping away from the gently dipping inner sills.

(5) Fault lineaments depict a dense NE-oriented curvy pattern over the northeastern to the central area, while in the southwestern area the NNE-SSW faults are linear and described by a less dense network. The faults form a structural network that may have assisted the emplacement of sills.

We demonstrate that, apart from the traditional seismic attributes (RMS amplitude, variance, dip, and azimuth), the vertical QR gradient successfully clarifies the seismic amplitude and enables the delineation of high-amplitude anomalies. In addition, the RGB color blending based spectral decomposition was essential for quantitative analyses of the seismic expression of magmatic sills.

## ACKNOWLEDGEMENTS

The authors gratefully acknowledge Equinor for supporting this research, and Sinochem and PGS for allowing the publication of the seismic data. This study was financed in part by Coordenação de Aperfeiçoamento de Pessoal de Nível Superior - Brasil (CAPES) - Finance Code 001. National Petroleum Agency's (ANP) Exploration and Production Database (BDEP) is appreciated for providing seismic and well log data. The authors also appreciate the academic software licenses provided by dGB Earth Sciences for OpendTect, by Schlumberger for Petrel, Kingdom by IHS Markit. Reviewers Kamal'deen Omosanya and Sverre Planke, and the Associate Editor Tiago Alves are thanked for the insightful review that substantially improved the original manuscript.

**REFERENCES**

Alves, T.M., Omosanya, K.D., Gowling, P., 2015. Volume rendering of enigmatic high-amplitude anomalies in southeast Brazil: A workflow to distinguish lithologic features from fluid accumulations. Interpretation, 3(2), A1-A14, http://dx.doi.org/10.1190/INT-2014-0106.1.

Brown, A., 2004. Interpretation of three-dimensional seismic data, 6th ed.: AAPG Memoir, vol. 42, http://dx.doi.org/10.1306/M4271346.

Brown, A., 2009. Phase and Polarity Issues in Modern Seismic Interpretation. In AAPG International Conference and Exhibition. AAPG, Cape Town, 1-22.

Cartwright, J., Hansen, D.M., 2006. Magma transport through the crust via interconnected sill complexes. Geology, 34(11), 929-932, http://dx.doi.org/10.1130/G22758A.1.

Castagna, J., Sun, S., Siegried, R., 2003. Instantaneous Spectral Analysis: Detection of Low Frequency Shadows Associated with Hydrocarbons. The Leading Edge, 22(2), 120-127, https://dx.doi.org/10.1190/1.1559038.

Chang, H.K., Kowsmann, R.O., Figueiredo, A.M.F., Bender, A.A., 1992. Tectonics and Stratigraphy of the East Brazil rift system: an overview. Tectonophysics, v. 213, p. 97–138, https://dx.doi.org/10.1016/0040-1951(92)90253-3.

Chopra, S., Marfurt, K.J., 2007. Volumetric curvature attributes add value to 3D seismic data interpretation. The Leading Edge, 26(7), 856-867, https://dx.doi.org/10.1190/1.2756864.

Chopra, S., Misra, S., Marfurt, K.J., 2011. Coherence and curvature attributes on preconditioned seismic data. The Leading Edge, 30(4), 386-393. https://dx.doi.org/10.1190/1.3575281.

Cortez, M.M.M., Santos, M.A.C., 2016. Seismic interpretation, attribute analysis, and illumination study for targets below a volcanic-sedimentary succession, Santos Basin, offshore Brazil. Interpretation, 4(1), SB37-SB50, http://dx.doi.org/10.1190/INT-2015-0097.1.

Delpino, D.H., Bermúdez, A.M., 2009. Petroleum systems including unconventional reservoirs in intrusive igneous rocks (sills and laccoliths). The Leading Edge, 28(7), 804-811, http://dx.doi.org/10.1190/1.3167782.

Ebrom, D., 2004. The low-frequency gas shadow on seismic sections. The Leading Edge, 23(8), 772-772, https://dx.doi.org/10.1190/1.1786898.

Fetter, M., 2009. The role of basement tectonic reactivation on the structural evolution of Campos Basin, offshore Brazil: Evidence from 3D seismic analysis and section restoration. Marine and Petroleum Geology, 26(6), 873-886, http://dx.doi.org/10.1016/j.marpetgeo.2008.06.005.

Fiduk, J.C., Brush, E.R., Anderson, L.E., Gibbs, P.B., Rowan, M.G., 2004. Salt deformation, magmatism, and hydrocarbon prospectivity in the Espirito Santo Basin, offshore Brazil. In Salt-sediment interactions and hydrocarbon prospectivity: Concepts, applications, and case studies for the 21st century: Gulf Coast Section SEPM 24th Annual Conference (pp. 370-392).

Francis, E.H., 1982. Magma and sediment-I Emplacement mechanism of late Carboniferous tholeiite sills in northern Britain. Journal of the Geological Society, 139, 1-20, http://dx.doi.org/10.1144/gsjgs.139.1.0001.

Galerne, C.Y., Galland, O., Neumann, E.R., Planke, S., 2011. 3D relationships between sills and their feeders: evidence from the Golden Valley Sill Complex (Karoo Basin) and experimental modelling. Journal of Volcanology and Geothermal Research, 202(3), 189-199, http://dx.doi.org/10.1016/j.jvolgeores.2011.02.006.

Galerne, C.Y., Neumann, E.R., Planke, S., 2008. Emplacement mechanisms of sill complexes: Information from the geochemical architecture of the Golden Valley Sill Complex, South Africa. Journal of Volcanology and Geothermal Research, 177(2), 425-440, http://dx.doi.org/10.1016/j.jvolgeores.2008.06.004.

Hansen, D.M., Cartwright, J., 2006. The three-dimensional geometry and growth of forced folds above saucer-shaped igneous sills. Journal of Structural Geology, 28(8), 1520-1535, http://dx.doi.org/10.1016/j.jsg.2006.04.004.

Hansen, D.M., Cartwright, J.A., Thomas, D., 2004. 3D seismic analysis of the geometry of igneous sills and sill junction relationships. In: Davies, R.J., Cartwright, J.A., Stewart, S.A., Lappin, M., Underhill, J.R. (Eds.), 3D Seismic Technology: Application to the Exploration of Sedimentary Basins, Geological Society, London, Memoirs 29, pp. 199–208, http://dx.doi.org/10.1144/GSL.MEM.2004.029.01.19.

Hansen, D.M., Redfern, J., Federici, F., Di Biase, D., Bertozzi, G., 2008. Miocene igneous activity in the Northern Subbasin, offshore Senegal, NW Africa. Marine and Petroleum Geology, 25(1), 1-15, http://dx.doi.org/10.1016/j.marpetgeo.2007.04.007.

Hansen, J., Jerram, D., McCaffrey, K., Passey, S., 2011. Early Cenozoic saucer-shaped sills of the Faroe Islands: An example of intrusive styles in basaltic lava piles: Journal of the Geological Society London, v. 168, p. 159–178, http://dx.doi.org/10.1144 /0016-76492010-012.

Henderson, J., Purves, S.J., Leppard, C., 2007. Automated delineation of geological elements from 3D seismic data through analysis of multichannel, volumetric spectral decomposition data. First Break, 25, 87–93.

Höcker, C., Fehmers, G., 2002. Fast structural interpretation with structure-oriented filtering. The Leading Edge, 21(3), 238-243, http://dx.doi.org/10.1190/1.1463775.

Honório, B.C.Z., Correia, U.M.da.C., Matos, M.C.De., Vidal, A.C., 2016. Similarity attributes from differential resolution components. Interpretation, 4, T65-T73, http://dx.doi.org/10.1190/INT-2015-0211.1.

Infante-Paez, L., Marfurt, K.J., 2017. Seismic expression and geomorphology of igneous bodies: A Taranaki Basin, New Zealand, case study. Interpretation, 5(3), SK121-SK140, http://dx.doi.org/10.1190/INT-2016-0244.1.

Jackson, C.A.-L, Schofield, N., Golenkov, B., 2013. Geometry and controls on the development of igneous sill–related forced folds: A 2-D seismic reflection case study from offshore southern Australia. Geological Society of America Bulletin, 125(11-12), 1874-1890, http://dx.doi.org/10.1130/B30833.1.

Magee, C., Jackson, C.A.-L., Schofield, N., 2013. The influence of normal fault geometry on igneous sill emplacement and morphology. Geology, 41(4), 407-410, http://dx.doi.org/10.1130/G33824.1.

Magee, C., Jackson, C.A.-L., Schofield, N., 2014. Diachronous sub-volcanic intrusion along deep-water margins: insights from the Irish Rockall Basin. Basin Research, 26(1), 85-105, http://dx.doi.org/10.1111/bre.12044.

Magee, C., Maharaj, S.M., Wrona, T., Jackson, C.A.L., 2015. Controls on the expression of igneous intrusions in seismic reflection data. Geosphere, 11(4), 1024-1041, https://dx.doi.org/10.1130/GES01150.1.

Maoshan, C., Shifan, Z., Zhonghong, W., Hongying, Z., Lei, L., 2011. Detecting carbonate-karst reservoirs using the directional amplitude gradient difference technique. In SEG Technical Program Expanded Abstracts 2011: pp. 1845-1849. Society of Exploration Geophysicists, https://dx.doi.org/10.1190/1.3627564.

Marfurt, K.J., 2006. Robust estimates of dip and azimuth. Geophysics, 71(4), P29–P40. https://dx.doi.org/10.1190/1.2213049.

Marfurt, K.J., Alves, T.M., 2015. Pitfalls and limitations in seismic attribute interpretation of tectonic features. Interpretation, 3(1), SB5-SB15, http://dx.doi.org/10.1190/INT-2014-0122.1.

Marfurt, K.J., Kirlin, R.L., Farmer, S.H., Bahorich, M.S., 1998. 3-D seismic attributes using a running window semblance-based algorithm: Geophysics, 63, 1150–1165, http://dx.doi.org/10.1190/1.1444415.

Mark, N.J., Schofield, N., Pugliese, S., Watson, D., Holford, S., Muirhead, D., Brown, R., Healy, D., 2018. Igneous intrusions in the Faroe Shetland basin and their implications for hydrocarbon exploration; new insights from well and seismic data. Marine and Petroleum Geology, http://dx.doi.org/10.1016/j.marpetgeo.2017.12.005.

McArdle, N.J., Iacopini, D., KunleDare, M. A., Paton, G.S., 2014. The use of geologic expression workflows for basin scale reconnaissance: A case study from the Exmouth Subbasin, North Carnarvon Basin, northwestern Australia. Interpretation, 2(1), SA163-SA177, http://dx.doi.org/10.1190/INT-2013-0112.1.

Meisling, K.E., Cobbold, P.R., Mount, V.S., 2001. Segmentation of an obliquely-rifted margin, Campos and Santos basins, southeastern Brazil. AAPG Bulletin, 85(11), 1903-1924, http://dx.doi.org/10.1306/8626D0A9-173B-11D7-8645000102C1865D.

Mohriak, W., Nemčok, M., Enciso, G., 2008. South Atlantic divergent margin evolution: rift-border uplift and salt tectonics in the basins of SE Brazil. Geological Society, London, Special Publications, 294(1), 365-398, http://dx.doi.org/10.1144/SP294.19.

Ojeda, H.A.O., 1982. Structural framework, stratigraphy, and evolution of Brazilian marginal basins. AAPG Bulletin, 66(6), 732-749.

Omosanya, K.O., Alves, T.M., 2013a. A 3-dimensional seismic method to assess the provenance of Mass-Transport Deposits (MTDs) on salt-rich continental slopes (Espírito Santo Basin, SE Brazil). Marine and Petroleum Geology, 44, 223-239, http://dx.doi.org/10.1016/j.marpetgeo.2013.02.006.

Omosanya, K.O., Alves, T.M., 2013b. Ramps and flats of mass-transport deposits (MTDs) as markers of seafloor strain on the flanks of rising diapirs (Espírito Santo Basin, SE Brazil). Marine Geology, 340, 82-97, https://dx.doi.org/10.1016/j.margeo.2013.04.013.

Omosanya, K.O., Johansen, S.E., Abrahamson, P., 2016. Magmatic activity during the breakup of Greenland-Eurasia and fluid-flow in Stappen High, SW Barents Sea. Marine and Petroleum Geology, 76, 397-411, http://dx.doi.org/10.1016/j.marpetgeo.2016.05.017.

Omosanya, K.O., Johansen, S.E., Eruteya, O.E., Waldmann, N., 2017. Forced folding and complex overburden deformation associated with magmatic intrusion in the Vøring Basin, offshore Norway. Tectonophysics, 706, 14-34, http://dx.doi.org/10.1016/j.tecto.2017.03.026.

Oreiro, S.G., Cupertino, J.A., Szatmari, P., Thomaz Filho, A., 2008. Influence of pre-salt alignments in post-Aptian magmatism in the Cabo Frio High and its surroundings, Santos and Campos basins, SE Brazil: An example of non-plume-related magmatism. Journal of South American Earth Sciences, 25(1), 116-131, http://dx.doi.org/10.1016/j.jsames.2007.08.00.

Penna, R., Araújo, S., Geisslinger, A., Sansonowski, R., Oliveira, L., Rosseto, J., Matos, M., 2018. Igneous rock characterization through reprocessing, FWI imaging, and elastic inversion of a legacy seismic dataset in Brazilian Pre-Salt Province. In SEG Technical Program Expanded Abstracts 2018: pp. 3277-3281. Society of Exploration Geophysicists. http://dx.doi.org/10.1190/segam2018-2996032.1.

Planke S., Svensen H., Myklebust R., Bannister S., Manton B., Lorenz L., 2015. Geophysics and Remote Sensing. In: Breitkreuz C., Rocchi S. (eds) Physical Geology of Shallow Magmatic Systems. Advances in Volcanology (An Official Book Series of the International Association of Volcanology and Chemistry of the Earth's Interior). Springer, Cham.

Planke, S., Rasmussen, T., Rey, S.S., Myklebust, R., 2005. Seismic characteristics and distribution of volcanic intrusions and hydrothermal vent complexes in the Vøring and Møre basins. In: A.G. Dore, and B.A. Vining (Eds.), North-West Europe and Global Perspectives: Proceedings of the Sixth Petroleum Geology Conference, Geological Society of London, 6, 833–844, http://dx.doi.org/10.1144/0060833.

Planke, S., Symonds, P.A., Alvestad, E., Skogseid, J., 2000. Seismic volcanostratigraphy of large-volume basaltic extrusive complexes on rifted margins. Journal of Geophysical Research: Solid Earth, 105 (B8), 19335-19351, https://dx.doi.org/10.1029/1999JB900005.

Polteau, S., Mazzini, A., Galland, O., Planke, S., Malthe-Sørenssen, A., 2008. Saucer-shaped intrusions: occurrences, emplacement and implications. Earth Planet Science Letters, 266(1-2), 195-204, http://dx.doi.org/10.1016/j.epsl.2007.11.015.

Rateau, R., Schofield, N., Smith, M., 2013. The potential role of igneous intrusions on hydrocarbon migration, West of Shetland. Petroleum Geoscience, 19(3), 259-272, http://dx.doi.org/10.1144/petgeo2012-035.

Roberts, A., 2001. Curvature Attributes and Their Application to 3D Interpreted Horizons. First Break, 19, 85-100, http://dx.doi.org/10.1046/j.0263-5046.2001.00142.x.

Schofield, N., Holford, S., Millett, J., Brown, D., Jolley, D., Passey, S.R., Dave, M., Grove, C., Magee, C., Murray, J., Hole, M., Jackson, C.A.-L., Stevenson, S., 2017. Regional magma plumbing and emplacement mechanisms of the Faroe- Shetland Sill Complex: implications for magma transport and petroleum systems within sedimentary basins. Basin Research, 29(1), 41-63, http://dx.doi.org/10.1111/bre.12164.

Schofield, N., Stevenson, C., Reston, T., 2010. Magma fingers and host rock fluidization in the emplacement of sills. Geology, 38(1), 63-66, https://doi.org/10.1130/G30142.1.

Schutter, S.R., 2003. Hydrocarbon occurrence and exploration in and around igneous rocks. Geological Society, London, Special Publications, 214(1), 7-33, http://dx.doi.org/10.1144/GSL.SP.2003.214.01.02.

Senger, K., Millett, J., Planke, S., Ogata, K., Eide, C.H., Festøy, M., Galland, O., Jerram, D.A., 2017. Effects of igneous intrusions on the petroleum system: a review. First Break, 35(6), 47-56, http://dx.doi.org/10.3997/1365-2397.2017011.

Smallwood, J.R., Maresh, J., 2002. The properties, morphology and distribution of igneous sills: modelling, borehole data and 3D seismic from the Faroe-Shetland area. Geological Society, London, Special Publications, 197(1), 271-306, http://dx.doi.org/10.1144/GSL.SP.2002.197.01.11.

Spacapan, J.B., Palma, O., Galland, O., Manceda, R., Rocha, E., D'Odorico, A., Leanza, H.A., 2018. Thermal impact of igneous sill-complexes on organic-rich formations and implications for petroleum systems: A case study in the northern Neuquén Basin, Argentina. Marine and Petroleum Geology, 91, 519-531, http://dx.doi.org/10.1016/j.marpetgeo.2018.01.018.

Sun, Q., Wu, S., Cartwright, J., Wang, S., Lu, Y., Chen, D., Dong, D., 2014. Neogene igneous intrusions in the northern South China Sea: Evidence from high-resolution three dimensional seismic data. Marine and Petroleum Geology, 54, 83-95, http://dx.doi.org/10.1016/j.marpetgeo.2014.02.014.

Svensen, H.H., Planke, S., Sørenssen, A.M., Jamtveit, B., Myklebust, R., Rasmussen, E.T., Rey, S.S., 2004. Release of methane from a volcanic basin as a mechanism for initial Eocene global warming: Nature, 429, 542-545, http://dx.doi.org/10.1038/nature02566.

Sydnes, M., Fjeldskaar, W., Løtveit, I.F., Grunnaleite, I., Cardozo, N., 2018. The importance of sill thickness and timing of sill emplacement on hydrocarbon maturation. Marine and Petroleum Geology, 89, 500-514, http://dx.doi.org/10.1016/j.marpetgeo.2017.10.017.

Taner, M.T., Koehler, F., Sheriff, R.E., 1979. Complex seismic trace analysis. Geophysics, 44(6), 1041-1063, https://dx.doi.org/10.1190/1.1440994.

Thomaz Filho A., Cesero P. de., Mizusaki A.M.P., Leão J.G., 2005. Hot spot Volcanic Tracks and their Implications for South American Plate Motion, Campos Basin (Rio de Janeiro State), Brazil. Journal of South American Earth Sciences, 18(3-4):383-389, http://dx.doi.org/10.1016/j.jsames.2004.11.006.

Thomaz Filho, A.T, Mizusaki, A.M.P., Antonioli, L., 2008. Magmatismo nas bacias sedimentares brasileiras e sua influência na geologia do petróleo, Revista Brasileira de Geociências, v. 38, n. 2, p. 128-137.

Thomson, K., 2007. Determining magma flow in sills, dykes and laccoliths and their implications for sill emplacement mechanisms. Bulletin of Volcanology, 70(2), 183-201, http://dx.doi.org/10.1007/s00445-007-0131-8.

Thomson, K., Hutton, D., 2004. Geometry and growth of sill complexes: insights using 3D seismic from the North Rockall Trough. Bulletin of Volcanology, 66(4), 364-375, http://dx.doi.org/10.1007/s00445-003-0320-z.

Trude, J., Cartwright, J., Davies, R.J., Smallwood, J., 2003. New technique for dating igneous sills. Geology, 31(9), 813-816, https://doi.org/10.1130/G19559.1.

Walker, R.J., 2016. Controls on transgressive sill growth. Geology, 44(2), 99-102, http://dx.doi.org/10.1130/G37144.1.

Watson, D., Holford, S., Schofield, N., Mark, N. 2019. Failure to predict igneous rocks encountered during exploration of sedimentary basins: A case study of the Bass Basin, Southeastern Australia. Marine and Petroleum Geology, 99, 526-547. https://dx.doi.org/10.1016/j.marpetgeo.2018.10.034

Widess, M.B. 1973. How thin is a thin bed?. Geophysics, 38(6), 1176-1180, https://dx.doi.org/10.1190/1.1440403

Zeng, H., Backus, M.M., 2005. Interpretive advantages of 90-phase wavelets: Part 1—Modeling. Geophysics, 70(3), C7-C15, https://dx.doi.org/10.1190/1.1925740

# 3. THE IMPORTANCE IGNEOUS-RELATED STRUCTURES FOR PETROLEUM RESERVOIRS: EXAMPLES FROM THE CAMPOS BASIN, SE BRAZIL

Ulisses M.C. Correia, Bruno C.Z. Honório, Leandro H. Melani, Alexandre C. Vidal

To be submitted to a peer-reviewed journal

# THREE-DIMENSIONAL SEISMIC ANALYSIS OF MAGMATIC SILL-RELATED STRUCTURES: EXAMPLES OF FORCED FOLDS, JUNCTIONS, STEPS, VENTS FROM THE SOUTHERN CAMPOS BASIN, SE BRAZIL

## ABSTRACT

The comprehension of intrusive bodies is essential for a wide range of geological studies across worldwide sedimentary basins. The structures related to intrusive bodies can be economically important as they may compartmentalize intervals of interest, and affect the thermal history of sedimentary basins. In this study, we used three-dimensional post-stack seismic data, calibrated with well logs, from the southern Campos Basin over the Cabo Frio tectonic domain, to illustrate some of the sub-volcanic structures (i.e. forced folds, vents, and junctions). This area reveals several magmatic events from Late Cretaceous to Early Tertiary period. The interpreted forced fold structures are characterized by dome-shaped strata overlying a saucer-shaped intrusion, which is, in turn, characterized by an inner and outer sill as well as inclined segments. The country rock is flexed, by the saucer-shaped intrusions, at a ratio between the sill length and sill depth ranging from 0.67 to 0.75. Sill length-to-depth ratio, which gives a quantitative idea of the how likely is the overburden deformed due to the emplacement of an igneous sill, in this study, ranges between 0.40 and 2.26 (0.92 mean). In addition, 66% of the sills mapped with a ratio between 0.67-2.09 (1.09 mean) have a supra-sill deformation. Interpreted steps and junctions suggest the local direction of the magma pattern, as they are often parallel to the axis of sill emplacement. We identified seismic features that look like ‘T’ and ‘J’ shaped junctions between the interpreted sills. Sills may also be responsible for the formation of vent structures, characterized by dome-shaped features with chaotic internal geometries, flat-lying concordant underlying reflectors. These suggest focused fluid flow produced by fault-related feeder dykes. Furthermore, these structures are onlapped by overlying reflectors suggesting a strong relationship with the overburden. The emplacement of saucer-shaped sills often favors the development of forced-fold structures on the overburden, as well as the creation of a series of local normal faults on the overburden. However, not always that the indicator ratio, from which country rock is flexed, is within the interval of interest a forced fold is formed. This evidence suggests that the formation of forced folds may also be associated with other controlling factors.

**Keywords:** Igneous related structures; Forced folds; Vents; Junctions

## 3.1. INTRODUCTION

The intrusive bodies and related structures (i.e. forced folds, vents, and junctions) are essential for a wide range of geological studies across worldwide sedimentary basins and for petroleum exploration, as they can be economically important (Hansen and Cartwright, 2006; Holford et al., 2013; Jackson et al., 2013). Furthermore, assessing these types of volcanic structures can be quite challenging due to the issues regarding detectability (i.e. separability and visibility) as Sydnes et al. (2018) mentioned for the seismic identification of sills. Also for petroleum exploration activities, it is extremely important to have these type of structures characterized, and when possible constrained by borehole data to tie the igneous rocks to the seismic events (Ran et al., 2014; De Luca et al., 2015).

Most of the times, the emplacement of igneous intrusions accommodate local forced folds, created immediately above the center of a sill body, which may act as hydrocarbon traps (Jackson et al., 2013). In addition, fractures associated with vents may impact on secondary migration and the local temperature history. In this study, we illustrate some structures in the overlying strata associated with the accommodation of deformation due to sill intrusions, as the overburden bends (Barnett and Gudmundsson, 2014). According to Mathieu et al. (2008), saucer-shaped intrusions flex the country rock at a ratio between the sill length and sill depth ranging from 0.5 to 0.6.

The focused fluid flow, which is important for the petroleum prospectivity within sedimentary basins, is generally associated with sub-vertical chaotic and reflection-free seismic zones, equivalent to the seismic chimneys (Thomson, 2007). These structures are comparable to the sub-vertical hydrothermal pipes that form at the sill edges and are associated with hydrothermal vent complexes defined by Planke et al. (2005), and pipes defined by Hansen (2006). Associated with the top of these seismic zones occur mounded structures (Magee et al., 2014). The strata below these mounds are concordantly deflected downwards providing an eye-shaped geometrical style and have an overburden relationship with strata diverging over the mound surface as described by Hansen (2006) and Magee et al. (2014). Furthermore, Hansen (2006) described two more geometrical styles for vent-related structures, with different internal geometries, as crater and dome-shaped with overlying reflectors concordant and onlapping onto the mound, respectively.

Hydrothermal vent and sill complexes are dyke-fed igneous structures as discussed in Planke et al. (2005) and Thomson (2007). However, the sill-to-sill junctions might be a consequence of overlapping sill tips as mentioned by Alves et al. (2015), which results in constructive interference of the seismic signal of sills, as pointed by Magee et al. (2015).

Bridges and junctions as one of the main features of the sill-to-sill interaction and connectivity allow constraining the associated magma flow pattern (Hutton, 2009; Schofield et al., 2012; Magee et al., 2014). Nested sill complexes may be associated with junctions due to its capacity to interconnect the several sills present in the same area (Hansen and Cartwright, 2006). These junctions, also described by Hansen et al. (2004) may provide insightful constraints on the reconstruction of sill complexes.

Techniques applied to high-quality seismic data have been used to extract information from the volcanic structures within sedimentary basins worldwide. Amongst successful techniques is the volume and opacity rendering that has already proven effective for visualizing the characteristics of sill complexes and associated structures (Smallwood and Maresh, 2002; Thomson and Hutton, 2004, Thomson, 2007; Schofield et al., 2012; Alves et al., 2015). Certainly, these techniques will speed up the seismic interpretation process and will contribute to insightful discussions on the three-dimensional architecture of these structures and the responsible processes for their generation.

Any type of hydrocarbon-bearing basin in Brazil has some sort of relation with volcanic activity, and yet there are still unresolved issues related to the impact of subvolcanic and related structures on the petroleum systems, namely in the post-salt and pre-salt reservoirs of the Brazilian margin basins. In addition, is still necessary to understand these impacts on the generation and secondary migration processes, and on the regional evolution of the rifted margins (Tissot and Welte, 1984; Magoon and Dow, 1994; England, 1994). In particular, the three most prolific Brazilian basins, Espírito Santo, Campos, and Santos Basins record an impact in reservoir presence and predictability due to the intense magmatic activity (Matias et al., 2015). The southern part of the Campos basin exposes evidence of vast volcanic activity, such as thermal uplift and occurrence of the extensive feeder and ring dykes, sills, and volcanic edifices (Oreiro et al., 2008).

Alvarenga et al. (2016) worked on the characterization and mapping the distribution of hydrothermal vent complexes in the rift section of Campos Basin based on 2D seismic lines and established correlations between those structures and the regional tectono-

magmatic events. Other studies have been developed that describe features such as, steps and bridges originated by the stresses during dyke intrusions and related faults as well. In addition, some of the identified sills are described as shallow emplacement magmatic intrusions resulted by the injection adjacent to volcanic cones (Oreiro, 2006; Almeida et al., 2013; Cortez and Santos, 2016).

Recently, Fornero et al. (2019) provided insights of a new characterization of extrusive lavas forming pahoehoe and rubbly flows within the pre-salt succession of the Santos Basin, based on borehole image logs constrained by sidewall cores. These authors are providing with controlled hard evidence (side wall cores) of a, perhaps, voluminous magmatic activity in the pre-salt Santos Basin. Despite this study was conducted in Campos Basin, still, there is a great area where this magmatism was active and probably fed all these regions, from Espírito do Santo Basin up in the North to the Santos Basin in the South Brazilian margin.

However, few studies have documented the detailed architecture of the intrusive bodies and related structures in the southern Campos Basin (e.g. Oreiro et al., 2008). In the light of that, we propose for this study a geological characterization of some of the intrusion-related structures to help in understanding the possible effects on the hydrocarbon systems. For that, we used a three-dimensional post-stack seismic survey from the southern Campos Basin calibrated with a log suite of 7 wells.

## 3.2. GEOLOGICAL SETTING OF THE CAMPOS BASIN

Campos Basin is a South Atlantic rifted margin basin (Chang et al., 1992) developed on a gneissic Pre-Cambrian basement, with NE-SW striking direction, similar to the strike of major extension axis of the basin (Cainelli and Mohriak, 1999). The lateral movement associated with the NW-SE transfer faults influenced the development of the initial structures. Inherited-basement structures, NE-trending, were reactivated as horsts and grabens during the Mesozoic drifting phase. In addition, the Cretaceous basement in the Cabo Frio area presents antithetic faults, which propagated to the upper units of post-rift sedimentary sequences (Mohriak et al., 1995; Meisling et al., 2001; Fetter, 2009).

Silva et al. (2012) described a volcanic complex striking E-W of the Cabo Frio formation, from Late Paleocene to Middle Eocene. In this time, a large volume of magmatic rocks emplaced into the Cretaceous sedimentary sequences, during the thermal uplift, recording ages of 55±11, 54±2, 53±2, 50±7, and 44±1 Ma (Thomaz-Filho et al., 2008). The

intercalation of basaltic and andesitic dome-like shape sills and dykes with sedimentary packages suggests several magmatic pulses intruding the soft rock succession, over the Cabo Frio magmatic province in southern Campos basin (Ojeda, 1982; Cainelli and Mohriak, 1999).

According to Mizusaki and Mohriak (1992), several stratigraphic levels registered intrusive and extrusive rocks, which occur intercalated with volcaniclastic and sedimentary sequences. Lobo et al. (2006) conducted geochemical studies in Pelotas and Campos Basins that led to the characterization of the tholeiitic basalts. Oreiro et al. (2008) also emphasized the largest occurrence of volcanic rocks, from Late Cretaceous to Early Tertiary, predominantly extrusive over intrusive rocks, and according to Thomaz-Filho et al. (2008), the former played a major role in the petroleum geology of the Albian Macaé Group.

Overall, two main phases of magmatic activity are responsible for the extrusive and intrusive igneous rocks in the Campos and Santos Basins, in the Early Cretaceous associated with the rifting stage and in the Late Cretaceous to Eocene, the latter more associated with intrusions (Mohriak et al., 2003).

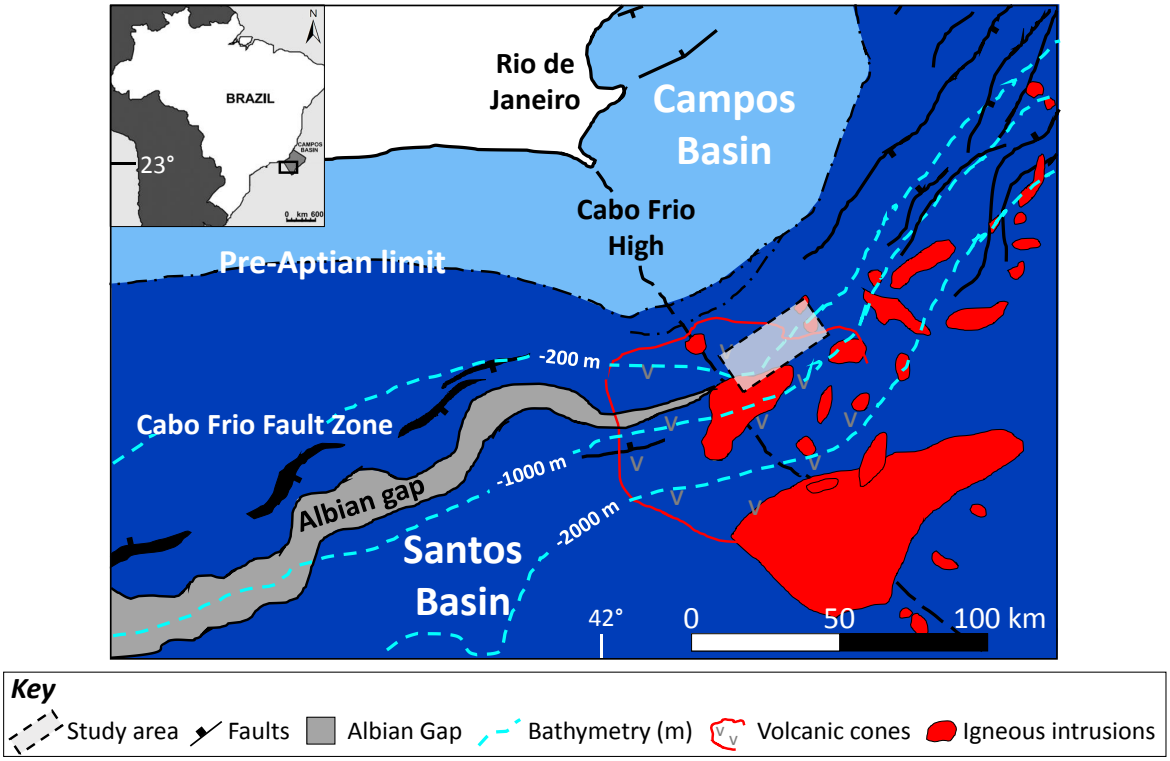


**Fig. 1.** Geological setting of Campos Basin depicting the location of the main faults, volcanic cones, and igneous intrusions (modified from Mohriak et al., 2008).

## 3.3. DATABASE AND METHODS

Located in the southern part of the Campos basin, the 3-D seismic data used covers approximately 183 $km^2$ (Fig. 1). The seismic inline and crossline spacing is 18.75 and 12.50 m, respectively. The seismic totalizes a record length of 4996 milliseconds with a vertical sampling interval of 4 milliseconds in two-way time (ms TWT). The dominant frequency is roughly 35 Hz within 0 to 125 Hz of total frequency content. The data is displayed accordingly to SEG standard polarity, i.e., a downward increase in impedance generates a positive amplitude reflection (Brown, 2008). We also used wireline log data from seven (7) boreholes consisting of gamma-ray, density, and sonic logs. The seismic data was calibrated using the wireline logs, specifically the density and sonic logs. This helped to tie some of the drilled igneous rocks to the seismic data.

The workflow is based on a 183 $km^2$ 3D post-stack seismic survey. This workflow can be divided into two main phases. The first one is the identification of seismic high-amplitude anomalies and their interpretation as igneous sills; later quantitative analyzed under certain morphometric parameters. The second phase is characterized by the application of volume rendering techniques (Thomson and Hutton, 2004) as an effective way of interpreting and extracting the characteristics of seismic-scale intrusion-related structures. The high-amplitude anomalies (HHA's) were extracted by opacity-rendering the mid-values of the amplitude spectrum. This method allows the extraction of geobodies, that is extremely useful for the calculation of magmatic volume and therefore to have a better idea of the impacted surrounding areas. In addition, it is possible to understand the sill-sill complex network and how the steps and junctions are related to interconnect the sills. We used indicator ratios to leave a possible, interpretation bias outside the estimation of the geometrical properties.

## 3.4. RESULTS

### 3.4.1. High-amplitude anomalies as sills

We have interpreted high-amplitude anomalies (HAA's) as igneous sills in the study area. These sills are generally characterized by blunt terminations (Fig. 2). We grouped the interpreted sills into three main types according to Planke et al. (2005) classification: strata-concordant sills (or layer-parallel), transgressive sills, and saucer-shaped sills. Within

each sill type, we may distinguish their characteristics. In particular, stepped-like features for the transgressive sills, flat inner and outer sills for the saucer-shaped geometry and concordant top and base for the layer-parallel geometries.

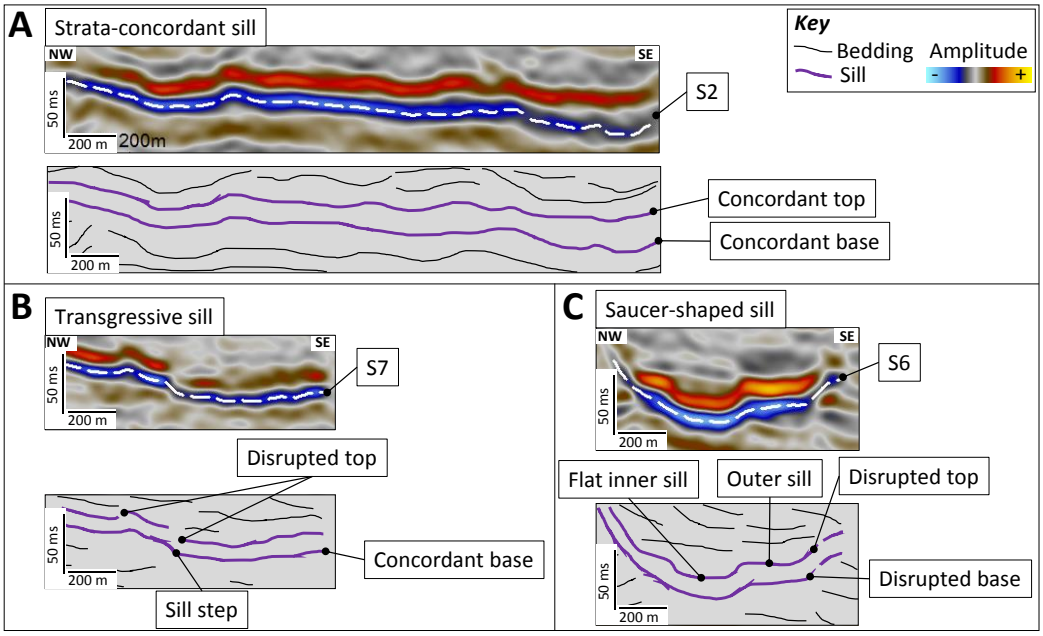


**Fig. 2.** Seismic dip sections highlighting geometric and strata relationship between intrusions (S2, S7, S6) and host rock bedding of (a) strata-concordant, (b) transgressive, and (c) saucer-shaped sills. To note that (a) show a relatively thicker and extensive strata-concordant sill, (b) a slight flat-ramp-flat geometry in the transgressive sill, (b) and (c) the disrupted top of sills, and (c) an approximately flat inner and outer sill.

### 3.4.2. Associated supra-sill deformation

These structures are interpreted as forced folds (Mathieu et al., 2008; Jackson et al., 2013) with dome-shaped strata overlying a saucer-shaped intrusion (S4) characterized by an inner and outer sill as well as inclined segments. This type of structures often occurs with faulting at the top (Jackson et al., 2013) as is shown in Figure 3. Furthermore, these saucer-shaped intrusions flex the country rock at a ratio between the sill length and sill depth ranging from 0.67 to 0.75. In particular, for the sill 4, the ratio is 0.72. Some of the sills occur associated with deformation in the overlain reflectors, and some do not.

Saucer-shaped sills (Type I, II and III), approximately 33% of the intrusions mapped are characterized by a ratio of 0.48-0.75 (0.63 mean). The ratio for the layer-parallel sills (Type V), which account for 47% of the intrusions of this study, ranges from 0.60 to 2.26 (1.26 mean). For the transgressive sills (Type IV), 20% of the intrusions, the ratio lie between 0.40 and 0.96 (0.63 mean).

Interpreted steps may suggest the direction of the emplacement of sills, as they are often parallel to the axis of sill emplacement described by Schofield et al. (2012).

On a more detailed observation, it is possible to note the effect intrusion has on the overburden by deforming it upwards; resulting in what it is called a forced fold (Jackson et al., 2013). Furthermore, the faults developed at the crest of this folded overburden strata may be a direct result of the emplacement of a sill. Either these faults may be sealed or leaky that will have a direct impact on the fluids entrapment or leakage.

The forceful intrusion of sill S4 originated the forced fold with faulted margins at both sides of the fold, in contrast with the also usually monoclinal folded flanks as in previous studies (e.g. Trude et al., 2003, Hansen and Cartwright 2006).

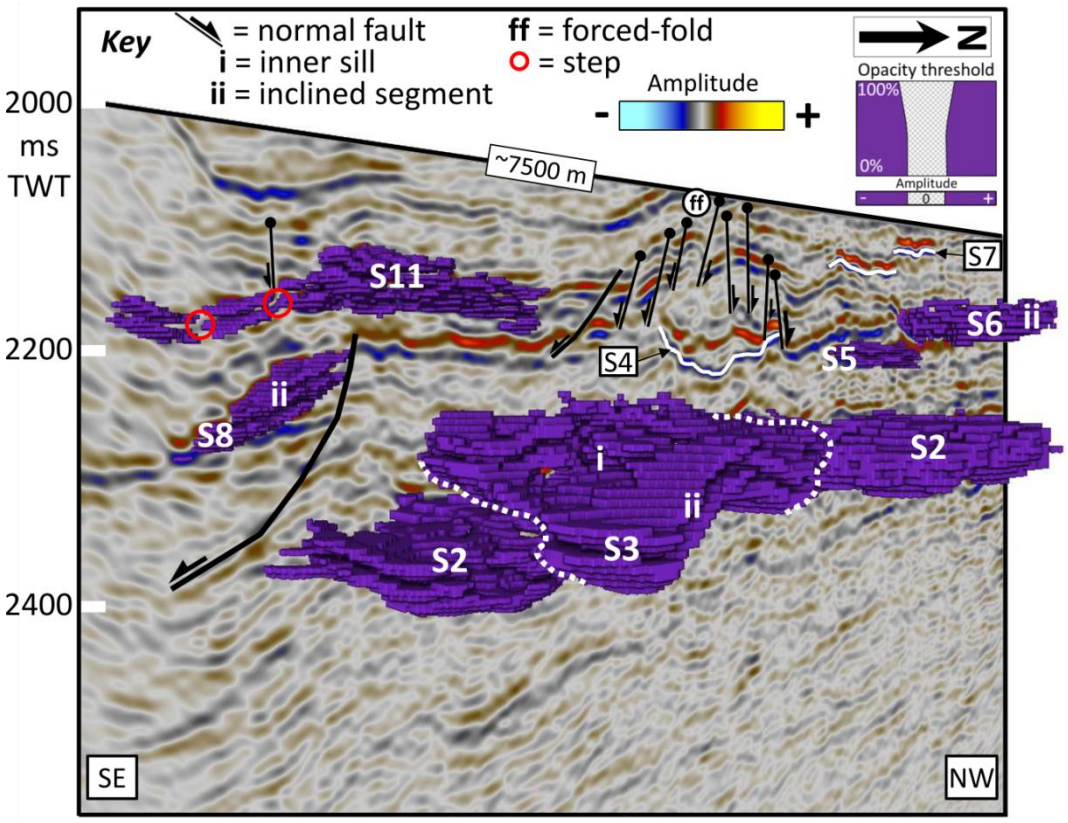


**Fig. 3.** NW-SE dip-oriented seismic section highlighting some of the extracted igneous geobodies and their relationship with the local faulting pattern and supra-sill deformation (forced-folds; ff). Note the sill S4 geometric shape influencing the overburden deformation by force-folding the overlying strata. Inner (i) and outer (ii) sill and steps (red circle) are also indicated. These geobodies extraction allow the calculation of the "true" magmatic volume.

### 3.4.3. Sub-vertical reflection-free seismic zones

The seismic chimney-like feature may be interpreted as a sub-vertical pipe, which is expressed as low-amplitudes reflections associated with an overlying convex-upward mound. These structures usually present a sub-circular morphology in plan view and a conic inverted geometry in cross-section (Magee et al., 2014). This feature may suggest focused fluid-flow produced (Fig. 4). These zones could also be comparable to the sub-vertical pipes that form at the sill edges and are associated with hydrothermal vent complexes defined by Planke et al. (2005) in the Vøring and Møre basins, and pipes defined by Hansen (2006) in the Paleocene sediments along northeastern Atlantic margin. These type of structures may also be associated with regions of intense fracturing and therefore with secondary migration of hydrocarbons. In addition, the top mounded structure may be useful for relative stratigraphic dating by targeting the morphological relationship between the surrounding reflectors onlapping onto the mounded structure.

The core of these structures could be associated to possible areas of higher concentration of hydrothermal fluids, which, in turn, may or may not enhance the porosity and permeability in this regions and in adjacent stratigraphic intervals. In particular, these structures may help the formation of petroleum reservoirs, such as travertines, or even silicification.

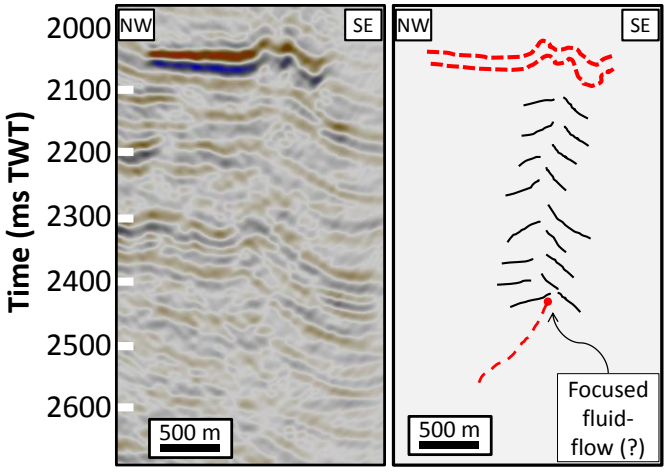


**Fig. 4.** NW-SE cross-sections of an example of a possible focused fluid-flow feature with several discontinuous and converging reflectors, underlying a slightly mounded and rugose high-amplitude anomaly (HHA). This could also describe a structure with an intense fracturing depending on the interpretation context, which may have an influence on secondary migration.

### 3.4.4. Junctions

We identified seismic features, similar to potential ‘T’ and ‘J’ shaped junction geometries that are connecting different sills upwards through a peripheral inclined limb on the inner saucers. It is possible to see the sill-to-sill junction facilitating an upwards stepping (Fig. 5). These pieces of evidence, such as sill abutment, are the type of geometrical features that form sill complexes, which may provide insights into the magmatic emplacement. This sill-to-sill interaction defined by the several types of junctions form the system connectivity and allows constraining the associated magma flow pattern (e.g. Cartwright and Hansen, 2006; Thomson, 2007). In addition, these external structures associated with sill complexes may have an important role on the secondary migration of hydrocarbons within petroleum systems (e.g., England, 1994).

In this example (Fig. 5) we may infer the main direction of the propagation of magma towards the northwest. This connection of the sills could also be through a dyke. However, igneous dykes usually appear as chaotic to a low-frequency seismic chimney feature along with a sub-vertical path connected to another igneous structure. These sill-to-sill junctions may also be a consequence of overlapping sill tips (Alves et al., 2015). Usually, overlapping sills result in constructive interference of the seismic signal (Magee et al., 2015). In the Figure 5, we actually cannot distinguish whether we are seeing a thick sill or an overlap of different sills. This difficulty in that distinction maybe related to the tuning effect of the seismic. That is one of the reasons for the extremely difficult that exist in mapping the correct form and estimating the true thickness of these sills.

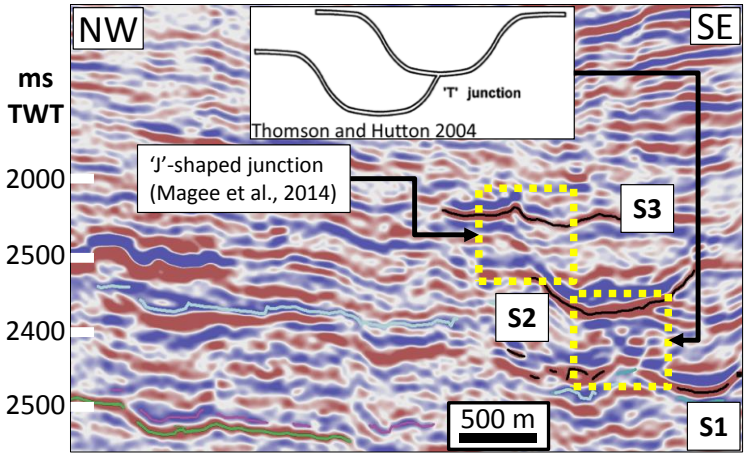


**Fig. 5.** NW-SE cross-sections of the ‘J’ and ‘T’ type sill-to-sill junction connecting different sills (S1, S2, and S3) and having a potential impact on the secondary migration processes of hydrocarbons.

### 3.4.5. Intrusion-related vent structures

We interpreted a seismic dome-shaped cross-sectional feature with a chaotic internal reflection configuration, and flat-lying concordant underlying reflectors (Fig. 6). The vent is approximately circular to elongate in plan view. From the cross-sectional point of view, the vent is characterized by highly dipping flanks toward the central axis and lower dipping angle flanks toward the margin. This vent structure is comparable to the structures recognized by Planke et al. (2005). The interpreted mound occur onlapped by overlying reflectors, which suggests a strong relationship with the overburden as described by Hansen (2006).

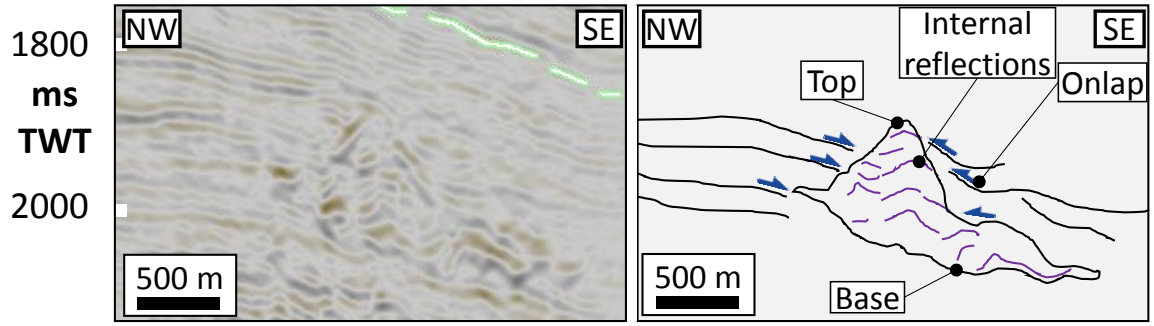


**Fig. 6.** NW-SE cross-sections of a mounded-like feature resembling volcanoes with top surface onlapped by apparently younger strata.

## 3.5. ARCHITECTURE OF MAGMATIC SILLS

Based on volume and opacity-rendering technique, it was possible to extract geobodies of the sill-sill complex network from the three-dimensional seismic cube (Fig. 7). It is possible to see how interconnected the interpreted sills are with one another by step, bridge, and junction structures.

From the volume and opacity-rendering technique applied to the interpreted anomalies (S2, S3, S5, S6, S8, S11, S14, S15) we may describe them with inner and thick zones grading to thin and slight to abrupt transgressing limbs. The top and base of the anomalies were extracted by opacity-rendering the mid-values of the amplitude spectrum as is possible to see in the opacity threshold insets in Figure 7.

The sill 2 (S2) is characterized by a low-frequency range feature. This is due to the slight transgressing segment of the southeastern portion of the sill. In addition, between

the portion well imaged and the one poorly-imaged occurs a discontinuity, inferred from the variance time slice panel, and also shown in Figure 7B.

An intriguing feature of the sill 2 (S2) and 3 (S3) is the small sub-circular features, also characterized by a low-frequency range, occurring in the portion well imaged (Fig. 7B and Fig. 7C). Both low-frequency features may suggest regions of depleted magma supply, described by Alves et al. (2015) as internal depletion zone, in similar structures. This zones might also suggest, the presence of faults intersecting the anomaly, and the transition between the inner sill and outer sill through an inclined limb and steps as depicted by sill 6 body in Figure 7D.

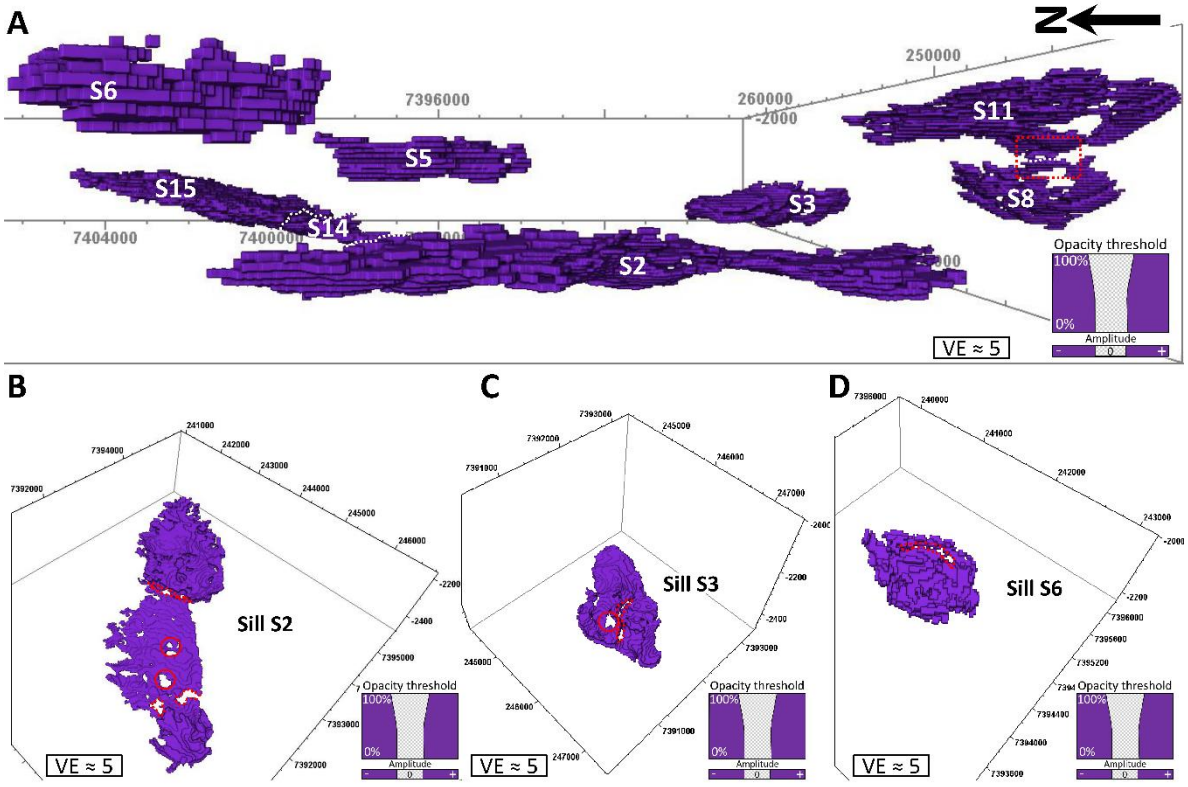


**Fig. 7.** (A) Volume rendering of the extracted geobodies characterizing the intrusive bodies. (B-D) Opacity-rendered layer-parallel (S2) and saucer-shaped (S3, S6) sills. The red-dotted circles in each of the sills highlights voxel-free zones are interpreted as possible magma depletion and red-dotted polygons as faults. In addition, there is the possibility to calculate the magmatic volume. The threshold of the amplitudes used to isolate and extract the geobodies are shown in the opacity panels.

## 3.6. DISCUSSION

The intrusion-related structures found in this study are comparable to the magma fingers described by Schofield et al. (2010) and Magee et al. (2015) and the forced folds described by Hansen and Cartwright (2006), Hansen et al. (2008) and Jackson et al. (2013). The intrusion fingers are expected as an elongated small-scale structure comprised by series of saucer-shaped sill lobes that suggests different phases of intrusion (Walker, 2016). In this study, the formation of forced folds agrees with the ratio between the sill length and the sill, previously described. In particular, Mathieu et al. (2008) described a ratio larger than 0.5-0.6 necessary to flex the overlain strata, based on analogue modeling experiments, for the cup-shaped intrusions that are similar in geometry to the saucer-shaped intrusions.

### 3.6.1. The relation between supra-sill deformation and underlying sills

Sill length-to-depth ratio, which gives a quantitative idea of the how likely is the overburden deformed due to the emplacement of an igneous sill, in this study, ranges between 0.40 and 2.26 (0.92 mean). Saucer-shaped sills (Type I, II and III), approximately 33% of the intrusions mapped are characterized by a ratio of 0.48-0.75 (0.63 mean). The ratio for the Layer-Parallel sills (Type V), which account for 47% of the intrusions of this study, ranges from 0.60 to 2.26 (1.26 mean). For the transgressive sills (Type IV), 20% of the intrusions, the ratio lies between 0.40 and 0.96 (0.63 mean) (Table 1 and Fig. 8).

In previous studies, were found ratios of 0.5-0.6 for cup-shaped intrusions (e.g. Mathieu et al., 2008). Mathieu et al. (2008) found that for cup-shaped intrusions, the country rocks upwards deform once this ratio is greater than 0.5-0.6. In our study, 66% of the sills mapped with a ratio between 0.67-2.09 (1.09 mean) have a supra-sill deformation, previously inferred from the seismic interpretation. It is important to refer that this kind of workflow is a major since it tries to leave the interpreter bias outside the estimations of sill geometric properties.

Even though there is an apparent relationship between the interpreted sills and overlying forced-folded strata, we always have to consider the great amount of uncertainty that is implicit. In particular, there is a significant uncertainty between the geometries and architecture of sill complexes seismically imaged in the subsurface and the true geometries seen exposed in outcrops (Magee et al., 2015; Eide et al., 2017). However, it is extremely

difficult or almost impossible to map the magmatic sills without seismic data, which, in turn, is of very low resolution if we want, for example, to see something varying a couple of meters that we would be able to see in outcrops. Therefore, we would only be able to see seismic events related to igneous intrusions that are more thick than 1/8 the wavelength (limit of detectability, see Magee et al., 2015), and to map those more thick than 1/4 the wavelength of the seismic data (limit of separability, see Magee et al., 2015).

Magmatic sills often occur as reflection tuned packages, where we hardly can separate and distinguish the top and base of the intrusion and for example measure their true thickness (Mark et al., 2018). Therefore, when analyzing these types of structures one need to be careful on what the interpretations are being made on so it is possible to avoid possible overestimation or underestimation of the true thicknesses of the structures and therefore their effects.

**Table 1.** Summary of the ratios between the measured characteristics of mapped sills.

| Sill | Sill type | Area (km2) | Height/long axis ratio | Height/depth ratio | Sill-length/depth ratio | Supra-sill deformation (Y/N) |
|---|---|---|---|---|---|---|
| S1 | I | 1.12 | 0.06 | 0.03 | 0.48 | N |
| S2 | VI | 7.55 | 0.02 | 0.05 | 2.09 | Y |
| S3 | II | 1.79 | 0.06 | 0.04 | 0.75 | Y |
| S4 | I | 1.61 | 0.09 | 0.07 | 0.72 | Y |
| S5 | V | 1.16 | 0.06 | 0.04 | 0.65 | N |
| S6 | I | 1.67 | 0.07 | 0.05 | 0.67 | Y |
| S7 | IV | 0.43 | 0.13 | 0.05 | 0.40 | N |
| S8 | IV | 3.12 | 0.09 | 0.09 | 0.96 | Y |
| S9 | IV | 0.82 | 0.06 | 0.03 | 0.54 | N |
| S10 | V | 2.11 | 0.03 | 0.02 | 0.68 | N |
| S11 | V | 4.39 | 0.04 | 0.06 | 1.37 | Y |
| S12 | VI | 0.85 | 0.06 | 0.03 | 0.60 | Y |
| S13 | VI | 4.21 | 0.05 | 0.05 | 1.14 | N |
| S14 | III | 1.27 | 0.11 | 0.06 | 0.54 | N |
| S15 | VI | 14.35 | 0.03 | 0.07 | 2.26 | N |

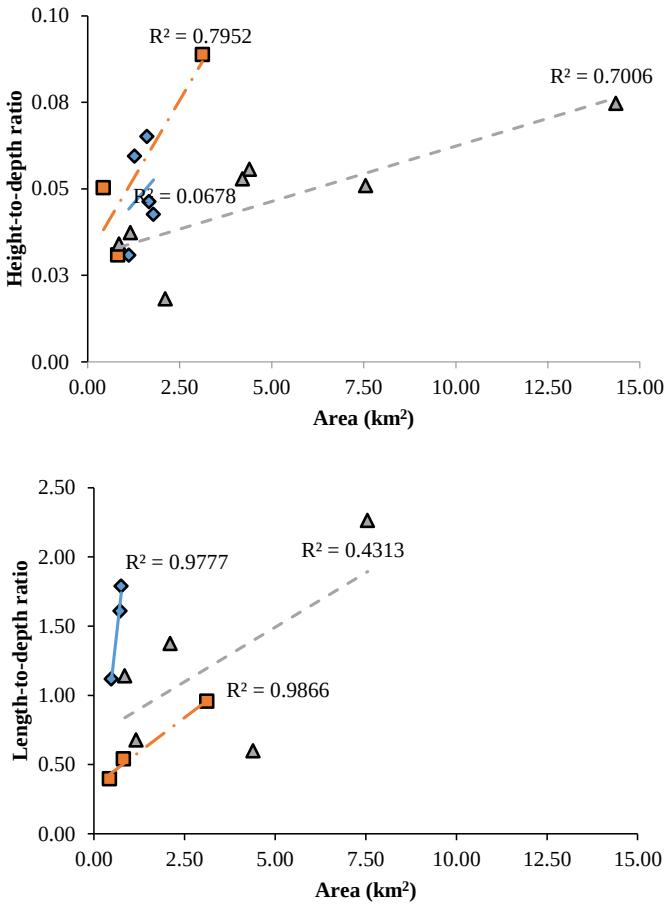


**Fig. 8.** Cross-plots with linear regressions for the morphometric parameters of each sill type (I to V), grouped into saucer-shaped (blue lozenges), transgressive (orange squares), and layer-parallel sills (green triangles).

### 3.6.2. Magma flow pattern

The magma flow direction is inferred from the stepped-like features of the igneous intrusions as well as body separation suggesting magma lobes separation (Schofield et al., 2012). Sill structures, like steps, bridges, and junctions are all magma flow indicators, developed along the direction of magma flow, at distal areas (Thomson, 2007; Schofield et al., 2012).

According to Magee et al. (2013), magma evolution can be partly known using the architecture of the sill-sill network as a tool for unveiling some of the igneous structures.

Sill steps that tend to climb the stratigraphy are consistent with features observed in the Streymoy sill, Faroe Islands (e.g. Walker, 2016). The distinct separated transgressive reflectors suggest sills splitting into separate segments while accommodated by the host rock.

## 3.7. CONCLUSIONS

We report a new study of magmatic sill related structures for the southern Campos Basin, southeastern Brazilian margin. In this study, we focused on the relationship between the magmatic sills and their related structures, i.e. forced folds, sub-vertical reflection-free seismic zones, junctions, steps, bridges, and vents, formed by associated supra-sill deformation, focused fluid flow, and magma flow pattern. A borehole integration with three-dimensional seismic data allow drawing some of the following conclusions:

(1) The architecture of the sub-volcanic sills emplaced in the southern Campos Basin allowed the characterization of the related structures (i.e. forced folds, junctions, and vents) that may help to constrain the volcanic activity in the study area.

(2) The volcanic structures may have a great impact on the petroleum systems in the study area and can be used to understand the impact of volcanic activity in other basins. In particular, the impacts in the secondary migration processes through the creation of new pathways for the hydrocarbons, and in the petrophysical properties, specifically the porosity and permeability enhancement through hydrothermal-induced activity.

(3) The evidence of connected and superposed sills on different levels suggest an emplacement through common and, perhaps, shared routes that led to the formation of the sill complex at the Cabo Frio High volcanic province.

(4) The emplacement of saucer-shaped sills is often accommodated by the development of forced-fold structures on the overburden. This forceful injection of sills often creates a series of local faults also on the overburden. This type of structure can be economically important as they may compartmentalize interest intervals.

(5) Sill length-to-depth ratio, which provides the likelihood of the overburden deformation due to the emplacement of an igneous sill, in this study, ranges between 0.40 and 2.26 (0.92 mean). In addition, 66% of the sills mapped with a ratio between 0.67-2.09 (1.09 mean) have a supra-sill deformation.

(6) Despite the emplacement of saucer-shaped sills favors forced-fold structures, not always that the indicator ratio, from which country rock is flexed, are at least 0.5-0.6 it forms a forced fold. This evidence suggests at least other controlling factors for the formation of intrusion-related forced folds. As for example the difference between the length and the thickness of the overburden may also influence the formation of forced

folds through the local stress field orientation at the sill tips that changes during the intrusion.

(7) Interpreted steps and junctions may suggest the direction of the emplacement of sills, as they are often parallel to the axis of sill emplacement.

(8) The volume and opacity-rendering technique applied allowed the extraction of interpreted HHA's (S2, S3, S5, S6, S8, S11, S14, S15) characterized by inner and thick zones grading to thin and slight to abrupt transgressing limbs that helps to constrain the volume of the magmatic emplacement. This in turn, may also help to constrain the local basin setting by correlating the magmatic activity with the margin rifting.

(9) This study also highlights the importance of using volume rendering techniques and extraction of geobodies as an effective way of interpreting the sub-volcanic structures and extracting the characteristics of a sill complex architecture.

## ACKNOWLEDGEMENTS

The authors gratefully acknowledge Equinor for supporting this research, and Sinochem and PGS for allowing the publication of the seismic data. This study was financed in part by Coordenação de Aperfeiçoamento de Pessoal de Nível Superior - Brasil (CAPES) - Finance Code 001. National Petroleum Agency's (ANP) Exploration and Production Database (BDEP) is appreciated for providing seismic and well log data. The authors also appreciate the academic software licenses provided by dGB Earth Sciences for OpendTect, Schlumberger for Petrel, IHS Markit for Kingdom.

## REFERENCES

Almeida, J.C.H de., Heilbron, M.C.P.L., Schmitt, R.S., Valeriano, C.M., Rubim, I.N., Mohriak, W.U., Júnior, D.L.M., Tetzner, W. 2013. Guia de campo na Área Continental do Alto de Cabo Frio. Boletim de Geociências da Petrobras, 21(2), 325-355.

Alvarenga, R.S., Iacopini, D., Kuchle, J., Scherer, C.M.S., Goldberg, K., 2016. Seismic characteristics and distribution of hydrothermal vent complexes in the Cretaceous offshore rift section of the Campos Basin, offshore Brazil. Marine and Petroleum Geology, 74, 12-25, https://doi.org/10.1016/j.marpetgeo.2016.03.030.

Alves, T.M., Omosanya, K.D., Gowling, P., 2015. Volume rendering of enigmatic high-amplitude anomalies in southeast Brazil: A workflow to distinguish lithologic features from fluid accumulations. Interpretation, 3(2), A1-A14, http://dx.doi.org/10.1190/INT-2014-0106.1.

Barnett, Z.A., Gudmundsson, A. 2014. Numerical modelling of dykes deflected into sills to form a magma chamber. Journal of Volcanology and Geothermal Research, 281, 1-11, https://doi.org/10.1016/j.jvolgeores.2014.05.018.

Brown, A. 2008. Phase and Polarity Issues in Modern Seismic Interpretation. In AAPG International Conference and Exhibition. AAPG, Cape Town, 1-22.

Cainelli, C., Mohriak, W.U., 1999. Some remarks on the evolution of sedimentary basins along the Eastern Brazilian continental margin. Episodes Journal of International Geoscience, 22(3), 206-216.

Chang, H.K., Kowsmann, R.O., Figueiredo, A.M.F., Bender, A.A., 1992. Tectonics and stratigraphy of the East Brazil rift system: an overview. Tectonophysics, 213(1-2), 97-138, http://dx.doi.org/10.1016/0040-1951(92)90253-3.

Cortez, M.M.M., Santos, M.A.C., 2016. Seismic interpretation, attribute analysis, and illumination study for targets below a volcanic-sedimentary succession, Santos Basin, offshore Brazil. Interpretation, 4(1), SB37-SB50, http://dx.doi.org/10.1190/INT-2015-0097.1.

Davies, R., Bell, B.R., Cartwright, J.A., Shoulders, S., 2002. Three-dimensional seismic imaging of Paleogene dike-fed submarine volcanoes from the northeast Atlantic margin. Geology, 30(3), 223-226, http://dx.doi.org/10.1130/0091-7613(2002)030<0223:TDSIOP>2.0.CO;2.

De Luca, P., Carballo, J., Filgueiras, A., Pimentel, G., Esteban, M., Tritlla, J., Villacorta, R., 2015. What is the Role of Volcanic Rocks in the Brazilian Pre-salt?. In 77th EAGE Conference and Exhibition, https://dx.doi.org/10.3997/2214-4609.201412890.

Eide, C.H., Schofield, N., Jerram, D.A., Howell, J.A., 2016. Basin-scale architecture of deeply emplaced sill complexes: Jameson Land, East Greenland. Journal of the Geological Society, http://dx.doi.org/10.1144/jgs2016-018.

Eide, C.H., Schofield, N., Lecomte, I., Buckley, S.J., Howell, J.A., 2017. Seismic interpretation of sill complexes in sedimentary basins: implications for the sub-sill imaging problem. Journal of the Geological Society, 175(2), 193-209, https://dx.doi.org/10.1144/jgs2017-096.

England, W.A., 1994. Secondary Migration and Accumulation of Hydrocarbons: Chapter 12: Part III. Processes.

Fetter, M. 2009. The role of basement tectonic reactivation on the structural evolution of Campos Basin, offshore Brazil: Evidence from 3D seismic analysis and section restoration. Marine and Petroleum Geology, 26(6), 873-886, http://dx.doi.org/10.1016/j.marpetgeo.2008.06.005.

Fornero, S.A., Marins, G.M., Lobo, J.T., Freire, A.F.M., de Lima, E.F., 2019. Characterization of subaerial volcanic facies using acoustic image logs: Lithofacies and log-facies of a lava-flow deposit in the Brazilian pre-salt, deepwater of Santos Basin. Marine and Petroleum Geology, 99, 156-174, https://doi.org/10.1016/j.marpetgeo.2018.09.029.

Goulty, N.R., Schofield, N. 2008. Implications of simple flexure theory for the formation of saucer-shaped sills. Journal of Structural Geology, 30, 812-817, http://dx.doi.org/10.1016/j.jsg.2008.04.002.

Hansen, D.M. 2006. The morphology of intrusion-related vent structures and their implications for constraining the timing of intrusive events along the NE Atlantic margin. Journal of the Geological Society, 163(5), 789-800, https://doi.org/10.1144/0016-76492004-167.

Hansen, D.M., Cartwright, J., 2006. The three-dimensional geometry and growth of forced folds above saucer-shaped igneous sills. Journal of Structural Geology, 28(8), 1520-1535, https://doi.org/10.1016/j.jsg.2006.04.004.

Hansen, D.M., Cartwright, J.A., Thomas, D., 2004. 3D seismic analysis of the geometry of igneous sills and sill junction relationships. Geological Society, London, Memoirs, 29(1), 199-208, https://doi.org/10.1144/GSL.MEM.2004.029.01.19.

Hansen, D.M., Redfern, J., Federici, F., Di Biase, D., Bertozzi, G., 2008. Miocene igneous activity in the Northern Subbasin, offshore Senegal, NW Africa. Marine and Petroleum Geology, 25(1), 1-15, https://doi.org/10.1016/j.marpetgeo.2007.04.007.

Holford, S.P., Schofield, N., Jackson, C.L., Magee, C., Green, P.F., Duddy, I.R., 2013. Impacts of igneous intrusions on source reservoir potential in prospective sedimentary basins along the western Australian continental margin. West Australian Basins Symposium, Perth, WA, 18-21 August.

Hutton, D.H.W. 2009. Insights into magmatism in volcanic margins: bridge structures and a new mechanism of basic sill emplacement–Theron Mountains, Antarctica. Petroleum Geoscience, 15(3), 269-278, http://dx.doi.org/10.1144/1354-079309-841.

Jackson, C.A.-L, Schofield, N., Golenkov, B., 2013. Geometry and controls on the development of igneous sill–related forced folds: A 2-D seismic reflection case study from offshore southern Australia. Geological Society of America Bulletin, 125(11-12), 1874-1890, http://dx.doi.org/10.1130/B30833.1.

Lobo, J.T., Duarte, B.P., Szatmari, P., Valente, S.C., 2016. Basaltos continentais do Cretáceo Inferior da bacia de Campos, SE do Brasil: compilação de dados e petrogênese. Revista Brasileira de Geociências, 37(2), 204-236.

Magee, C., Jackson, C.A.-L., Schofield, N., 2013. The influence of normal fault geometry on igneous sill emplacement and morphology. Geology, 41(4), 407-410, http://dx.doi.org/10.1130/G33824.1.

Magee, C., Jackson, C.A.-L., Schofield, N., 2014. Diachronous sub- volcanic intrusion along deep- water margins: insights from the Irish Rockall Basin. Basin Research, 26(1), 85-105, http://dx.doi.org/10.1111/bre.12044.

Magee, C., Maharaj, S.M., Wrona, T., Jackson, C.A.-L., 2015. Controls on the expression of igneous intrusions in seismic reflection data, https://doi.org/10.1130/GES01150.1.

Magoon, L.B., Dow, W.G., 1994. The petroleum system – from source to trap: AAPG Memoir 60. American Association of Petroleum Geologists, Tulsa, 25-49.

Mark, N.J., Schofield, N., Pugliese, S., Watson, D., Holford, S., Muirhead, D., Brown, R., Healy, D., 2018. Igneous intrusions in the Faroe Shetland basin and their implications for hydrocarbon exploration; new insights from well and seismic data. Marine and Petroleum Geology, http://dx.doi.org/10.1016/j.marpetgeo.2017.12.005.

Mathieu, L., De Vries, B.V.W., Holohan, E.P., Troll, V.R. 2008. Dykes, cups, saucers and sills: Analogue experiments on magma intrusion into brittle rocks. Earth and Planetary Science Letters, 271(1-4), 1-13, https://doi.org/10.1016/j.epsl.2008.02.020.

Matias, H.C., Ninci, B., Guangsheng, X., Pessoa, M.C., Mattos, F., Margem, R., Carballo, J., Esteban, M., Tritlla, J., Loma, R., Pimentel, G., 2015. Unlocking Pandora-Insights from Pre-salt Reservoirs in Campos and Santos Basins (Offshore Brazil). In 77th EAGE Conference and Exhibition, https://dx.doi.org/10.3997/2214-4609.201412891.

Mavko, G., Mukerji, T., Dvorkin, J., 2009. The rock physics handbook: Tools for seismic analysis of porous media. 2nd edition. New York: Cambridge University Press. 524p.

Meisling, K.E., Cobbold, P.R., Mount, V.S., 2001. Segmentation of an obliquely-rifted margin, Campos and Santos basins, southeastern Brazil. AAPG Bulletin, 85(11), 1903-1924.

Mizusaki, A.M.P., Mohriak, W.U. 1992. Seqüências Vulcano-sedimentares na Região da Plataforma Continental de Cabo Frio, RJ. In: Congresso Brasileiro de Geologia, 37. São Paulo. Resumos expandidos, São Paulo: Sociedade Brasileira de Geologia, 2, 468-469.

Mohriak, W., Nemčok, M., Enciso, G., 2008. South Atlantic divergent margin evolution: rift-border uplift and salt tectonics in the basins of SE Brazil. Geological Society, London, Special Publications, 294(1), 365-398, http://dx.doi.org/10.1144/SP294.19.

Mohriak, W.U., Paula, O.B., Szatmari, P., Sobreira, J.F.F., Parsons, M., MacQueen, J., Undli, T.H., Berstad, S., Weber, M., Horstad, I., 2003. Volcanic provinces in the Eastern Brazilian margin: geophysical models and alternative geodynamic interpretations. In 8th International Congress of the Brazilian Geophysical Society.

Mohriak, W.U., Macedo, J.M., Castellani, R.T., Rangel, H.D., Barros, A.Z.N., Latgé, M.A.L., Ricci, J.A., Mizusaki, A.M.P., Szatmari, P., Demercian, L.S., Rizzo, J.G., Aires, J.R.. 1995. Salt tectonics and structural styles in the deep water province of the Cabo Frio region, Rio de Janeiro, Brazil. In: M.P.A. Jackson, D.G. Roberts, and S. Snelson (eds), Salt tectonics: a global perspective. AAPG Memoir, 65, 273-304.

Ojeda, H.A.O. 1982. Structural framework, stratigraphy, and evolution of Brazilian marginal basins. AAPG Bulletin, 66(6), 732-749.

Omosanya, K.O., Johansen, S.E., Eruteya, O.E., Waldman, N., 2017. Forced folding and complex overburden deformation associated with magmatic intrusion in the Vøring Basin, offshore Norway. Tectonophysics, http://dx.doi.org/10.1016/j.tecto.2017.03.026.

Oreiro, S.G. 2006. Magmatismo e Sedimentação em uma Área na Plataforma Continental de Cabo Frio, Rio de Janeiro, Brasil, no intervalo Cretáceo Superior – Terciário. Boletim de Geociências da Petrobras, 14(1), 95-112.

Oreiro, S.G., Cupertino, J.A., Szatmari, P., Thomaz Filho, A. 2008. Influence of pre-salt alignments in post-Aptian magmatism in the Cabo Frio High and its surroundings, Santos and Campos basins, SE Brazil: An example of non-plume-related magmatism. Journal of South American Earth Sciences, 25(1), 116-131, http://dx.doi.org/10.1016/j.jsames.2007.08.00.

Planke, S., Rasmussen, T., Rey, S.S., Myklebust, R., 2005. Seismic characteristics and distribution of volcanic intrusions and hydrothermal vent complexes in the Vøring and Møre basins. In: A.G. Dore, and B.A. Vining (Eds.), North-West Europe and Global Perspectives: Proceedings of the Sixth Petroleum Geology Conference, Geological Society of London, 6, 833–844, http://dx.doi.org/10.1144/0060833.

Ran, Q., Wang, Y., Sun, Y., Yan, L., Tong, M., 2014. Volcanic gas reservoir characterization. Elsevier.

Schofield, N., Heaton, L., Holford, S.P., Archer, S.G., Jackson, C.A.-L., Jolley, D.W., 2012. Seismic imaging of ‘broken bridges’: linking seismic to outcrop-scale investigations of intrusive magma lobes. Journal of the Geological Society, 169(4), 421-426, http://dx.doi.org/10.1144/0016-76492011-150.

Schofield, N., Stevenson, C., Reston, T., 2010. Magma fingers and host rock fluidization in the emplacement of sills. Geology, 38(1), 63-66, http://dx.doi.org/10.1130/G30142.1.

Silva, O.B., Santos, P.R., Caixeta, L.B., Ribeiro, C., Barros, P. 2012. Main Trap Models of OGX's Oil Discovery from Albian/Cenomanian Carbonate Reservoirs—Cabo Frio High, Southern Campos Basin. In: N.C. Rosen, P. Weimer, S.C. dos Anjos, S. Henrickson, E. Marques, M. Mayall, R. Fillon, T. D'Agostino, A. Saller, K. Campion, T. Huang, R. Sarg, and F. Schroeder (eds), New Understanding of the Petroleum Systems of Continental Margins of the World: 32nd Annual, 32, 347-364. http://dx.doi.org/10.5724/gcs.12.32.0347.

Smallwood, J.R., Maresh, J., 2002. The properties, morphology and distribution of igneous sills: modelling, borehole data and 3D seismic from the Faroe-Shetland area. Geological Society, London, Special Publications, 197(1), 271-306, http://dx.doi.org/10.1144/GSL.SP.2002.197.01.11.

Svensen, H., Jamtveit, B., Planke, S., Chevallier, L., 2006. Structure and evolution of hydrothermal vent complexes in the Karoo Basin, South Africa. Journal of the Geological Society, 163(4), 671-682, http://dx.doi.org/10.1144/1144-764905-037.

Sydnes, M., Fjeldskaar, W., Løtveit, I.F., Grunnaleite, I., Cardozo, N., 2018. The importance of sill thickness and timing of sill emplacement on hydrocarbon maturation. Marine and Petroleum Geology, 89, 500-514, http://dx.doi.org/10.1016/j.marpetgeo.2017.10.017.

Thomaz-Filho, A.T, Mizusaki, A.M.P., Antonioli, L. 2008. Magmatismo nas bacias sedimentares brasileiras e sua influência na geologia do petróleo. Revista Brasileira de Geociências, 38(2), 128-137.

Thomson, K. 2007. Determining magma flow in sills, dykes and laccoliths and their implications for sill emplacement mechanisms. Bulletin of Volcanology, 70(2), 183-201, https://doi.org/10.1007/s00445-007-0131-8.

Thomson, K., Hutton, D. 2004. Geometry and growth of sill complexes: insights using 3D seismic from the North Rockall Trough. Bulletin of Volcanology, 66(4), 364-375, https://doi.org/10.1007/s00445-003-0320-z.

Tissot, B.P., Welte, D.H., 1984 Petroleum Formation and Occurrence. 2nd Edition, Springer-Verlag Berlin Heidelberg, 699 p., https://dx.doi.org/10.1007/978-3-642-87813-8.

Trude, J., Cartwright, J., Davies, R.J., Smallwood, J., 2003. New technique for dating igneous sills. Geology, 31(9), 813-816, http://dx.doi.org/10.1130/G19559.1.

Walker, R.J., 2016. Controls on transgressive sill growth. Geology, 44(2), 99-102, http://dx.doi.org/10.1130/G37144.1.

# 4. THE IMPACT OF FAULTS, FRACTURES, AND KARST IN CARBONATE ROCKS: EXAMPLES FROM A SANTOS BASIN PRE-SALT RESERVOIR

Ulisses M.C. Correia, Leandro H. Melani, Felipe M. Oliveira, Luana G. Lima, Michelle C. Kuroda, Alexandre C. Vidal

In preparation to be submitted to a peer-reviewed journal

# THE IMPACT OF FAULTS, FRACTURES, AND KARST IN CARBONATES: EXAMPLES FROM A SANTOS BASIN PRE-SALT RESERVOIR

## ABSTRACT

The presence of faults, fractures, karst structures in petroleum reservoirs has been a challenge in for the reservoir characterization. These post-depositional structures influence the overall assessment of the true potential and productivity that they might yield over the development and production years. Therefore, understanding how these structures relate to each other and quantify their impact on the static reservoir behavior is paramount, in the majority of the worldwide carbonate reservoirs that usually are classified as naturally fractured reservoirs. One of the tools commonly used to conduct reservoir characterization is the integration of the borehole image logs, wireline logs, and seismic data, core data when available, and outcrop analogue if possible. In this work, we used borehole image logs, conventional wireline logs, from two boreholes, and three-dimensional seismic data from the Barra Velha Formation in the pre-salt succession of Santos Basin for the characterization of faults, fractures, and karst in a carbonate reservoir. We applied a discrete fracture network modeling methodology to represent the fractures and faults as stochastic discrete and deterministic discrete elements in the geological model grid to build a dual-porosity, dual-permeability geological model. To assist the modeling stage, we first conducted regional fault and horizon interpretation on the seismic data in order to build a structural framework. Then we applied a multi-attribute analysis to detect high-amplitude anomalies possibly associated with karst structures, which is a possible indication for regions with increased porosity within the reservoir. We used the fracture data from borehole images to estimate the in situ tectonic stress field and the faulted horizons to estimate the local far stress field. The tectonic stress field corroborates the small-scale fractures (from borehole images) and the large-scale faults (from seismic interpretation).

**Keywords:** Faults, Fractures, Karst, Modeling, Pre-Salt Santos Basin

## 4.1. INTRODUCTION

The naturally fractured reservoirs (NFRs) in particular the ones from the Brazilian pre-salt are extremely heterogeneous in terms of the fracture network patterns (Matias et al., 2015). These carbonates present an apparent independence of sedimentary facies from the porosity and permeability. It is plausible that the fracture networks are controlling the distribution of the petrophysical properties. For a better reservoir characterization of NFRs, it is usual to do geological modeling of dual-medium systems (dual-porosity, dual-permeability - DPDP) considering matrix and fractures, which in turn, are modeled as discrete elements (DFN – Discrete Fracture Networks) within a geological grid (Correia et al., 2015; 2017). This type of fracture modeling is generally used to understand the relationship between the fracture networks and the petrophysical properties (Bourbiaux et al., 2002).

The fracture networks affect the transport efficiency of fluids (Valentini et al., 2007). The quantification of such efficiency impact remains a challenge. Fracture networks may be beneficial or detrimental for a variety of geological processes, increasing the fluid transport efficiency (Valentini et al., 2007). The impact of the fracture networks on oil and gas migration, implies a fluid transfer with or without significant modifications depending on the efficiency of transport (Valentini et al., 2007). Furthermore, fractures are critical to increase the productivity index on low-permeability geological formations (Santiago et al., 2016) and to evaluate the reservoir's potential in general (Procter and Sanderson, 2018).

Previous work have been successfully implementing different techniques to extract properties of a fracture network system using seismic data (e.g. Ben Amor et al., 2017), sub-seismic scale data from fieldwork (e.g. Santiago et al., 2016; Silva et al., 2017; Bisdom et al., 2017), and in a much smaller scale, from well log data (e.g. Sanderson and Nixon, 2015; 2018). All the previous efforts made to characterize complex fracture networks have been leading current research on challenging issues regarding fractures in geological formations (Correia and Schiozer, 2018). These structural features vary from isolated microscopic fissures to a kilometer-wide collection (“fracture swarms” or “corridors”) (Ghosh and Mitra, 2009). In order to understand the interplay between the fractures topological features and flow properties with implications in the quantification of the fluids transport efficiency and therefore the migration, efforts are being made. These efforts include research on mapping critical areas for the development of karst features (e.g. Yu et al., 2016), the

communicability indices (Santiago et al., 2016), and on the understanding of the connectivity of such fracture networks (Fang et al., 2017, Spagnuolo et al., 2018).

The characterization of paleokarst systems is still a challenge, due to the complex geometries at several scales, principally in the pre-salt reservoirs that are highly impacted. The karst-related features, which may have developed during the period of sub-aerial exposure (Wright and Barnett, 2017), are often revealed as seismic bright spot features (e.g. Zeng et al., 2011; Chen et al., 2012; Zhao et al., 2014; Yu et al., 2016). Previous authors connect these anomalies to karst structures within carbonate build-ups, in Kwanza (e.g. Saller et al., 2016) and Campos (e.g. De Luca et al., 2017) basins, as they may occur in pre-salt from the Santos Basin. Furthermore, these build-ups are characterized by great vuggy and cavernous porosities potentially influenced by high temperature or hydrothermal fluids and by the Mg-silicate to carbonate interaction (e.g. Tosca and Wright, 2015; Poros et al., 2017).

The interpretation of enigmatic seismic features, as karst structures, often requires processing techniques and seismic attributes to highlight information and to facilitate the overall understanding of the paleokarst system (Yu et al., 2016). Therefore, one of the objectives of this work is to test different computational techniques to reveal desired features by seismic attributes to guide a robust interpretation and to understand whether the karstification was beneficial or detrimental for the Barra Velha Formation.

The main objective of this work is to distribute the key fracture attributes in the geological grid so it is possible to provide insights on the high-density fracturing regions of the reservoir and overall enhancement of the prediction of natural fractures within carbonate reservoirs.

## 4.2. GEOLOGICAL SETTING OF THE SANTOS BASIN

Santos Basin is considered to be both a passive and active margin basin, greatly influenced by both passive and active basins formation mechanisms that overall shaped this basin in terms of the structural framework (e.g., Demercian, 1996; Zalán and Oliveira, 2005) that undergone two main periods of tectonic activity responsible for the overall structures spanning the basin (Fig. 1). These periods include, (1) the syn-rift tectonism, mainly characterized by the extension during the continental rifting between South America and West Africa, and (2) the post-rift tectonism succeeding thermally induced subsidence and relative rise of the sea level (Alves et al., 2017). Therefore, several asymmetric grabens and tilted-

block systems, as well as transfer fault structures took place (Davison, 2012). The overall stratigraphy of the basin is summarized into three main sedimentary sequences overlain the Early Cretaceous pre-rift basement igneous rocks. These sequences include the syn-rift, post-rift, and drift deposits separated by regional erosive unconformities (Davison, 2012). The continental breakup is characterized by a series of half-graben basins formation filled with non-marine strata of the Piçarras and Itapema Formations, overlain by the carbonates of the Barra Velha Formation with proximal microbial carbonates, stromatolites and laminites, and distal shales (Moreira et al., 2007). These carbonates are believed to be developed in a non-marine to transitional setting (Szatmari and Milani, 2016; Wright and Rodriguez, 2018). Noteworthy is the relatively fast accumulation of the Ariri Formation (the approximately 2 km-thick salt package) (Chang et al., 1992), which is overlying the carbonates of the Barra Velha Formation (Moreira et al., 2007). This evaporite sequence is a regional package at the end of the rifting stage and the beginning of a basinwide thermal stage over the Brazilian margin (Caixeta et al., 2014).

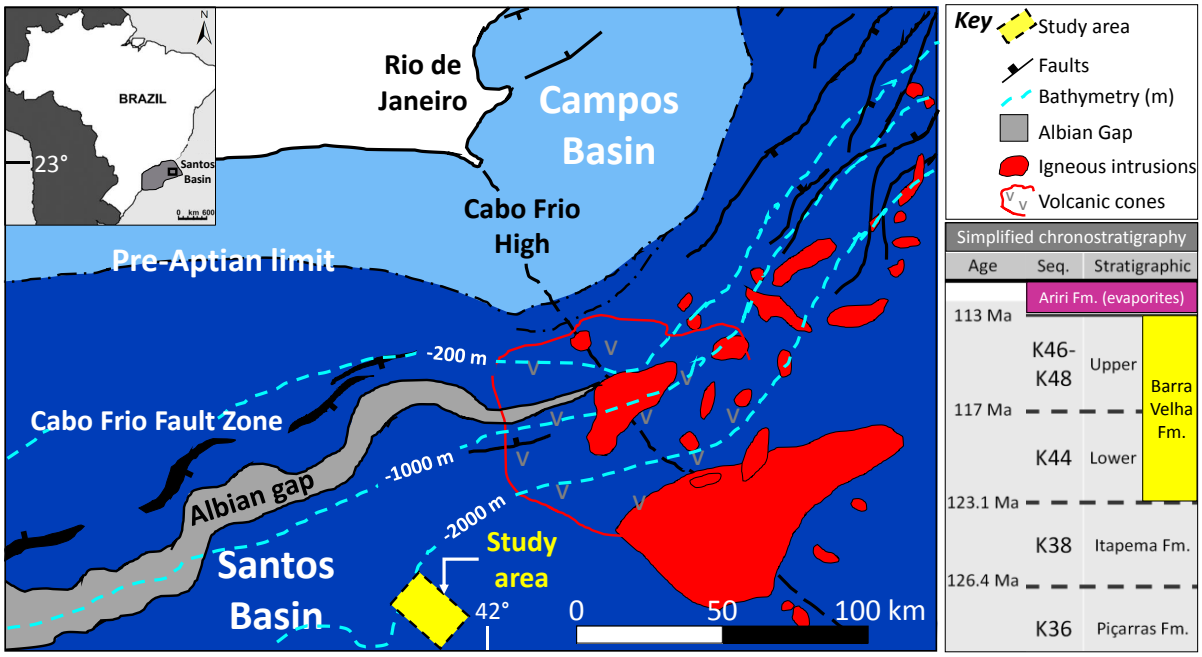


**Fig. 1.** Location of the study area (yellow polygon) within the Santos Basin (modified from Mohriak et al., 2008) and the simplified chronostratigraphic chart highlighting the Barra Velha Fm. of the pre-salt carbonate succession (modified from Moreira et al., 2007).

## 4.3. DATABASE

We used a 3-D seismic dataset 400 $km^2$. The inline and crossline bin size is 18.75 m, sampling 2000 samples at a 5 m rate. The data is zero-phase processed and the polarity convention we used followed the American convention for seismic display, which means a downwards increase in acoustic impedance generates a positive reflection, shown as a black loop peak (Brown, 2004). We also used borehole image logs and conventional wireline logs from two boreholes. This well database includes fracture point data, gamma ray, density, sonic, neutron porosity, permeability, water saturation, and net-to-gross logs.

## 4.4. METHODS

### 4.4.1. Faults interpretation

We used oriented seismic cross-sections and depth slices to interpret the main regional faults based on the recognition of the reflectors offset, abrupt changes in the dip and in seismic patterns, associated folding or sag and discontinuities in general. To characterize the structural framework, we followed a workflow that includes seismic data analysis (pre-conditioning), which means noise removal in order to increase the signal-to-noise ratio, and filtering when necessary to highlight major fault structures. Then, we computed several seismic discontinuity attributes, such as dip and azimuth, residual dip, variance, and variance-derived ant tracking volume.

These seismic discontinuity attributes highlight potential fault and fractures. However, the interpreted fault structures must be internally consistent by intersecting on different crossing lines in a reasonable way, meaning very small offsets in between. In the light of that, the quality control is a key step in this interpretation phase.

Despite the result from the attributes provided by the first cycle of seismic attributes generation, it might be still necessary to eliminate noise-related features (i.e., random noise, spikes, acquisition footprint) and try not to create artifacts, instead of highlighting real fault and fracture structures. In addition, it is necessary to highlight both large- and small-scale structures, since the seismic expression of noise is very similar to small-scale structures.

### 4.4.2. Fracture modeling

The fracture modeling was based on borehole image data (information of dip angle and dip azimuth of fracture sets), well logs (porosity, permeability, water saturation, and net-to-gross), main horizons and several small to large-scale faults from the seismic interpretation, and ant tracking seismic attribute as a geological driver. We used a workflow for the geological modeling (Cosentino, 2001). The workflow we used, included fractures as discrete elements and allows computing the fracture permeability and porosity (Bourbiaux et al., 2002; Fang et al., 2017). We distributed the fracture intensity (P32, Dershowitz and Herda, 1992) per fracture set into the geological grid conditioned to ant tracking volume.

We used a sector model derived from a full-field static model grid to first generate the discrete fracture networks, estimate the petrophysical properties within the fracture networks divided by different fracture sets according to the type (open or closed, and continuous or discontinuous). Due to the high computational cost we had to first built a sector model (a smaller portion of the full-field model) to compute the representation of individual fractures as discrete features, which is the Discrete Fracture Network (DFN) modeling approach (Dershowitz and Herda, 1992). For the scale averaging of the network properties into the geological grid, we used the statistical method of Oda (Oda, 1985). This method allows for fast testing the iterative process of generating the petrophysical properties from the discrete fractures into the geological grid. The Oda method is the simplest amongst the available ones in commercial software, which uses the total area of the fracture network to calculate secondary porosity and permeability in each grid-cell and performs a numerical integration for the implicit fractures. However, the Oda method assumes an upscaled fracture network fully connected that leads to overestimation of the degree of communication, and hence the permeability of the system (Chesnaux et al., 2009; Vaughan et al., 2015).

### 4.4.3. Karst characterization

We used a multiattribute approach to detect and characterize the high-amplitude anomalies (bright spots) possibly associated with karst features. This may help to guide a robust interpretation and to understand the karst development. The bright spots were detected by texture attributes, using a combination of Hilbert transform, Energy, and Gray-Level Co-occurrence Matrix (GLCM) Maximum Probability (Chopra and Marfurt, 2007; Yenugu et al.,

2010). We conducted an interpretation of seismic bright spots that usually relates to karst-related features.

## 4.5. RESULTS

### 4.5.1. Fault framework interpretation

The interpreted faults are associated with the syn-rift and sag sections. This interpretation allowed obtaining a glimpse of the overall regional faults framework. To obtain the discontinuity volume we tested a series of discontinuity attributes. In particular, in the Sag section, the discontinuities show an overall strike (ENE-WSW to E-W) different from the well-established strike of the NW-trending Syn-Rift section. The variability in the interval of interest suggests a spatial correlation between the major Syn-Rift and the Sag structures. Thus, apparently, the Syn-Rift structures have conditioned the smaller sag structures. In addition, major NW-trending faults occur near the wells (Fig. 2).

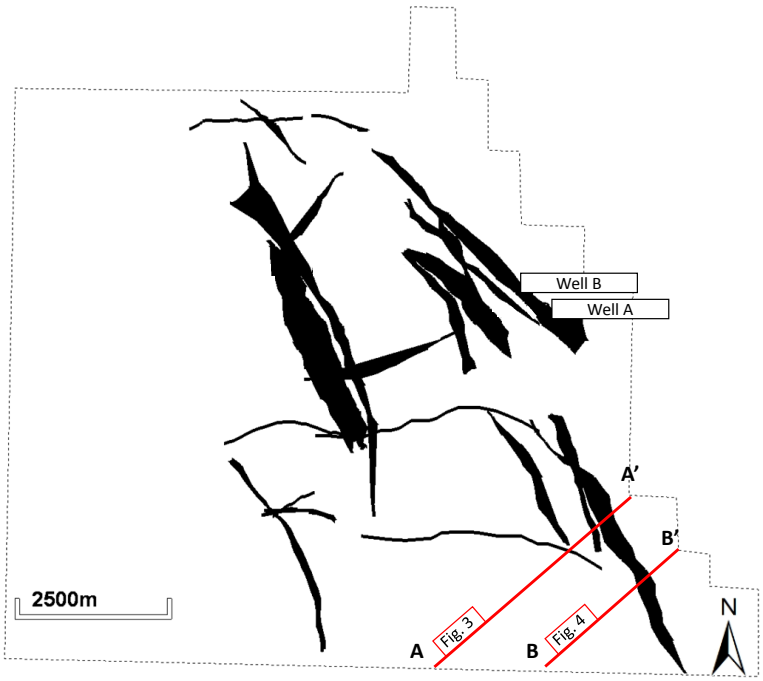


**Fig. 2.** The main regional faults and lineaments are depicted over the study area. Note that the overall strike is NW-SE with fewer structures in a different direction (ENE-WSW to E-W).

The interpreted faults are crossing seismic units correlated to the Syn-Rift, Lower Sag, and Upper Sag sections (Fig. 3). From the cross-sections, we recognize an apparent increase in thickness of the NW-trending Syn-Rift hanging-wall faults that suggests a relatively large throw when compared with the other smaller faults (i.e., the ENE-WSW to E-W) (Fig. 3 and Fig. 4). The major NW faults clearly displace and apparently rotate reflectors over the Syn-Rift section. However, within the Sag section, it is still a challenge to map the faults due to the apparent smaller offsets on both sides of the faults. From the cross-sections, it is easier to interpret the faults by recognizing the offsets of the high-amplitude reflectors. However, the continuity of the faults is better assessed using the depth slices.

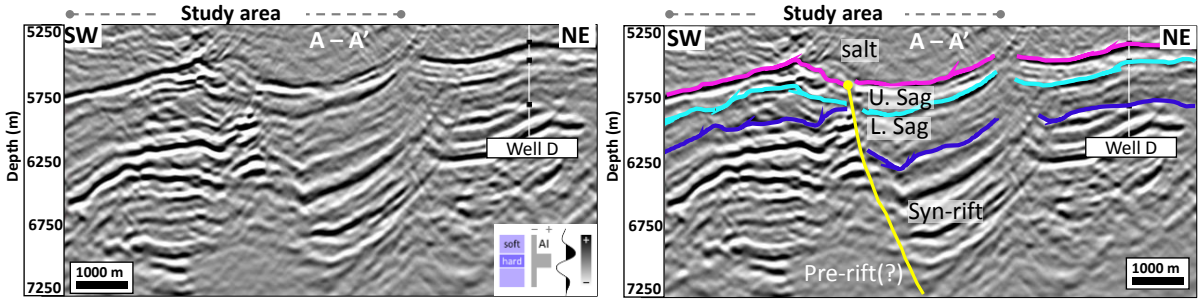


**Fig. 3.** Seismic cross-section highlighting a regional fault crossing the Syn-rift, Lower and Upper Sag sections. Noteworthy is the apparent higher throw on the hanging-wall block.

Some of the Syn-Rift faults are characterized by opposite dips to form positive features. These features may be associated to the paleotopographic highs (Gomes et al., 2012), which may also be associated to the Campos Basin rift shoulders (Mohriak et al., 2008; Kattah, 2017). It is on top of those rift shoulders that most of the microbialites are developed (Kattah, 2017). Some of those seismic features are illustrated in cross-sections (Fig. 4).

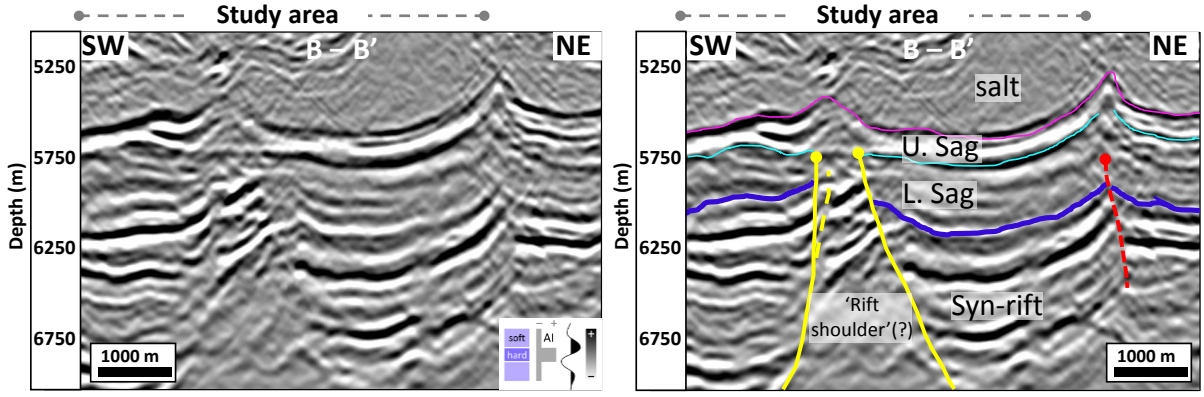


**Fig. 4.** Seismic cross-sections highlighting a positive feature interpreted as rift shoulder as in Campos Basin, formed by two opposing dip normal fault structures that cross the strata up to the base of the Upper Sag.

The fault interpretation allowed the definition of the structural framework with the regional faults that cross-cuts the pre-salt sag interval. This helps to constrain the further fracture modeling.

The overall orientation of the interpreted faults follows an NW-SE trend, which is coinciding with the NW-trending microbial build-ups interpreted over the study area and other nearby pre-salt discoveries that present a similar structural trend.

### 4.5.2. Seismic characterization of potential karst-related features

Interpreted seismic cross-sections display bright spots occurring at different depths. To detect the high-amplitude anomalies, this interpretation included a seismic texture attribute and filtered seismic data, based on a multiattribute approach that combined the Hilbert transform, Energy, and the GLCM Maximum Probability. High-amplitude anomalies that occur with large values of the texture attribute suggest potential karst-related features (Fig. 5). In addition, evidence of onlapping seismic reflectors suggests that the pre-salt sag section undergone a period of sub-aerial exposure. The center of the interpreted sag structure (SF1) is characterized by low amplitude and is bounded by high-amplitude continuous reflectors. This could be correlated to the seismic-scale karst cavities described in the Ordovician carbonates of the Tarim Basin (Chen et al., 2012). The Upper Sag horizon presents a similar expression, regarding the low amplitude, on top of the mounded features that could be correlated to the pre-salt carbonate build-up structures.

These results suggest an association of the high-amplitude seismic anomalies, expressed as bright spots, with potential karst-related features.

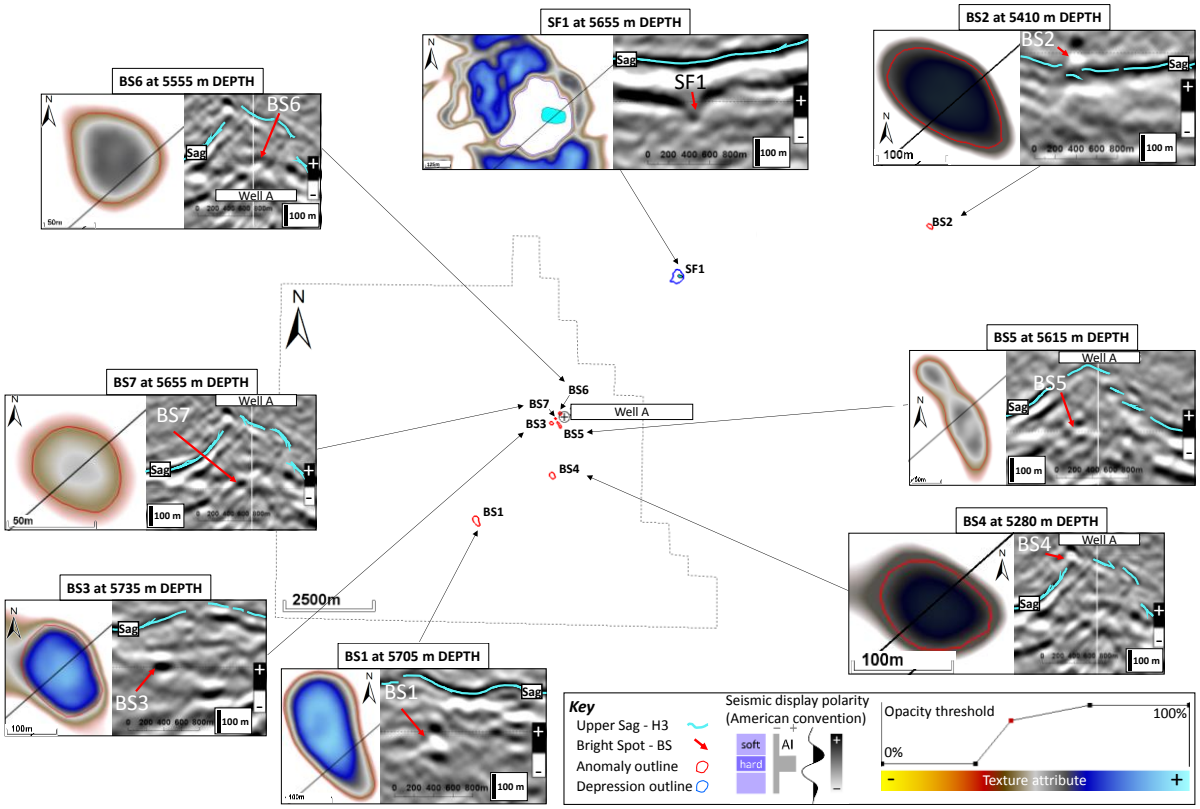


**Fig. 5.** High-amplitude anomalies map and NE-oriented original seismic crossing lines showing bright spots with a similar expression of karst-related features. Note that all the mapped features are characterized by an approximately sub-circular to elliptical plan-view morphologies illustrated in the texture attribute depth slices.

The available seismic data and the texture attribute allowed the detection of approximately 0.16 x 0.09 km horizontally high-amplitude anomalies possibly associated to karst-related features, interpreted as bright spots and sag structures associated to paleocave collapse that according to McDonnell et al. (2007) are typically collapse structures often defined by sub circular geometries in plan view. These interpreted features that vertically extend up to a height of 0.16 km occur at different depths, ranging from 5.3 to 5.7 km, and within a distance, between the top reflection and the Upper Sag horizon, of approximately 0.15 km, except for two of the bright spots (BS2 and BS4) that appear to occur on the Upper Sag horizon. The overall long-to-short axis (L/S) ratio that gives us a quantitative measurement of how circular an anomaly is, range from 1.13 to 4.18 km. Most of the interpreted features (75%) are NNW to NW-oriented, while the resting two (25%) are NNE-oriented. The depression feature interpreted as a sag structure (SF1) that occur at approximately 5.6 km, is characterized by a total area of 0.09 and an L/S ratio of 1.25, meaning a relatively circular plan-view shape (Table 1).

**Table 1.** Morphometric parameters of the interpreted seismic high-amplitude anomalies (bright spots - BS) and the depression feature (sag feature - SF).

| Features No. | Depth (km) | Area ($km^2$) | Height (km) | Long axis (km) | Short axis (km) | L/S ratio | Long axis azimuth (°) | Direction | Distance from Upper Sag (km) | Seismic unit |
|---|---|---|---|---|---|---|---|---|---|---|
| BS1 | 5.705 | 0.03 | 0.16 | 0.29 | 0.14 | 2.11 | 13.24 | NNE-SSW | 0.16 | L. Sag |
| BS2 | 5.410 | 0.01 | 0.16 | 0.19 | 0.09 | 2.02 | 352.58 | NNW-SSE | 0.00 | U. Sag |
| BS3 | 5.735 | 0.02 | 0.12 | 0.19 | 0.13 | 1.40 | 352.23 | NNW-SSE | 0.11 | L. Sag |
| BS4 | 5.280 | 0.01 | 0.10 | 0.10 | 0.08 | 1.26 | 161.56 | NNE-SSW | 0.00 | U. Sag |
| BS5 | 5.615 | 0.01 | 0.11 | 0.21 | 0.05 | 4.18 | 138.02 | NW-SE | 0.23 | L. Sag (?) |
| BS6 | 5.555 | 0.01 | 0.09 | 0.09 | 0.08 | 1.13 | 340.56 | NNW-SSE | 0.21 | U. Sag |
| BS7 | 5.655 | 0.00 | 0.11 | 0.05 | 0.04 | 1.14 | 334.77 | NNW-SSE | 0.34 | U. Sag |
| SF1 | 5.655 | 0.09 | 0.10 | 0.36 | 0.29 | 1.25 | 320.71 | NW-SE | 0.23 | U. Sag |

We also interpreted seismic fluid-escape features, which can be associated with the hydrothermal activity, commonly originated from the hydrothermal-induced fluid-rock interactions that may affect the host rock fabric structure and consequently the reservoir (Baomin and Jingjiang, 2009). These features may provide insights into the karstic systems in deeply buried carbonate reservoirs (Heward et al., 2000). Examples of features associated with fluid escape include pipe-like structures, documented worldwide (Klimchouk et al., 2016; Zhu et al., 2017; Belka et al., 2018; Gao et al., 2019). We described examples of seismic features possibly associated with focused fluid escape characterized by ‘reflection-free’ to acoustic blanking zones with a distinctive seismic reflector character (Fig. 6). Their cross-sectional shapes consist of several inward-dipping reflectors resembling a shallow depression, with an abrupt transition to the horizontal surrounding reflectors (Fig. 6). In plan view, they can be recognized by an approximately sub-circular to elliptical morphology, measuring, typically between 500 m and 1000 m wide (Fig. 6). There is a possibility that the hypogenic karst structures might have influenced the static behavior of the reservoir, since hydrothermal fluids could cause dissolution and therefore enhance porosity and permeability. This may help the hypotheses proposed to explain the karstic influence in the Brazilian pre-salt carbonates.

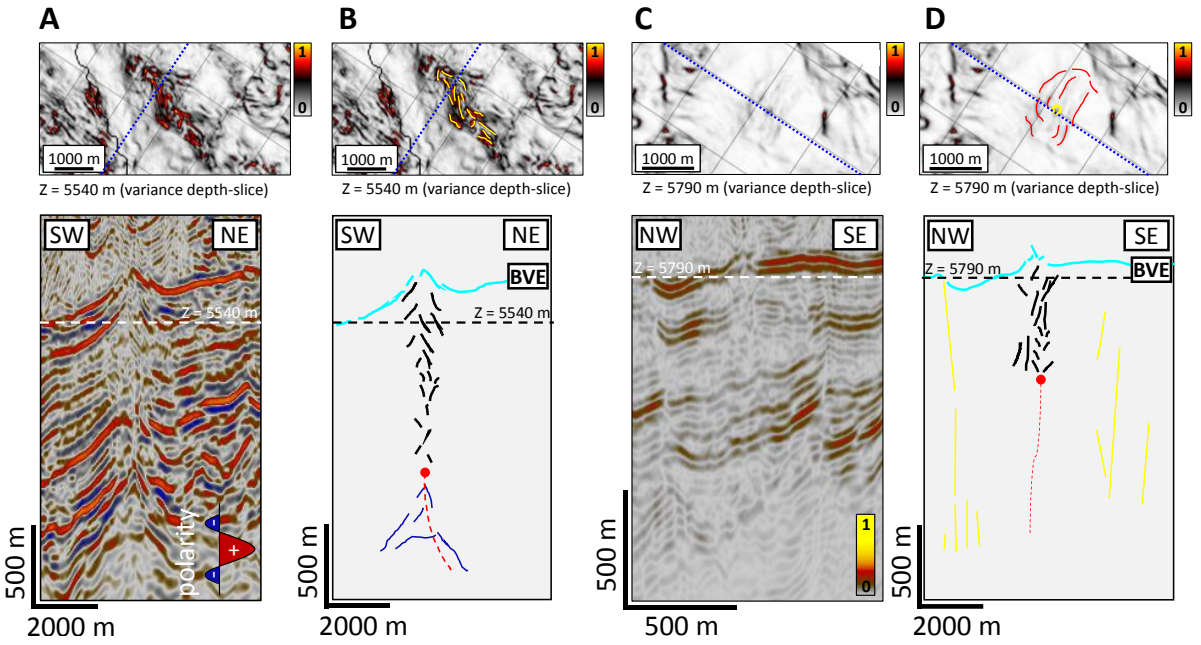


**Fig. 6.** Uninterpreted (A and C) and interpreted (B and D) morphology of fluid-escape features in plan view (depth slices) and cross-sections. The variation between an inward and outward configuration of the disrupted reflectors on the pipe-like structures might suggest focused fluid flow. We used original seismic amplitude volume (e.g. A) and RMS amplitude seismic attribute (i.e., C) for the cross-section interpretation and variance seismic attribute for the depth-slice interpretation (A-D). BVE is the top of the Barra Velha Formation in Santos Basin.

### 4.5.3. Discrete fracture networks modeling

The full-field geological model is defined by an approximately 98 million-cell grid with 299x842x389 cells spaced by a horizontal increment of approximately 25x25 m and a vertical increment of 2 m (Fig. 7). The sector model is defined by an approximately 1.35 million-cell grid with 39x89x389 cells spaced by a horizontal increment of approximately 25x25 m and a vertical increment of 2 m (Fig. 7). The chosen cell thickness (vertical discretization) might be able to capture the heterogeneities of the reservoir.

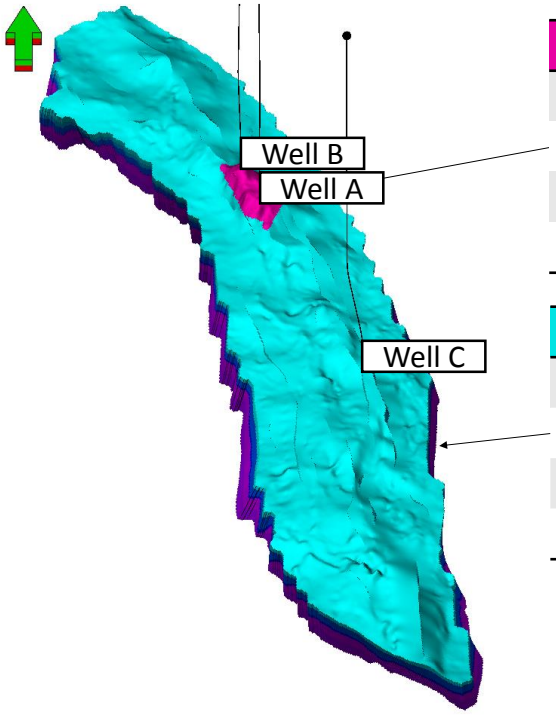


| Sector geogrid resolution (metric) | | | |
|---|---|---|---|
| Cells | I (X) | J (Y) | K (Z) |
| Dimension | 24.49 | 25.12 | 2.08 |
| Number | 39 | 89 | 389 |
| Total number | | 1.350.219 | |

| Full-field geogrid resolution (metric) | | | |
|---|---|---|---|
| Cells | I (X) | J (Y) | K (Z) |
| Dimension | 24.49 | 25.12 | 2.08 |
| Number | 299 | 842 | 389 |
| Total number | | 97.933.862 | |

**Fig. 7.** Geological grid highlighting the full-field scale model grid and the sector scale model grid for the DFN modeling.

The DFN model incorporated five stochastic fracture sets (continuous and discontinuous open and closed fractures), and one deterministic set based on interpreted faults (Fig. 8). Differences in the fracture trends of the model might be explained by the conditioning seismic attribute volumes. The ant tracking attribute and the distance from faults, used as collocated co-kriging of the fracture intensity, have questionable correlation coefficients for some of the reservoir intervals. It could be due to sparse fracture data in some parts, or to a lack of parametrization. We used the DFN model to distribute fracture porosity and permeability throughout the field. The fracture porosity and permeability that this DFN model predicted need to be calibrated with well tests.

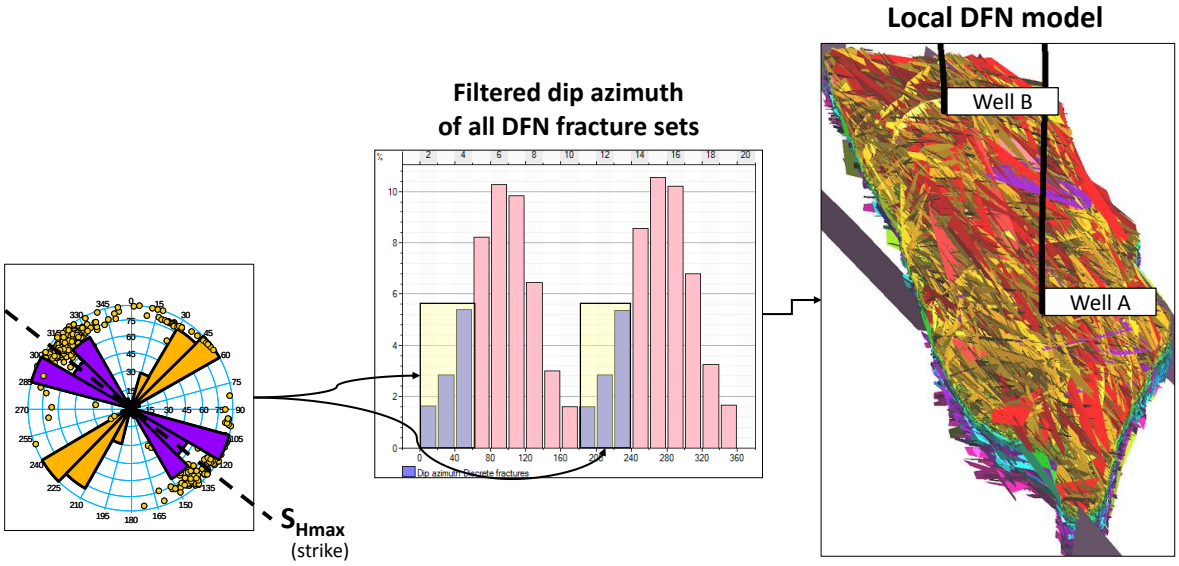


**Fig. 8.** Local DFN model defined by orientation and depth interval for different deterministic and stochastic fracture sets: Deterministic faults; Closed continuous fractures; Closed discontinuous fractures; Open continuous fractures; Open discontinuous fractures.

The tectonic regime analysis describes an overall extensional regime. The Upper Sag horizon in the tectonic modeling corresponds to the third tectonic phase, the Lowe Sag horizon corresponds to the second tectonic phase, and the Rift horizon corresponds to the first tectonic phase (Fig. 9). The main directions of the fracture sets for the in situ stress estimation from the borehole fracture point data correlate well with the predicted local tectonic model.

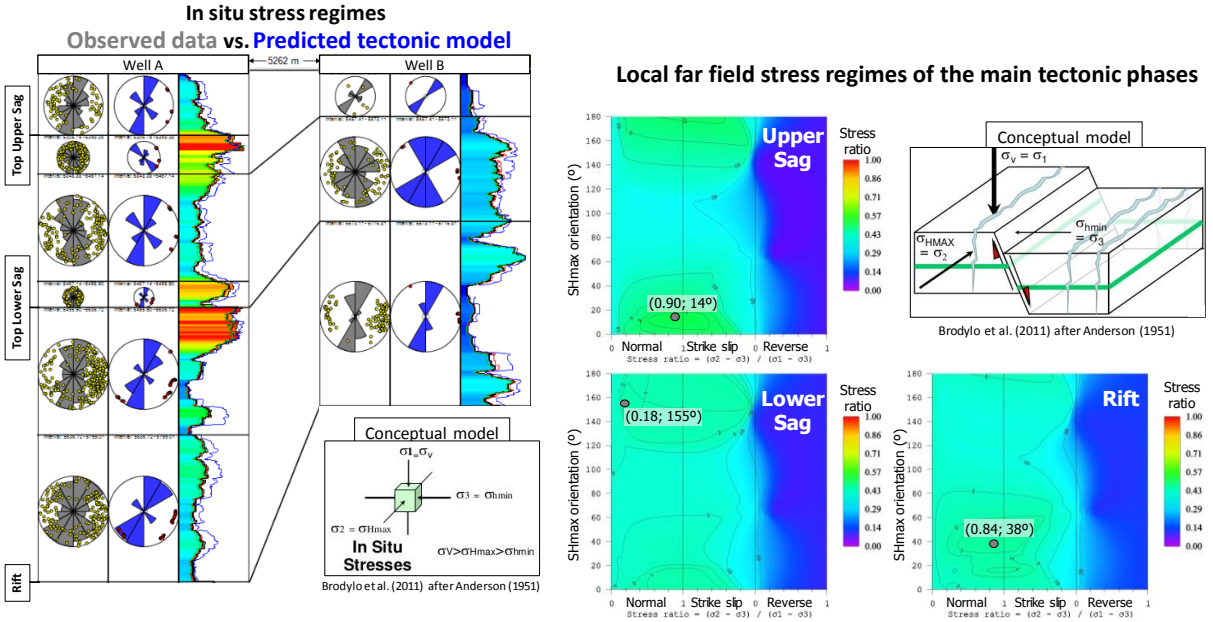


**Fig. 9.** Present-day in-situ principal stresses at each reservoir level for the Top Upper Sag, Top Lower Sag, and Top Rift. Contour lines express uncertainty levels (%) defining the tectonic regime (given by the stress ratio). A conceptual model for an extensional deformation case where the following stresses relationship applies: Sv > SHmax > Shmin (modified from Brodylo et al., 2011 after Anderson, 1951).

The permeabilities are associated with the fracture aperture, length, and connectivity. The upscaled permeabilities are illustrated in Fig. 10 for the permeability tensor of anisotropy.

We made assumptions for the DFN modeling that certainly impact the overall result of the model. In particular, the permeability volumes in the three directions were influenced by the input aperture values, which we could not estimate from the dataset; instead, we assumed different aperture values regarding the type of fracture set. Therefore, for the open fractures, we set higher apertures, for the closed ones we set lower values. The orientation of the tectonic stress field was also a criterion for the aperture values set, in a way that every fracture set in the direction of the SHmax would be set to have higher aperture values, whereas the fracture sets in the direction of the Shmin would be set to have lower aperture values.

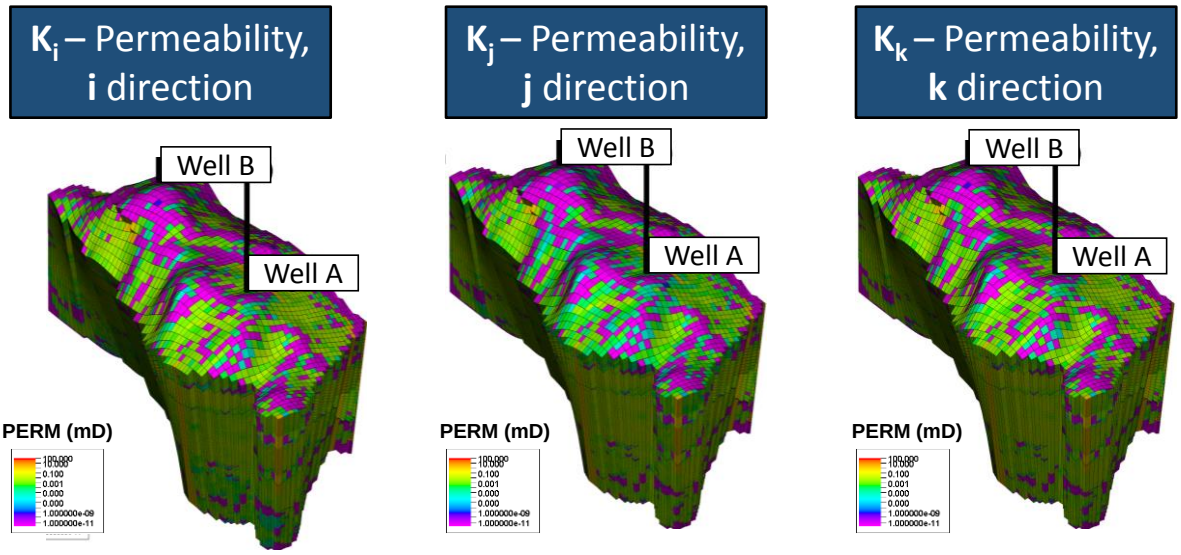


**Fig. 10.** Equivalent fracture permeability tensor ($k_i$, $k_j$, and $k_k$) for the sector model grid DFN of one of the realizations and one scenario, just to exemplify.

## 4.6. DISCUSSION

### 4.6.1. Fault framework

The interpreted major regional faults that cross-cut both the syn-rift and the sag sedimentary successions follow the overall syn-rift architecture and the minor faults lying within the sag succession appear to be conditioned by the pre-existing structures due to its spatial and geometrical correlation (Karner and Gambôa, 2007; Mohriak et al., 2008). However, the influence of the syn-rift faults on the sag succession requires a more thorough analysis, to assess the role of the previous fault in conditioning the later structuration.

According to Karner and Gambôa (2007), the extensional faults developed up to the base of the evaporites sequence overlying the sag succession, which has undergone a period of regional sub-aerial exposure, based on an interpreted erosive unconformity. During the period of exposure may have developed karst-related features (Wright and Barnett, 2017). According to Alves et al. (2017), the syn-rift package occurring truncated presents another evidence of an exposure period between the syn-rift Barra Velha Formation and the deposition of the Ariri Formation (salt). A small number of large faults produce up to 4 km-offsets at the evaporites base, often associated with smaller faults as a result of the late pre-salt tectonics (Alves et al., 2017), which is in accordance with Davison et al. (2012) that recognized smaller fault offsets. The basement presents paleotopographic highs originated from the later structuration, post-deposition lake sediments prior to salt deposition and spatially correlated with the carbonate build-up structures of the Barra Velha Formation (Wright and Barnett, 2017). The paleotopographic highs and combined 4-way closures form structural traps beneath the salt in microbial carbonate platforms, and occasionally isolated microbial build-ups (Santos et al., 2013; Kattah, 2015; Saller et al., 2016; Kattah, 2017). Furthermore, the study area is lying in the Central Santos microbial platform with NW-trending isolated build-up complexes (Fig. 11) (Kattah, 2017).

Noteworthy are the yet unclear nature of seismic mounded features, whether they are originated by the carbonate build-ups or another geologic structure. Such structures are being inferred based on the seismic character of their external geometries and internal facies pattern by several authors (e.g. Kattah and Balabekov, 2015; Kattah, 2017; De Luca et al., 2017). As for example, the pre-salt Elena Kay Complex in Campos Basin illustrates features that resemble microbial platforms appearing to be developed on top of volcanic complexes,

controlled by faults and expressed as mounded features (Kattah, 2017). Thus, it is clear that different geologic structures may produce seismic mounded features, which is why their characterization and relation with fault structures are important.

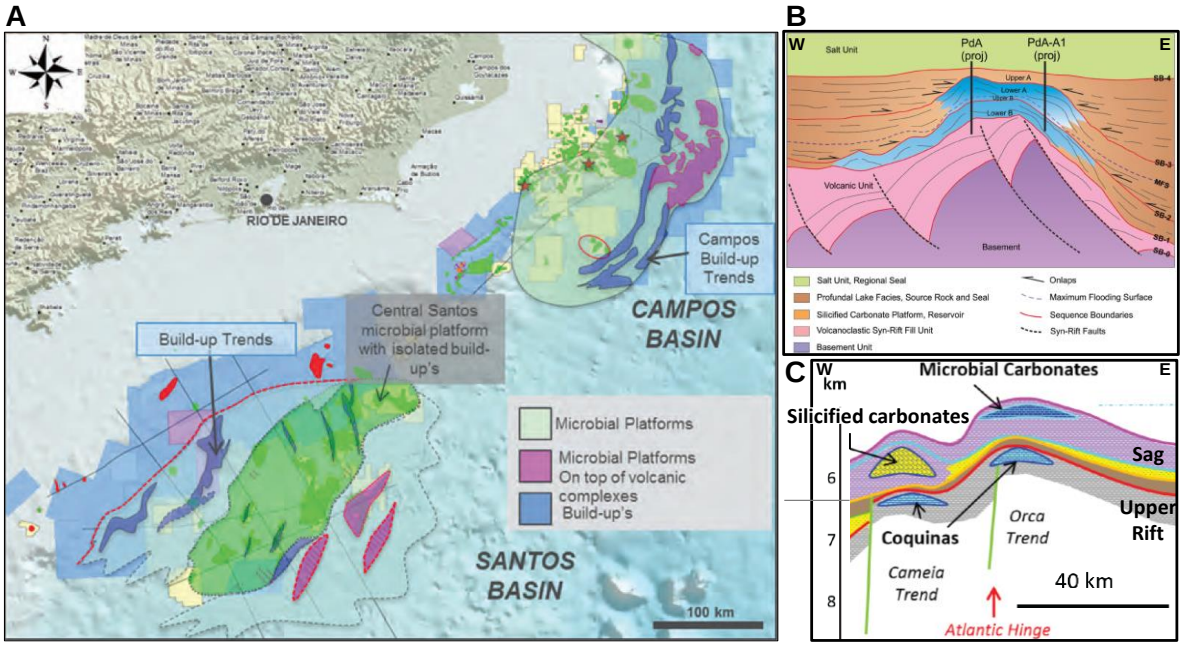


**Fig. 11.** (A) Microbial build-ups complexes trends occurring associated with microbial platforms, both in Campos and Santos basins (extracted from Kattah, 2017). (B) Some of the microbial platforms developed on top of volcanic rocks as the Pão de Açúcar pre-salt discovery in Campos Basin (extracted from De Luca et al., 2017). (C) Microbial and silicified carbonate build-ups in the counterpart margin of West Africa depicting the Cameia and Orca pre-salt discoveries. Note that the limit between Sag and Upper Rift is given by the red horizon (extracted from Poros et al., 2017).

### 4.6.2. Tectonic stress field

The model allowed to estimate the present-day tectonic regime at each of the reservoir level (Top Upper Sag, Top Lower Sag, Top Rift) (Figure 2). At the Top Upper Sag, the SHmax orientation is approximately NW-SE, while at the Top Lower Sag varies between NNE-SSW and NW-SE, and at the Top Rift is NE-SW. The tectonic model indicates that a hypothetical normal stress regime dominates the study area, with gravity driving normal faulting and creating extensional deformation, defined by the following relationship, Sv > SHmax > Shmin (Anderson, 1951). The study area has an apparently great contribution of an also possible strike-slip stress regime, where the relationship between the principal stresses changes to SHmax ≥ Sv ≥ Shmin, with a difference between the two horizontal stresses dominating the deformation and resulting in strike-slip faulting (Anderson, 1951). This estimation of the tectonic regime might be biased by the interpreted faults. Nevertheless, these results are consistent with detailed observations from the seismic interpretation. The borehole

image log analysis is also consistent with these results. The drilled-induced tensile fractures (NW-SE, roughly parallel to present-day in-situ stress SHmax) and borehole breakouts (NE-SW, roughly parallel to present-day in-situ stress Shmin) dip azimuths agree with these results. The uncertainties must be dealt with using different scenarios to better illustrate the stress changes during the tectonic evolution of the study area. The tectonic model may help us to know more about the Brazilian pre-salt carbonate reservoirs, specifically the Barra Velha Formation, which conceptual model is still unclear (e.g. Wright and Rodriguez, 2018).

## 4.7. CONCLUSIONS

In the fracture modeling study, we were able to produce a model that characterize the fractured zones discretized within the geological grid. In addition, these results might help to characterize the reservoir into one of the main types of Nelson's (2001) classification through the understanding of the contribution amount of the matrix. This helps to predict the reservoir behavior and to test the conceptual model underlying the structural characterization.

Our results support the following conclusions:

1. The integration of the seismic interpretation of faults and main horizons (Upper Sag, Lower Sag, and Rift) with well log-derived fracture orientations allowed the construction of this model that can be used as a predictive tool to locate potential fractured regions in the field.
2. The fault framework of the study area is characterized by regional fault structures that corroborate the in-situ stress field and the local far stress field.
3. The dominant tectonic stress at each top of main reservoir sequence varies from the base to the top, between normal and strike-slip with different orientations for SHmax. The model is consistent with the borehole breakouts and drilled-induced fractures.
4. The karst-related features characterized by seismic interpretation and multi-attribute co-rendering indicate a potential increase of porosities for the reservoir.

## ACKNOWLEDGEMENTS

The authors gratefully acknowledge Shell for supporting this research. This study was financed in part by Coordenação de Aperfeiçoamento de Pessoal de Nível Superior - Brasil (CAPES) - Finance Code 001. National Petroleum Agency's (ANP) Exploration and Production Database (BDEP) is acknowledged for providing seismic and well log data. The authors also acknowledge the academic software licenses provided by dGB Earth Sciences for OpendTect, by Schlumberger for Petrel, Kingdom by IHS Markit.

**REFERENCES**

Alves, T. M., Fetter, M., Lima, C., Cartwright, J. A., Cosgrove, J., Gangá, A., Queiroz, C.L., Strugale, M., 2017. An incomplete correlation between pre-salt topography, top reservoir erosion, and salt deformation in deep-water Santos Basin (SE Brazil). Marine and Petroleum Geology, 79, 300-320, https://dx.doi.org/10.1016/j.marpetgeo.2016.10.015.

Anderson, E.M., 1951. The dynamics of faulting and dyke formation with application to Britain. 2nd edition, Oliver and Boyd, Edinburgh, 206p.

Baomin, Z., Jingjiang, L., 2009. Classification and characteristics of karst reservoirs in China and related theories. Petroleum Exploration and Development, 36(1), 12-29, https://doi.org/10.1016/S1876-3804(09)60107-5.

Belka, Z., Skompski, S., Dopieralska, J., Feist, R., 2018. Flow paths of hydrothermal vent fluids in the Devonian Kess-Kess mounds, Anti-Atlas, Morocco. Neues Jahrbuch für Geologie und Paläontologie-Abhandlungen, 290(1-2), 49-63, https://doi.org/10.1127/njgpa/2018/0779.

Ben Amor, F., Kindi, Z., Kriplani, S., Panda, A., Darous, C., Akram, A.H., 2017. An Innovative Approach for Integrated Characterization and Modeling of a Complex Carbonate Reservoir. In SPE Middle East Oil & Gas Show and Conference. Society of Petroleum Engineers, https://dx.doi.org/10.2118/183800-MS.

Bisdom, K., Bertotti, G., Bezerra, F.H., 2017. Inter-well scale natural fracture geometry and permeability variations in low-deformation carbonate rocks. Journal of Structural Geology, 97, 23-36, https://doi.org/10.1016/j.jsg.2017.02.011.

Bourbiaux, B., Basquet, R., Cacas, M.C., Daniel, J.M., Sarda, S., 2002. An integrated workflow to account for multi-scale fractures in reservoir simulation models: implementation and benefits. In Abu Dhabi International Petroleum Exhibition and Conference. Society of Petroleum Engineers, https://doi.org/10.2118/78489-MS.

Brodylo, J., Chatellier, J-Y., Matton, G., Rheault, M., 2011. The stability of fault systems in the south shore of the St. Lawrence lowlands of Québec: Implications for shale gas development. SPE-149307-MS, 15-17 November, Calgary, Alberta, Canada.

Brown, A., 2004. Interpretation of three-dimensional seismic data, 6th ed.: AAPG Memoir, vol. 42, http://dx.doi.org/10.1306/M4271346.

Caixeta, J.M., Ferreira, T.S., Machado Jr., D.L., Teixeira, J.L., Romeiro, M.A., 2014. Albian rift systems in the northeastern brazilian margin: an example of rifting in hyper-extended Continental crust. AAPG Search and Discovery. Article, 30378.

Chen, Q., Zhao, Y., Li, G., Chu, C., Wang, B., 2012. Features and controlling factors of epigenic karstification of the Ordovician carbonates in Akekule arch, Tarim Basin. J. Earth Sci. 23, 506–515, https://dx.doi.org/10.1007/s12583-012-0271-4.

Chopra, S., Marfurt, K.J., 2007. Seismic attributes for prospect identification and reservoir characterization. Tulsa, Oklahoma: Society of Exploration Geophysicists. Vol. 11, p.481, https://dx.doi.org/10.1190/1.9781560801900.

Chesnaux, R., Allen, D.M., Jenni, S., 2009. Regional fracture network permeability using outcrop scale measurements. Engineering Geology, 108(3-4), 259-271, https://doi.org/10.1016/j.enggeo.2009.06.024.

Correia, M.G., Maschio, C., Schiozer, D.J., 2015. Integration of multiscale carbonate reservoir heterogeneities in reservoir simulation. Journal of Petroleum Science and Engineering, 131, 34-50, https://dx.doi.org/10.1016/j.petrol.2015.04.018.

Correia, M.G., Maschio, C., Schiozer, D.J., 2017. Development of complex layered and fractured reservoir models for reservoir simulation. Journal of the Brazilian Society of Mechanical Sciences and Engineering, 39(1), 219-233, https://dx.doi.org/10.1007/s40430-016-0606-7.

Correia, M.G., Schiozer, D.J., 2018. An Integrated Workflow to Combine Static and Dynamic Uncertainties in Reservoir Simulation Models. In 80th EAGE Conference and Exhibition, https://dx.doi.org/10.3997/2214-4609.201800807.

Cosentino, L., 2001. Integrated reservoir studies. Series: Fundamentals of Exploration and Production. Institute Français du Pétrole Publications. Editions Technip, 310 pp.

Davison, I., Anderson, L., Nuttall, P., 2012. Salt deposition, loading and gravity drainage in the Campos and Santos salt basins. Geological Society, London, Special Publications, 363(1), 159-174, https://dx.doi.org/10.1144/SP363.8.

Demercian, S., Szatmari, P., Cobbold, P.R., 1993. Style and pattern of salt diapirs due to thin-skinned gravitational gliding, Campos and Santos basins, offshore Brazil. Tectonophysics, 228(3-4), 393-433, https://doi.org/10.1016/0040-1951(93)90351-J.

Dershowitz, W.S., Herda, H.H., 1992. Interpretation of fracture spacing and intensity. Proceedings of the 33rd U.S. Symposium on Rock Mechanics, eds Tillerson, J.R. and W.R. Wawersik, Rotterdam, Balkema. Pp. 757-766.

Fang, J., Fengde, Z., Tang, Z., 2017. Discrete fracture network modeling in a naturally fractured carbonate reservoir in the Jingbei Oilfield, China. Energies, 10, 183.

Gao, J., Bangs, N., Wu, S., Cai, G., Han, S., Ma, B., Wang, J., Xie, Y., Huang, W., Dong., Wang, D., 2019. Post- seafloor spreading magmatism and associated magmatic hydrothermal systems in the Xisha uplift region, northwestern South China Sea. Basin Research, https://doi.org/10.1111/bre.12338.

Ghosh, K., Mitra, S., 2009. Structural controls of fracture orientations, intensity, and connectivity, Teton anticline, Sawtooth Range, Montana. AAPG bulletin, 93(8), 995-1014, https://doi.org/10.1306/04020908115.

Gomes, P.O., Kilsdonk, B., Grow, T., Minken, J., Barragan, R., 2012, Tectonic evolution of the Outer High of Santos Basin, southern São Paulo Plateau, Brazil, and implications for hydrocarbon exploration, in D. Gao, ed., Tectonics and sedimentation: Implications for petroleum systems. AAPG Memoir 100, p. 1 – 14, https://dx.doi.org/10.1306/13351550M1003530.

Hansen, D., 2006. The morphology of intrusion-related vent structures and their implications for constraining the timing of intrusive events along the NE Atlantic margin. Journal of the Geological Society, 163(5), 789-800.

Heward, A. P., Chuenbunchom, S., Mäkel, G., Marsland, D., Spring, L., 2000. Nang Nuan oil field, B6/27, Gulf of Thailand: karst reservoirs of meteoric or deep-burial origin?. Petroleum Geoscience, 6(1), 15-27, https://doi.org/10.1144/petgeo.6.1.15.

Karner, G. D., Gambôa L. A. P. 2007. Timing and origin of the South Atlantic pre-salt sag basins and their capping evaporites. Geological Society, London, Special Publications, 285, 15-35, 2007, https://dx.doi.org/10.1144/SP285.2.

Kattah, S., 2017. Exploration Opportunities in the Pre-Salt Play, Deepwater Campos Basin, Brazil, Society for Sedimentary Geology, The Sedimentary Record, 15, pp. 4-8, https://dx.doi.org/10.2110/sedred.2017.1.4.

Kattah, S., 2015. Pre-Salt Limestone Plays in Campos and Santos Basins, Brazil: Additional Potential Identified. In OTC Brasil. Offshore Technology Conference, https://dx.doi.org/10.4043/26101-MS.

Kattah, S., Balabekov, Y., 2015. Seismic facies/geometries of the pre-salt limestone units and newly-identified exploration trends within the Santos and Campos basins, Brazil. 14th International Congress of the Brazilian Geophysical Society & EXPOGEF, Rio de Janeiro, Brazil, 3-6 August, pp 288-293. https://dx.doi.org/10.1190/sbgf2015-057.

Klimchouk, A., Auler, A.S., Bezerra, F.H., Cazarin, C.L., Balsamo, F., Dublyansky, Y., 2016. Hypogenic origin, geologic controls and functional organization of a giant cave system in Precambrian carbonates, Brazil. Geomorphology, 253, 385-405, https://doi.org/10.1016/j.geomorph.2015.11.002.

Luca, P.H.V., Matias, H., Carballo, J., Sineva, D., Pimentel, G.A., Tritlla, J., Esteban, M., Loma, R., Alonso, J.L.A., Jiménez, R.P., Pontet, M., Martinez, P., Vega, V., 2017. Breaking Barriers and Paradigms in Presalt Exploration: The Pão de Açúcar Discovery (Offshore Brazil) in R. K. Merril and C. A. Sternbach, eds., Giant fields of the decade 2000-2010. AAPG Memoir 113, p. 177-194.

Matias, H.C., Ninci, B., Guangsheng, X., Pessoa, M.C., Mattos, F., Margem, R., Carballo, J., Esteban, M., Tritlla, J., Loma, R., Pimentel, G., 2015. Unlocking Pandora-Insights from Pre-salt Reservoirs in Campos and Santos Basins (Offshore Brazil). In 77th EAGE Conference and Exhibition, https://dx.doi.org/10.3997/2214-4609.201412891.

McDonnell, A., Loucks, R.G., Dooley, T., 2007. Quantifying the origin and geometry of circular sag structures in northern Fort Worth Basin, Texas: Paleocave collapse, pull-apart fault systems, or hydrothermal alteration?. AAPG bulletin, 91(9), 1295-1318, https://doi.org/10.1306/05170706086.

Mohriak, W., Nemčok, M., Enciso, G., 2008. South Atlantic divergent margin evolution: rift-border uplift and salt tectonics in the basins of SE Brazil. Geological Society, London, Special Publications, 294(1), 365-398, https://dx.doi.org/10.1144/SP294.19.

Moreira, J.L.P., Madeira, C.V., Gil, J.A., Machado, M.P., 2007. Bacia de Santos. Boletim de Geociências da Petrobras, 15(2), 531-549.

Nelson, R.A., 2001. Geological analysis of naturally fractured reservoirs, 2nd edition, Houston: Gulf Publishing Company, 320 p.

Oda, M., 1985. Permeability tensor for discontinuous rock masses. Geotechnique 35, 483–495, https://dx.doi.org/10.1680/geot.1985.35.4.483.

Poros, Z., Jagniecki, E., Luczaj, J., Kenter, J., Gal, B., Correa, T. S., Ferreira, E., McFadden, K.A., Elifritz, A., Heumann, M., Johnston, M., Matt, V.S., 2017. Origin of Silica in Pre-Salt Carbonates, Kwanza Basin, Angola. AAPG Annual Convention and Exhibition, Houston, Texas. Search and Discovery Article #51413.

Procter, A., Sanderson, D.J., 2018. Spatial and layer-controlled variability in fracture networks. Journal of Structural Geology, 108, 52-65, https://doi.org/10.1016/j.jsg.2017.07.008.

Saller, A., Rushton, S., Buambua, L., Inman, K., McNeil, R., Dickson, J.A.D., 2016. Presalt Stratigraphy and Depositional Systems in the Kwanza Basin, Offshore Angola: American Association of Petroleum Geologists Bulletin, v. 100, p. 1135-1164, https://dx.doi.org/10.1306/02111615216.

Sanderson, D.J., Nixon, C.W., 2015. The use of topology in fracture network characterization. Journal of Structural Geology, 72, 55-66, https://doi.org/10.1016/j.jsg.2015.01.005.

Sanderson, D.J., Nixon, C.W., 2018. Topology, connectivity and percolation in fracture networks. Journal of Structural Geology, 115, 167-177, https://doi.org/10.1016/j.jsg.2018.07.011.

Santiago, E., Velasco-Hernández, J.X., Romero-Salcedo, M., 2016. A descriptive study of fracture networks in rocks using complex network metrics. Computers & Geosciences, 88, 97-114, https://doi.org/10.1016/j.cageo.2015.12.021.

Santos, E.C.Dos, Ayres, H.F., Pereira, A.D.F., Machin, J.D., Tritlla, J.D., Leite, K.D.S., Silva, E.P., 2013. Santos Microbial Carbonate Reservoirs: A Challenge. In OTC Brasil. Offshore Technology Conference, https://dx.doi.org/10.4043/24446-MS.

Silva, O.L., Bezerra, F.H., Maia, R.P., Cazarin, C.L. 2017. Karst landforms revealed at various scales using LiDAR and UAV in semi-arid Brazil: Consideration on karstification processes and methodological constraints. Geomorphology, 295, 611-630, https://doi.org/10.1016/j.geomorph.2017.07.025.

Spagnuolo, M., Scalise, F., Leoni, G., Bigoni, F., Contento, F. M., Diatto, P., Francesconi, A., Cominelli, A., Osculati, L., 2018. Driving Reservoir Modelling Beyond the Limits for a Giant Fractured Carbonate Field-Solving the Puzzle. In Abu Dhabi International Petroleum Exhibition & Conference. Society of Petroleum Engineers, https://dx.doi.org/10.2118/192708-MS.

Szatmari, P., Milani, E.J., 2016. Tectonic control of the oil-rich large igneous-carbonate-salt province of the South Atlantic rift. Marine and Petroleum Geology, 77, 567-596, https://doi.org/10.1016/j.marpetgeo.2016.06.004.

Tosca, N.J., Wright, V.P., 2015. Diagenetic pathways linked to labile Mg-clays in lacustrine carbonate reservoirs: a model for the origin of secondary porosity in the Cretaceous pre-salt Barra Velha Formation, offshore Brazil. Geological Society, London, Special Publications, 435(1), 33-46, https://dx.doi.org/10.1144/SP435.1.

Valentini, L., Perugini, D., Poli, G., 2007. The “small-world” topology of rock fracture networks. Physica A: Statistical Mechanics and its Applications, 377(1), 323-328, https://doi.org/10.1016/j.physa.2006.11.025.

Vaughan, R.L., 2015. Practical Fracture Modeling Workflows: An Example from a Large Carbonate Field Development. In SPE Middle East Oil & Gas Show and Conference. Society of Petroleum Engineers, https://dx.doi.org/10.2118/172652-MS.

Wright, P., Rodriguez, K., 2018. Reinterpreting the South Atlantic Pre-Salt ‘Microbialite’ reservoirs: petrographic, isotopic and seismic evidence for a shallow evaporitic lake depositional model. Special topic: Modeling/Interpretation. First Break, 36, 71-77.

Wright, V. P., Barnett, A., 2017. Critically Evaluating the Current Depositional Models for the Pre-Salt Barra Velha Formation, Offshore Brazil. AAPG/SEG International Conference and Exhibition, London, England, pp. 15-18, Search and Discovery Article #90310.

Yenugu, M., Marfurt, K.J., Matson, S., 2010. Seismic texture analysis for reservoir prediction and characterization. The Leading Edge, 29 (9), p. 1116-1121, https://dx.doi.org/10.1190/1.3485772.

Yu, J., Li, Z., Yang, L., 2016. Fault system impact on paleokarst distribution in the Ordovician Yingshan Formation in the central Tarim basin, northwest China. Marine and Petroleum Geology, 71, 105-118, https://dx.doi.org/10.1016/j.marpetgeo.2015.12.016.

Zalán, P.V., Oliveira, J.A., 2005. Origem e evolução estrutural do Sistema de Riftes Cenozóicos do Sudeste do Brasil. Boletim de Geociencias da PETROBRAS, 13(2), 269-300.

Zeng, H., Loucks, R., Janson, X., Wang, G., Xia, Y., Yuan, B., Xu, L., 2011. Three-dimensional seismic geomorphology and analysis of the Ordovician paleokarst drainage system in the central Tabei Uplift, northern Tarim Basin, western China. AAPG bulletin, 95(12), 2061-2083.

Zhao, W., Shen, A., Qiao, Z., Zheng, J., Wang, X., 2014. Carbonate karst reservoirs of the Tarim Basin, northwest China: Types, features, origins, and implications for hydrocarbon exploration. Interpretation, 2(3), SF65-SF90, http://dx.doi.org/10.1190/INT-2013-0177.1.

Zhu, H., Zhu, X., Chen, H., 2017. Seismic characterization of hypogenic karst systems associated with deep hydrothermal fluids in the Middle-Lower Ordovician Yingshan formation of the Shunnan area, Tarim basin, NW China. Geofluids, 2017, https://doi.org/10.1155/2017/8094125.

# 5. CONCLUSIONS

This thesis emphasizes the documentation of post-depositional structures in the Campos and Santos Basin. These structures include igneous sills, and related structures (forced folds, junctions, and vents), fractures and karst. With all that, one may be able to better constrain the geological studies with a focus on the characterization of reservoirs. The characterization of the magmatic sill geometries, related structures, faults, fractures, and karst-related structures will certainly help to reduce the geological uncertainties before drill boreholes. Therefore, the type of predictive models that are able to perhaps close the gap between the expected seismic response of an intrusion and a prospective fractured and/or karstified carbonate or sand reservoir may be key to avoid negative exploration outcomes hence improving the success

In seismic based studies is important to try to keep the analysis as much as simple and with the minimum interpreter bias. This, in turn, is extremely challenging because the evidence found on seismic must somehow be interpreted using some a priori background and geological or geophysical knowledge.

The way this study was conducted may be applicable to similar geologic contexts in sedimentary basins worldwide, at least with the similar occurrence of the structures here identified.

Combining the characterization of some of these structures, interpreters should be able to conduct a better constraining of carbonate reservoirs, both for the pre-salt and for the post-salt sedimentary successions within the Brazilian margin basins or in other basins.

The Brazilian pre-salt reservoirs could benefit from a hypothesis where deep-seated faults might act as of feeder systems. However, the vent-related fractures are sub-seismic scale (Wright and Rodriguez, 2018). These types of structures may be recognized as sub-vertical seismic chimney-like structures, with a dominant low frequency content and reflectors occurring tilted upwards surrounding a reflection-free zone, which may indicate focused fluid flow (e.g. Hansen, 2006). That is why it is important to build predictive geological models taking into account the fractures. These carbonates may present an apparently independence between the sedimentary facies and the porosity and permeability. Therefore, it is plausible that fracture networks are controlling the distribution of porosity and permeability.

**REFERENCES**

Bisdom, K., Bertotti, G., Bezerra, F.H., 2017. Inter-well scale natural fracture geometry and permeability variations in low-deformation carbonate rocks. Journal of Structural Geology, 97, 23-36, https://doi.org/10.1016/j.jsg.2017.02.011.

Chen, Q., Zhao, Y., Li, G., Chu, C., Wang, B., 2012. Features and controlling factors of epigenic karstification of the Ordovician carbonates in Akekule arch, Tarim Basin. Journal of Earth Science, 23(4), 506-515, https://doi.org/10.1007/s12583-012-0271-4.

Ghosh, K., Mitra, S., 2009. Structural controls of fracture orientations, intensity, and connectivity, Teton anticline, Sawtooth Range, Montana. AAPG bulletin, 93(8), 995-1014, https://doi.org/10.1306/04020908115.

Gong, J., Rossen, W.R. 2017. Modeling flow in naturally fractured reservoirs: effect of fracture aperture distribution on dominant sub-network for flow. Petroleum Science, 14(1), 138-154, https://doi.org/10.1007/s12182-016-0132-3.

Narr, W., 1996. Estimating average fracture spacing in subsurface rock. AAPG bulletin, 80(10), 1565-1585.

Price, N.J., Cosgrove, J.W., 1990. Analysis of geological structures. Cambridge University Press.

Sanderson, D.J., Nixon, C.W., 2015. The use of topology in fracture network characterization. Journal of Structural Geology, 72, 55-66, https://doi.org/10.1016/j.jsg.2015.01.005.

Sanderson, D.J., Nixon, C.W., 2018. Topology, connectivity and percolation in fracture networks. Journal of Structural Geology, 115, 167-177, https://doi.org/10.1016/j.jsg.2018.07.011.

Singhal, B.B.S., Gupta, R.P., 2010. Applied hydrogeology of fractured rocks. Springer Science & Business Media.

Yu, J., Li, Z., Yang, L., 2016. Fault system impact on paleokarst distribution in the Ordovician Yingshan Formation in the central Tarim basin, northwest China. Marine and Petroleum Geology, 71, 105-118, https://doi.org/10.1016/j.marpetgeo.2015.12.016.

# APPENDICES

## APPENDIX A – SEISMIC POLARITY DISPLAY CONVENTION

Typical seismic response for a carbonate build-up and intrusive igneous rock.

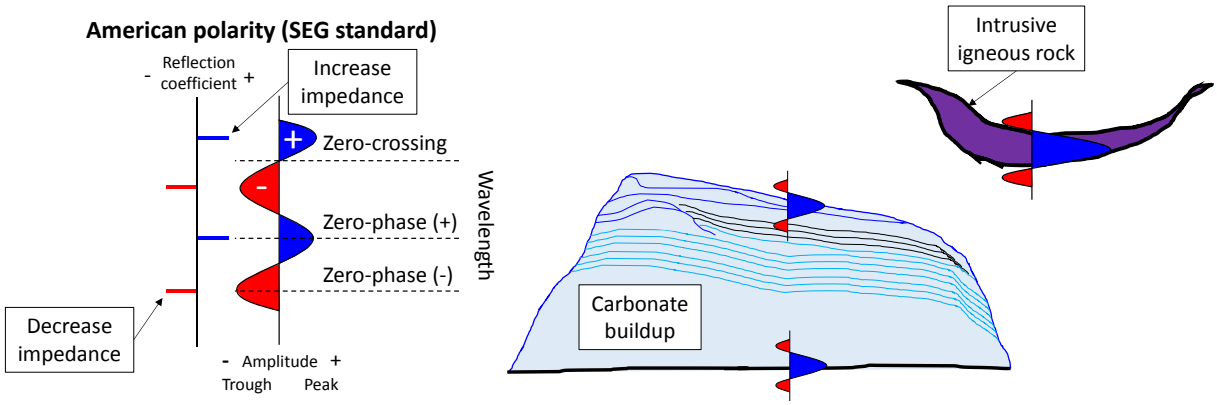


**Fig. A1.** The polarity convention according to the SEG standards (the American polarity). The typical seismic wavelet response of top and base of a carbonate build-up and the often seismic tuned reflection of an igneous intrusive rock. Most of the times, interpreters cannot distinguish the top and base contacts of the intrusion due to the side lobe effect of the wavelet.

# APPENDIX B – SEISMIC VERTICAL AND HORIZONTAL RESOLUTION

To calculate the vertical resolution of the seismic data it is necessary to first define an interval of interest, then measure the frequency content of that interval. If possible interpreters should estimate the velocity (often interval velocity) from the borehole data so it is possible to calibrate the seismic data. It should be interesting to assume an uncertainty and to work with possible ranges for the frequency content, which is often difficult to extract or measure without uncertainty.

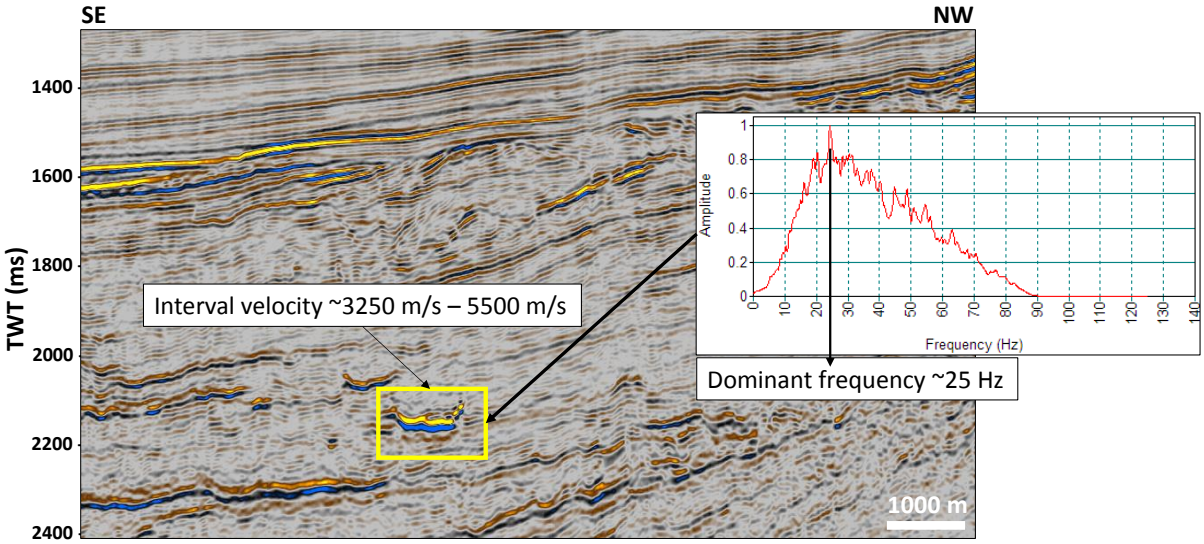


**Fig. B1.** Example from a seismic section from the study area 1 (Campos Basin) showing the frequency content and an estimated interval velocity for an igneous body, which can be used to compute the vertical resolution for an interval of interest. In the light of that, one may estimate the vertical resolution. This is from the Campos Basin study area.

The seismic horizontal resolution can be calculated using the Fresnel zone definition. To calculate the horizontal resolution it is also necessary to define the depth of the reflector under investigation. Therefore, this resolution will strongly depend on the depth, velocity, and dominant frequency. Commonly it is assumed a horizontal resolution from the lateral sampling of the seismic survey given by the CDP's spacing.

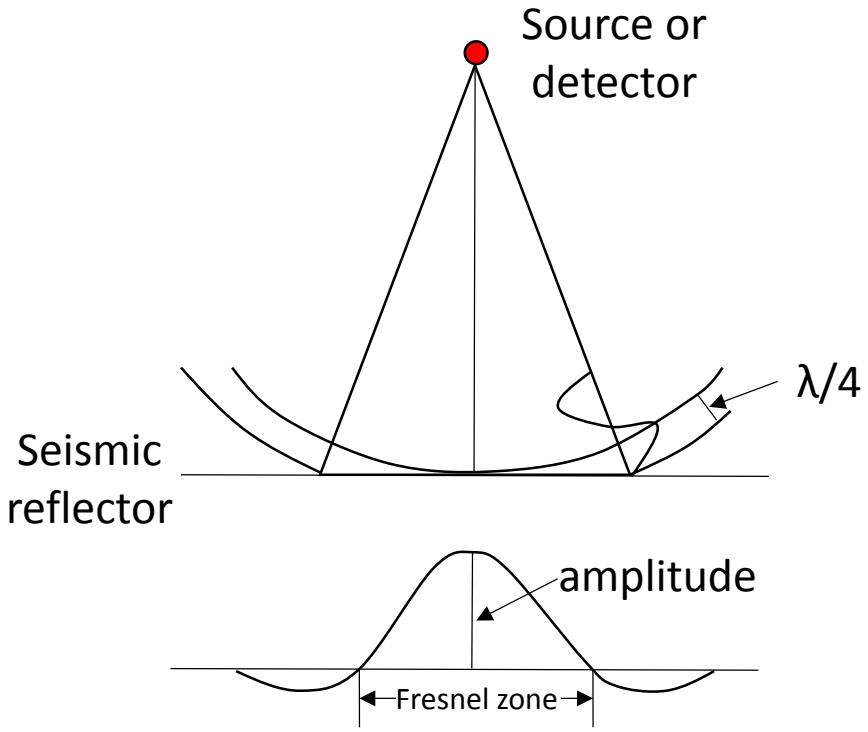


**Fig. B2.** Sketch of the Fresnel zone and the elements for calculating the seismic horizontal resolution (modified from Veeken, 2007).

## APPENDIX C – WIRELINE LOG CHARACTERISTICS REGARDING THE VARIATION IN SILICA CONTENT OF IGNEOUS ROCKS

Typical wireline log characteristics of gamma ray (GR), density (DEN), and compressional velocity (Vp) for different magmatic rocks regarding the silica content.

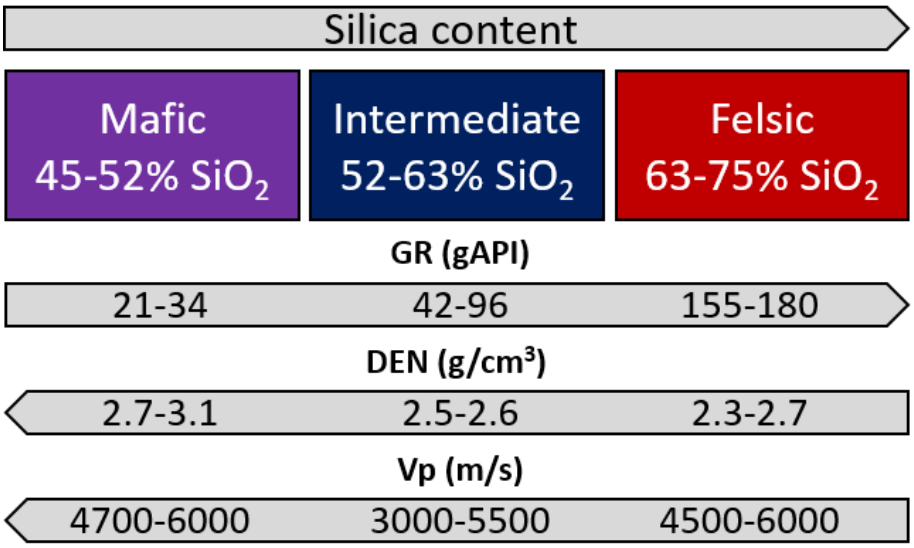


**Fig. C1.** Summary of theoretical averaged values for well log properties of mafic to felsic volcanic rocks, characterized by low to high silica-content (% SiO2) respectively, based on Planke et al. (2000, 2005), Mavko et al. (2009), and Delpino and Bermúdez (2009). In this summary ultramafic rocks are not considered (<45% SiO2), expected to be denser and higher velocity rocks. To note that SiO2 does not totalize 100% due to the presence of other oxides in the composition of magmas. Low gamma ray values are associated with high density and velocity values. Although, there are volcanic rocks with high gamma ray values associated with low to high density values as well.

## APPENDIX D – POST-STACK SEISMIC ATTRIBUTES USED IN THIS STUDY

Some examples of the seismic attributes that were used in this thesis.

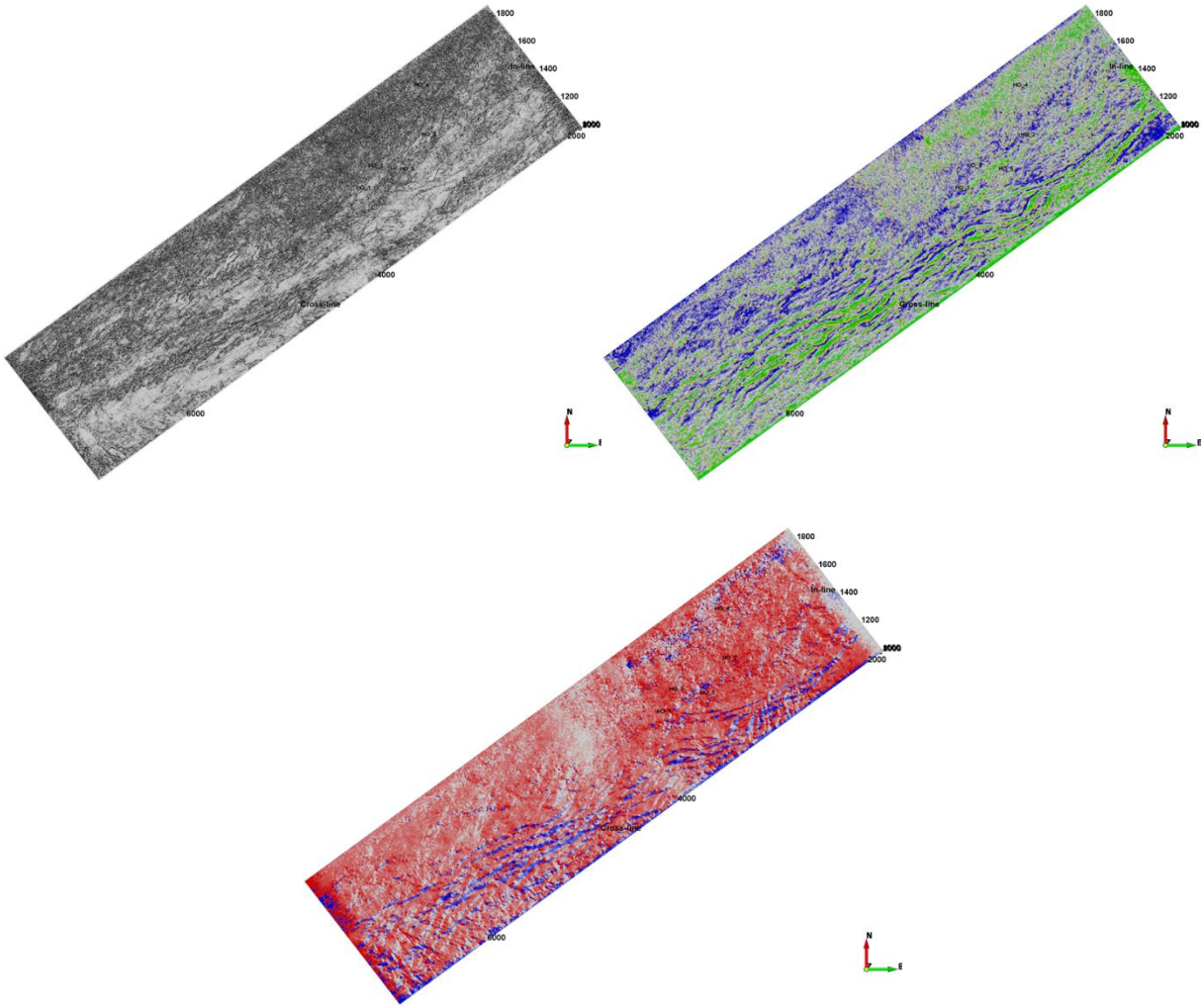


**Fig. D1.** Time-slices, from the study area in Campos Basin, of (a) steered minimum similarity attribute, (b) dip-steering filter in the strike direction and maximum curvature attribute, and (c) dip azimuth attribute.

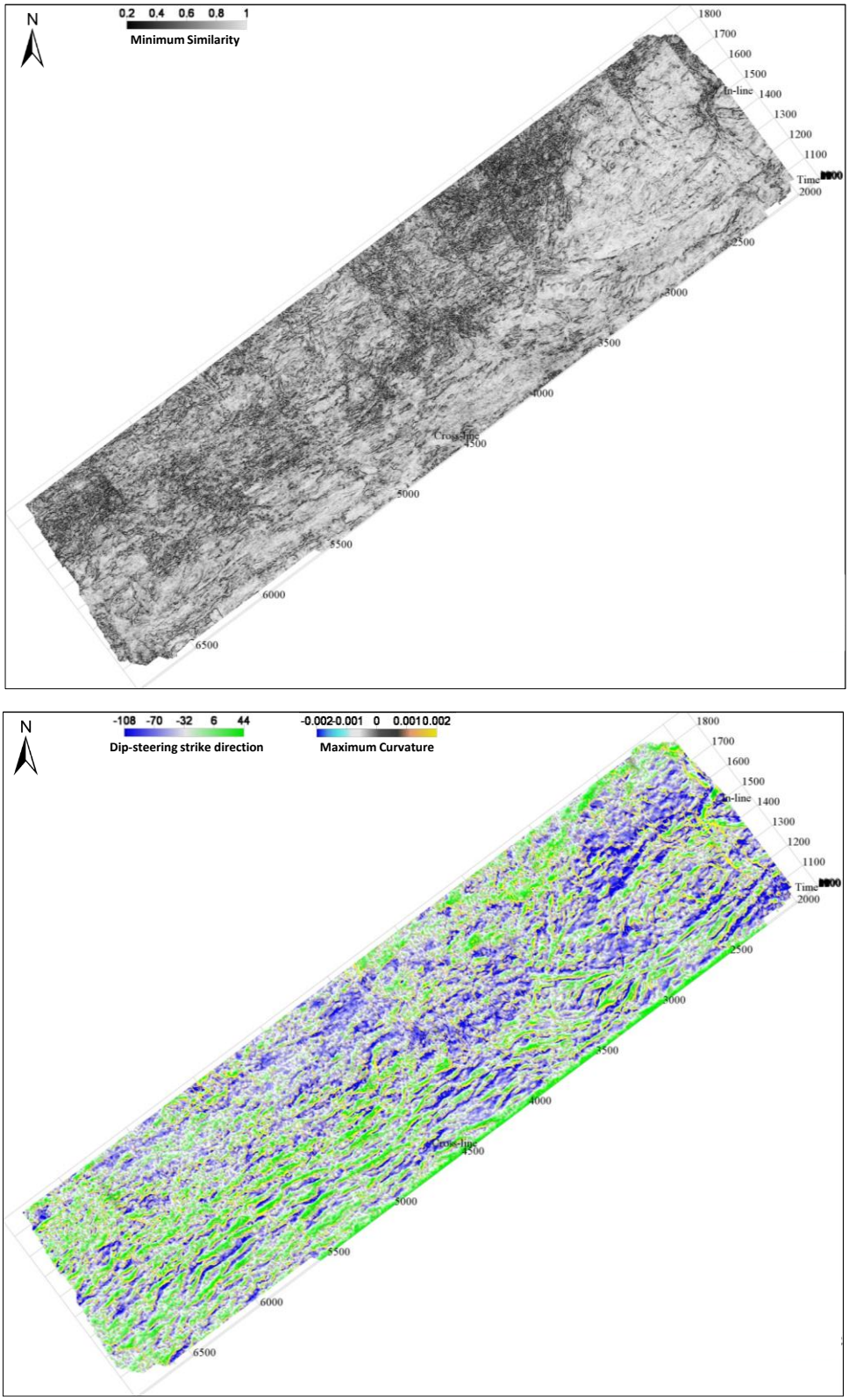


**Fig. D2.** Top Macaé Group surface with seismic attributes, from the study area in Campos Basin, of (a) steered minimum similarity attribute, (b) dip-steering filter in the strike direction and maximum curvature attribute, utilized in the structural interpretation.

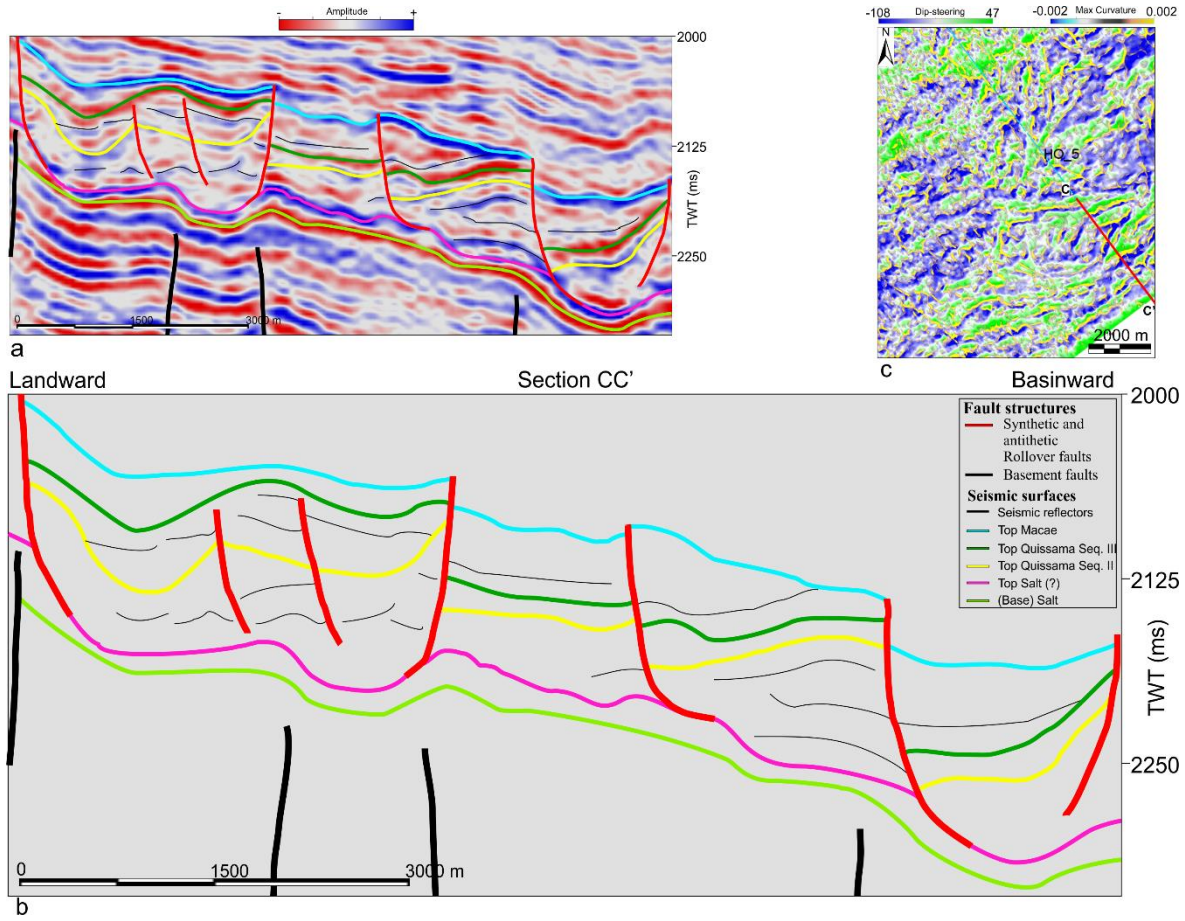


**Fig. D3.** Synthetic and antithetic listric faults, accommodating tilted blocks and rollover systems, from the study area in Campos Basin. The internal reflection pattern shows an increase of the tilting degree of the reflectors downslope. This fault system is rooted at the Top of Salt. Note some of the basement faults at the similar position of the Albian fault system. The insert show (c) the dip section location overlying the Macaé Group dip-steering horizon.

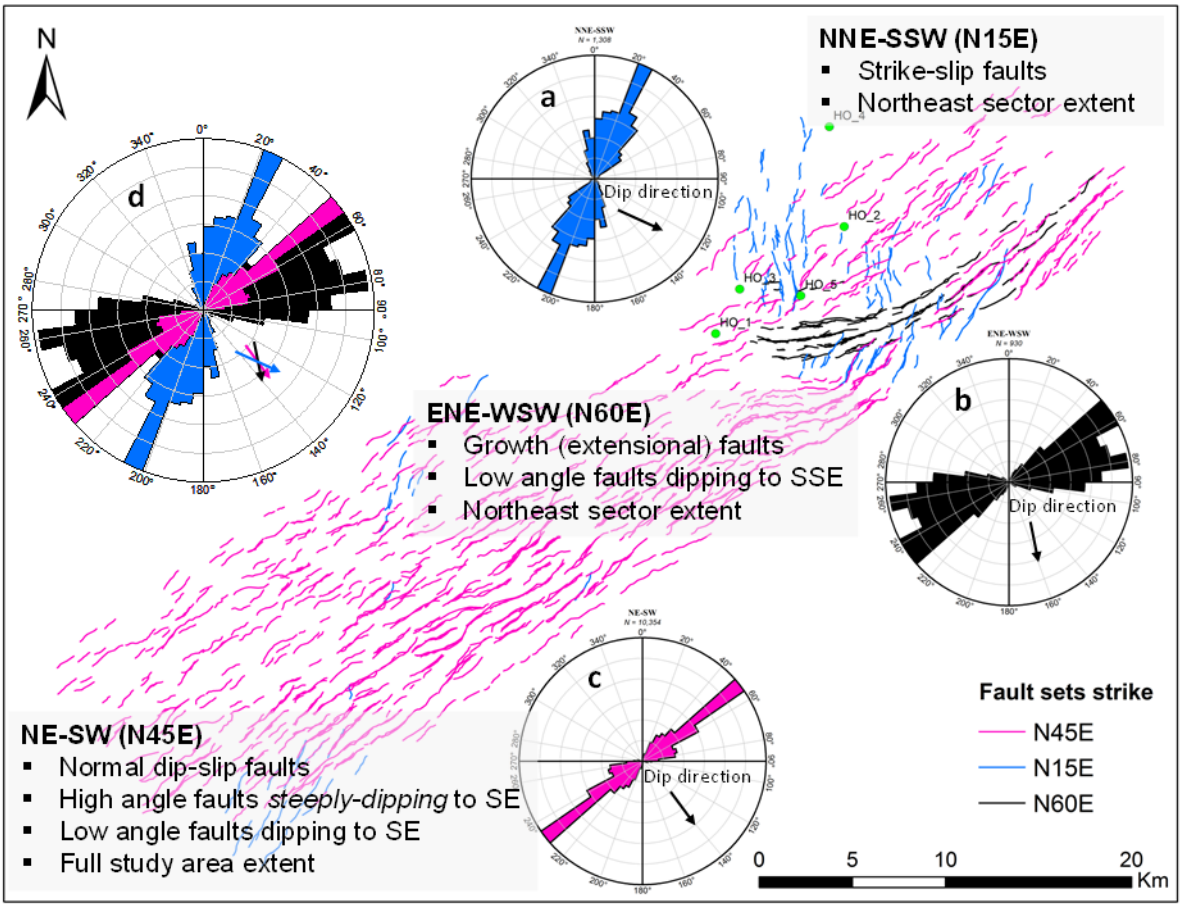


**Fig. D4.** Fault surface lineaments strike direction and rose diagrams showing the azimuth for each fault set, from the study area in Campos Basin: (a) NNE-SSW occurring both in the East portion and in the Southwest portion of the area; (b) WSW-ENE comprised of the easternmost portion of the area; and (c) NE-SW widespread over the whole area.

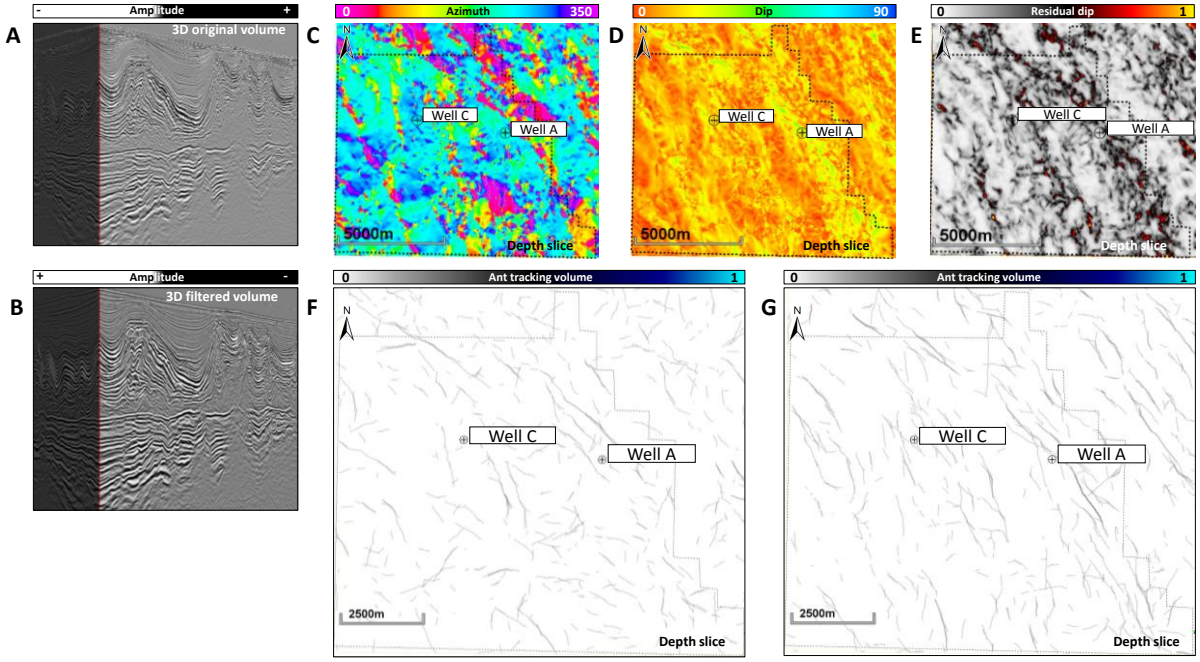


**Fig. D5.** Seismic attributes used for highlighting discontinuities interpreted as faults from the study area in Santos Basin, for the 3D original (A) and filtered seismic data (B). Examples of depth slices of filtered attributes: azimuth (C), dip (D) and residual dip (E). Note the distinct pattern in the Sag (F) and Syn-Rift (G) sections.

## APPENDIX E – WELL TO SEISMIC TIES METHOD

The well-to-seismic tie method used in this thesis describes the traditional convolution of the reflectivity with a statistical (theoretical) or deterministic (extracted from the data) wavelet to produce a synthetic trace. This well and seismic calibration aims to relate the waveforms with stratigraphy and rock properties to provide a solid ground for quantitative seismic interpretation. The workflow used is described by the following steps: (1) quality control of the seismic quality and the well logs in order to apply corrections if needed; (2) determine a time-depth relationship per well; (3) estimate statistical and extract deterministic wavelets from the well locations; (4) generate synthetic seismograms; and (5) quantify the accuracy of the well-to-seismic tie.

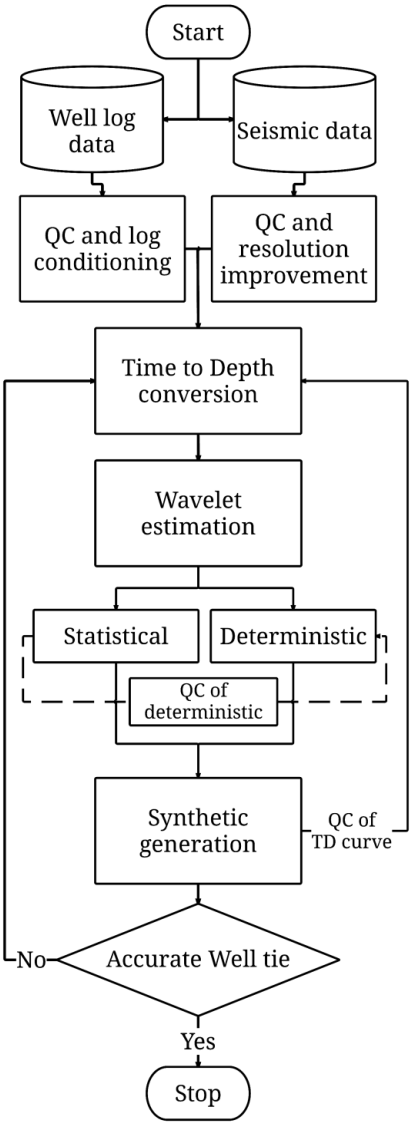


**Fig. E1.** Simplified flow chart used for the well-to-seismic ties in this thesis.

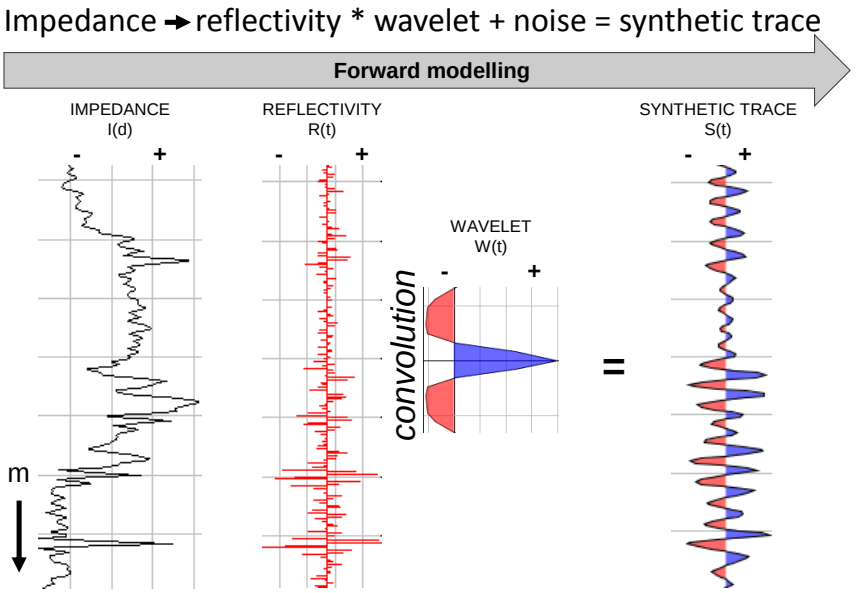


**Fig. E2.** Workflow for seismic forward modeling, to get synthetic seismograms, by predicting seismic from geology (modified from Zoeppritz, 1919).

$$PEP = \frac{Output\ Energy - Residual\ Energy}{Output\ Energy} \qquad S.E.\{\phi(f)\} \simeq \sqrt{\frac{NMSE}{2}}(radians) \qquad S.E.\{\phi\} \simeq \sqrt{1 + \frac{12\bar{f}^2}{(B^2 - b^2)}}\sqrt{\frac{PEP^{-1} - 1}{2bT}}(radians)$$

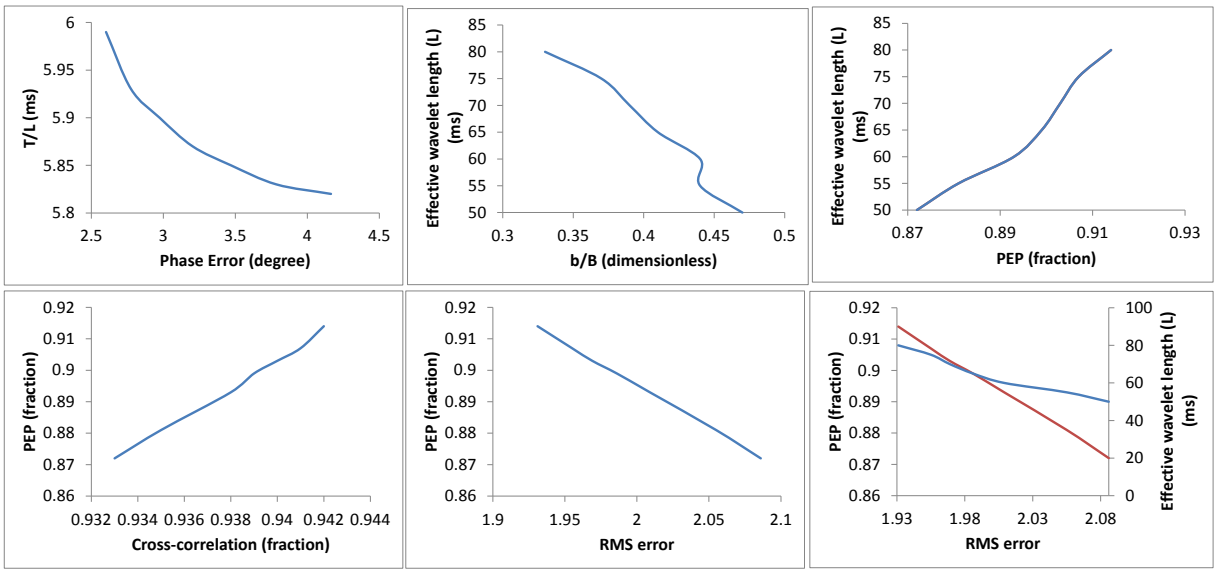


**Fig. E3.** Parameters used by RokDoc version 6.2.1.27 to run a quality control of the quality of well-to-seismic tie. **T** – The time window used for the analysis; **L** – The effective wavelet length, must be lower than the half of cross-correlation window. Typical 60-120 ms. RokDoc uses 124 as default. Smoother wavelets are generated with decreasing L; **T/L** – The time

window to wavelet length ratio, should be between 3 and 7 (5 is advisable); **Phase error** - Should be lower than 15º because this is an estimate of the likely phase error of the wavelet. In practice, phase errors vary with frequency of the seismic signal. Loss of phase error with increasing B; **b** – The analysis of bandwidth should be at least <B/2; **B** – The bandwidth of seismic data controls temporal (vertical) resolution. B controls the wavelet's resolving power and the detail available from inversion. A match that is coherent to the high frequency limit of B is good evidence of accurate log calibration and timing (log conditioning); **b/B** - should be in the range 0.25 - 0.5; **PEP** - proportion of energy predicted or predictability, should be high >70%. It is approximately the square of the cross-correlation coefficient between the synthetic seismogram and data; **Cross-correlation** – Should be high because it is representing the 'goodness-of-fit'. It is the cross-correlation at input range, between the synthetic and seismic data.

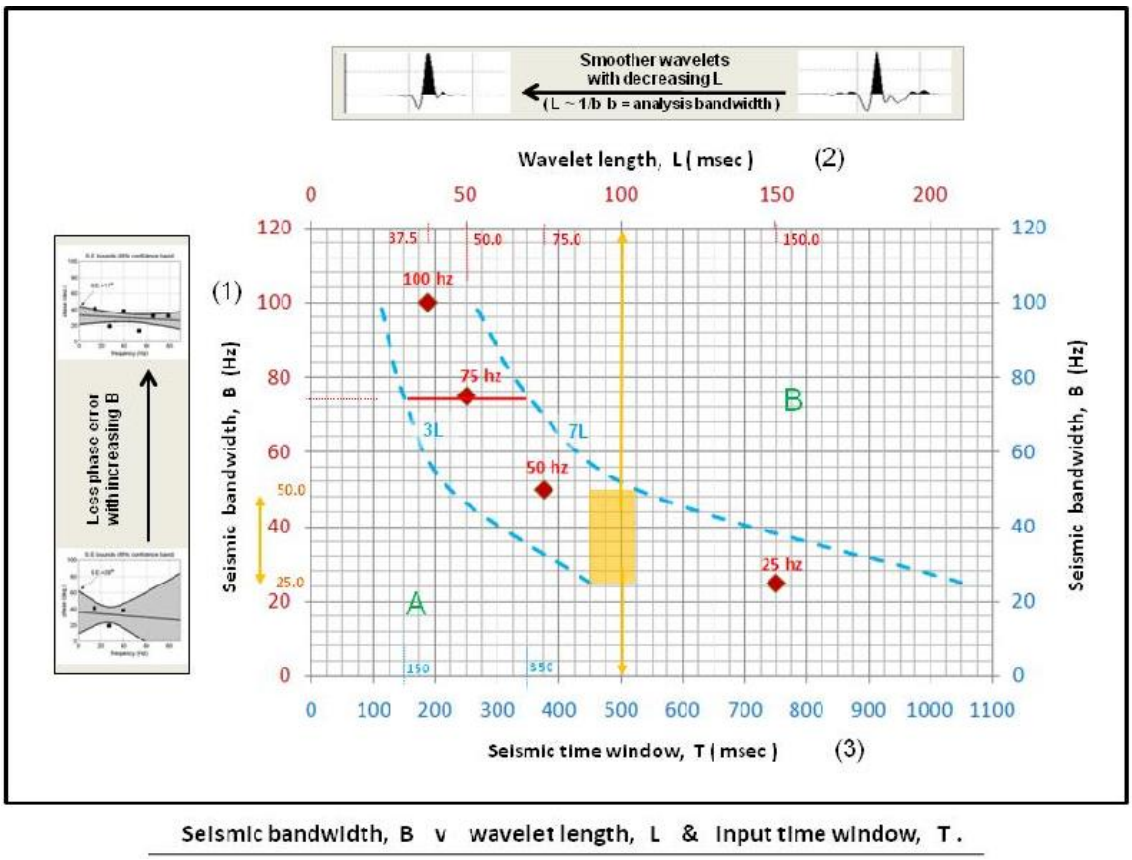


**Fig. E4.** Cross plot between the seismic bandwitdh (B in Hz) and seismic time window (T in msec) that help to chose the combination of parameters for the wavelets extraction. Extracted from the software manual of RokDoc version 6.2.1.27.

## APPENDIX F – COMMERCIAL SOFTWARES USED IN THIS THESIS FOR SEISMIC INTERPRETATION AND GEOLOGICAL MODELING

The interpretation of the three-dimensional seismic data, generation of the post-stack seismic attributes, well-to-seismic ties, tuning thickness analysis, borehole image log analysis, and fracture modeling, was carried out in several commercial software provided under academic licenses for the Institute of Geosciences, Center for Petroleum Studies, and laboratory of Geological Modeling of Reservoirs (MGR). Petrel versions 2015 and 2017 from Schlumberger, Kingdom version 2018 from IHS Markit, OpendTect versions 5.0.0 and 6.0.0 from dGB Earth Sciences, RokDoc version 6.2.1.27 from IkonScience, and Interactive Petrophysics version 4.4 from Lloyd's Register.

# APPENDIX G – LICENSE AGREEMENTS FROM PUBLISHERS GRANTING PERMISSION TO REPRODUCE PUBLISHED ARTICLES IN THIS THESIS